Image Processing Results of One Week Covid-19 Evolution Pneumonia X-Rays

Abhishek Bansal†
Self-Employed, Amateur Scholar, Independent Researcher
Delhi, India
abhishekbansaL006@gmail.com

Abstract

This paper presents the collection of 385 new images and results, obtained after performing many known image processing algorithms and digital image transformations techniques like adding noises namely Gaussian with variances, Poisson and speckle with variances; double precision, methods of Sobel,Prewitt and Robert; dehazing algorithm, pixel intensities,vector quantization, k-means clustering, fuzzy logic and morphological segmentation. Images used in this paper are five X-Rays at day 0, day 3, day 4 and day 6, which are Posterior to Anterior (PA) views of the patient's lungs who was diagnosed with covid-19 Pneumonia. All results are included in the paper as well as separate images have also been uploaded on the open-access page. The data has been analyzed with histogram and mathematical polynomial fitting equations and matrices have been also submitted which can used in the digital testing of machines or computer diagnostic solutions. As these results reveal certain patterns,these further processed X-Ray results can help researchers or doctors in understanding ailment or diagnosing and to pharmacologists in making medicine or machine/therapy.

† His ORCiD Identification Number is 0000-0002-2572-9004

Index Terms

image processing, pneumonia, X-Ray, Laplacian operator, Sobel–Feldman operator, mathematical morphology,Gaussian,white noise,variances,Poisson,speckle,single precision,double precision,Sobel,Prewitt, Robert,dehazing algorithm, pixel intensities,vector quantization, k-means clustering,fuzzy logic,edge detection, fuzzy inference system, FIS,Gaussian smoothing, intermediate difference,central difference,polynomial regression,convolution,morphological segmentation,COVID, windpipe,covid-19 ,respiratory tract

I Introduction

It is known that images can be processed through computer using algorithms. There are many open-source and proprietary tools and softwares like in Python[1], OpenCV[3], FuzzyLite[4], PyTorch[10],TensorFlow[11] etc. The techniques like Laplacian Operator[5], Sobel–Feldman operator[6], Mathematical morphology[7], Fuzzy Logic[8],double precision, methods of Sobel,Prewitt and Robert gradients,Gaussian,Canny, dehazing algorithm, pixel intensities,vector quantization, k-means clustering, fuzzy logic and morphological segmentation. are known and widely implemented in digital camera images, Face detection, Edge Detection, traffic vehicles, etc.

The author has used all these various digital image transformations techniques on the X-rays or Datasets from[1]. **The use of these image processing algorithms is in research by many researchers/post-doctorate fellows/clinical doctors**, even the source[1] has python script and other scripts on tensorflow, openCV or proprietary software scripts can be located on internet. The techniques used in this paper are mentioned along side with the processed-image. Algorithms have not been explained as they are known and

it would be a plagiarism.‡ *

The further processed images or results are included within manuscript file and all these images (in .png) are also separately available for study, which can be downloaded freely from open-access page[9]. For this particular manuscript, pls refer Paper2.zip[9] for collection of images.

The paper is organized : In the Section II, five original-rays are included. The subsequent five sections are related to the results of processed images of Day0(L), Day0(PA), Day3(PA), Day4(PA) and Day6(PA). **The Day0(L) results are from page 4-33. The Day0(PA) results are from page 34-60. The Day3(PA) results are from page 61-86. The Day4(PA) results are from page 87-113.The Day6(PA) results are from page 114-140. The conclusion is given on page 141** .

The subsections are organized as :

1) Firstly X-Ray of the section is converted to single precision grayscale and double precision in *Subsection 1* titled as 'X-Ray Converted'
2) In *Subsection 2*- 'Double Precision Noise Addition', noises namely Gaussian, Poisson and speckle noises are added to the converted double-precision X-Ray.
3) In *Subsection 3*-'Gradient Magnitude and Direction' of single precision X-Ray are plotted using four methods.
4) In *Subsection 4*-'Directional Gradients' of single precision X-Ray are plotted using four methods.

*‡ Many will say just known code and image processing, elementary, which is true as the author has modified known scripts and image results obtained. On the other side, many paid freshers or paid employees! will want to know code. **Modified code is not shareable** but the author can render services at some monetary price. *Overload computations have caused many times computer crashes with complete corruption of files*.

5) In *Subsection 5*- 'Gaussian Noises & Sobel Gradient', Gaussain noise with variances are added to single precision grayscale X-Ray.
6) In *Subsection 6*- 'Poisson Noise & Sobel Gradient', noise is added to single precision grayscale X-Ray.
7) In *Subsection 7*- 'Speckle Noise & Sobel Gradient', Speckle noise with variances are added to single precision grayscale X-Ray.
8) In *Subsection 8*- 'Pixel Intensities & Contrast', orignial X-Ray is contrasted and mathematical formulation of the pixels are given.
9) In *Subsection 9*- 'Fuzzy Logic' is used and edge detection using FIS and edge algorithm given.
10) In *Subsection 10*- 'K-means Clustering', a vector quanization technique is used to obtain clusters and the mathematical formulation is again given.
11) *Subsection 11*- 'Morphological Segmentation' results are given.
12) *Subsection 12*- 'Dehazing Algorithm' is used and its results are given.

II Original X-Rays

The five X-Rays are taken from [1] are shown in Fig. 1, which are evolution of covid-19-pneumonia over a week from Day 0 to Day 6. On these X-rays, the above mentioned popular elemenetary and advanced algorithms will be implemented.

III Results : Day 0,Lateral

1 X-Ray Converted

In this subsection, X-Ray(L) of Day 0 is converted to single precision grayscale and double precision,on which all further image processings will be done. These are shown in Fig. 2.

2 Double Precision Noise Addition

In this subsection, the double precision X-Ray of Day 0 (Fig 2(b)) of the previous subsection is subjected to noises namely Gaussian with variance 0.01, Poisson Noise and speckle noise with variance 0.05. These are shown in Fig. 3.

3 Gradient Magnitude and Direction

In this subsection, the gradient of the single precision X-Ray of Day 0 (Fig 2(a)) is obtained and its magnitude and direction is plotted using methods of Sobel, Prewitt, central difference and intermediate difference. These are shown in Fig. 4.

4 Directional Gradients

In this subsection, the directional gradient of the single precision X-Ray of Day 0 (Fig 2(a)) is plotted using methods of Sobel, Prewitt, central difference and intermediate difference. These are shown in Fig. 5.

5 Gaussian Noises & Sobel Gradient

In this subsection, the single precision X-Ray of Day 0 (Fig 2(a)) is subjected to Gaussian noise with three variances of 0.01, 0.001 and 0.0001. These are shown in Fig. 6. The gradient magnitude of these noisy X-Rays are plotted using Sobel method, which are shown in Fig. 7. The figures of gradient magnitude of Fig. 7 are further smoothed using 2-D Gaussian smoothing. The Gaussian smoothing and central difference gradient are shown in Fig. 8. The Gaussian smoothing and intermediate difference gradient are shown in Fig. 9.

6 Poisson Noise & Sobel Gradient

In this subsection, the single precision X-Ray of Day 0 (Fig 2(a)) is subjected to Poisson Noise,Fig. 10(a). The gradient magnitude of Poisson noise X-Ray is plotted using Sobel method, which are shown in Fig. 10(b). This is further smoothed using 2-D Gaussian smoothing and central difference gradient in Fig. 10(c); and 2-D Gaussian smoothing and intermediate difference gradient in Fig. 10(d).

7 Speckle Noise & Sobel Gradient

In this subsection, the single precision X-Ray of Day 0 (Fig 2(a)) is subjected to Speckle noise with four variances of 0.05, 0.01, 0.001 and 0.1. These are shown in Fig. 11[a-d]. The gradient magnitude of these noisy X-Rays are plotted using Sobel method, which are shown in Fig. 12. These are further smoothed using 2-D Gaussian smoothing. The Gaussian smoothing and central difference gradient are shown in Fig. 13. The Gaussian smoothing and intermediate difference gradient are shown in Fig. 14.

8 Pixel Intensities & Contrast

In this subsection, the original X-Ray (without converting to single precision or double precision) is contrasted for study and analysis.

Let the center fit $z = \dfrac{(x - 127.5)}{74.05}$, then from polynomial regression

$$y = -1049 \times z^9 + 2661 \times z^8 + 6199 \times z^7 - 1.429 \times 10^4 \times z^6 - 1.22 \times 10^4 \times z^5 + 2.406 \times 10^4 \times z^4 + 7439 \times z^3 - 1.476 \times 10^4 \times z^2 + 1640 \times z + 5288$$

Let $\bar{y}$ be the mean of y, $\hat{y}$ the calculated values of y, then the coefficient of determination, $R^2 = 1 - \frac{\sum_{\iota=1}^{n}(y_i - \hat{y})^2}{\sum_{\iota=1}^{n}(y_i - \bar{y})^2} = 0.6302$

The measure of the goodness of fit given by norm of residuals is 2.758×10^4. Here, the polynomial of degree 9 chosen here is the global which can be focused on the areas of interest (to be decided by infection part or researchers/doctors interest) and separate equations can be obtained for each particular area of interest. This gives insight in mathematical formulation and has been used in the Novel $\mathcal{B}$-Mathematical Modeling of Respiratory System.

TABLE I: Data Statistics for Fig. 15(b)

	X	Y
min	0	0
max	255	3.214×10^4
mean	127.5	2668
median	127.5	2082
mode	0	300
std deviation	74.05	2840
range	255	3.214×10^4

The Fig.15(a) shows that X-Ray contrast is improved for analysis when compared with Fig. 1(a). Fig. 15(b) shows the distribution of X-Ray pixel intensities. Fig. 15(c) shows the error estimation plot, which is the plot of the residuals. Fig. 15(d) shows the X-Ray histogram equalization which is the spreading of the intensity values over the full range.

In Fig. 16, X-Ray Contrast is improved with five local luminances. The original

Fig. 2(a) X-Ray contrast is improved with four more local luminances by varying the intensity values at low and high intensities. These are shown in Fig 16(a), Fig. 16(b) and Fig. 16(c). In Fig. 16(d), the original Fig. 2(a) X-Ray is contrasted with fifth value of improvement but smoothing technique is applied after it.

9 Fuzzy Logic

In this subsection, the images obtained using fuzzy logic edge-detection algorithm and Fuzzy Inference System (FIS) are given. Two 2-D Convolution are performed. The x-axis of directional gradient is convolved with x-axis gradients of double-precision X-Ray obtained in Fig. 2(b) and the X-Ray gradient of fuzzy logic x-axis is given in Fig. 17(a). The y-axis of directional gradient is convolved with y-axis gradients of double-precision X-Ray obtained in Fig. 2(b) and the X-Ray gradient of fuzzy logic y-axis is given in Fig. 17(b). The edge detection is shown in Fig. 17(c).

10 K-means Clustering

In this subsection, the popular vector quantization technique of K-Means clustering is applied to X-Ray. In this technique, firstly CIE XYZ tristimulus technique is used to know the color information and thus, the information of luminosity layer 'L*', chromaticity-layer 'a*' and chromaticity-layer 'b*' is obtained. Then every pixel is clustered with its pixel label and partitioned into three clusters. The clustering obtained is shown in Fig. 18(a), Vector Quantization Cluster Label. And three clusters Cluster 1, Cluster 2 and Cluster 3 obtained are shown in Fig. 18(b), Fig. 18(c) and Fig. 18(d) respectively.

In Fig. 19(a), segmentation is applied and Fig. 19(b) and Fig. 19(c) shows respectively the cluster plot and the plot of error estimation, that is, the plot of residuals.

Moving in similar way as in the *Subsection-8* and choosing same $z = \frac{(x - 127.5)}{74.05}$, we have

$$y = -1091 \times z^9 + 2695 \times z^8 + 6434 \times z^7 - 1.445 \times 10^4 \times z^6 - 1.263 \times 10^4 \times z^5 + 2.43 \times 10^4 \times z^4 + 7715 \times z^3 - 1.487 \times 10^4 \times z^2 + 1595 \times z + 5292$$

$R^2 = 0.6213$, and Norm of Residuals $= 2.828 \times 10^4$

TABLE II: Data Statistics for Fig. 18(b)

	X	Y
min	0	0
max	255	3.308×10^4
mean	127.5	2668
median	127.5	2075
mode	0	0
std deviation	74.05	2878
range	255	3.308×10^4

11 Morphological Segmentation

In this subsection, known morphological segmentation technique is applied on X-Rays. Three morphological openings are used. The morphological opening with structuring element of disk shaped with three different radius are shown in Fig. 20(a), Fig. 20(c) and Fig. 21(a). The background approximation images of X-Ray obtained after subtracting from the original image are shown in Fig. 20(b), Fig. 20(d) and Fig. 21(b).

12 Dehazing Algorithm

In Fig. 22(a), the original Fig. 2(a) X-Ray is inverted and the low-light areas and focused and the new X-Ray is obtained. The hazing obtained in Fig.22(a) is reduced by hazing reduction algorithm.

On the new X-Ray of Fig.22(b), dehazing algorithm is applied and its result is in Fig.22(c,d). Fig. 23[a-d] has four more such combinations on which dehazing algorithm is implemented.

(a) Day 0, Lateral

(b) Day 0, Posterior to Anterior

(c) Day 3, Posterior to Anterior

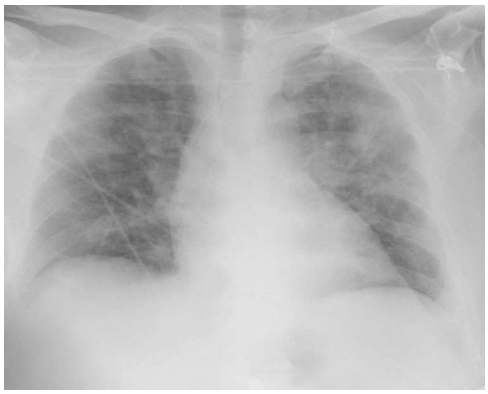

(d) Day 4, Posterior to Anterior

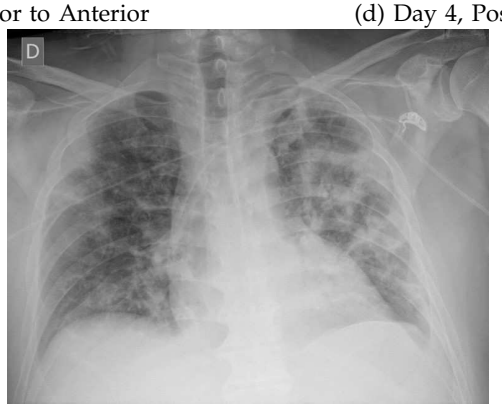

(e) Day 6, Posterior to Anterior

Fig. 1: Original X-Rays from [1]

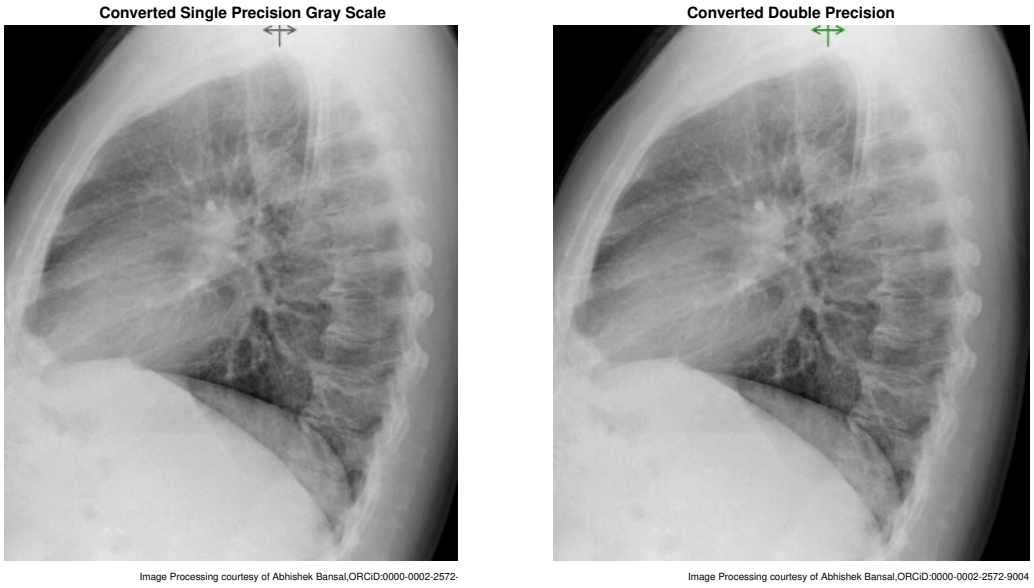

(a) Single Precision (b) Double Precision

Fig. 2: Converted to Single Precision & Double Precision

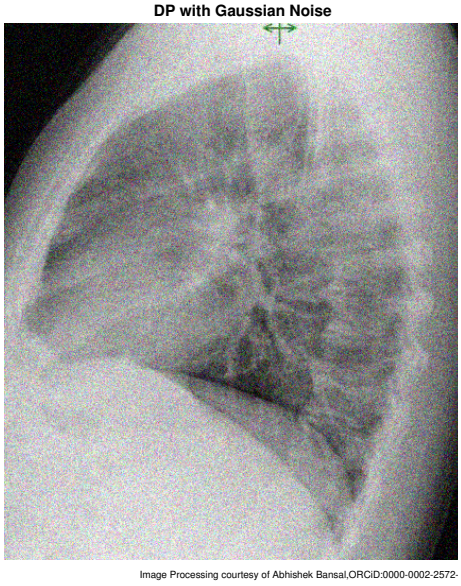

(a) Gaussian Noise

(b) Poisson Noise

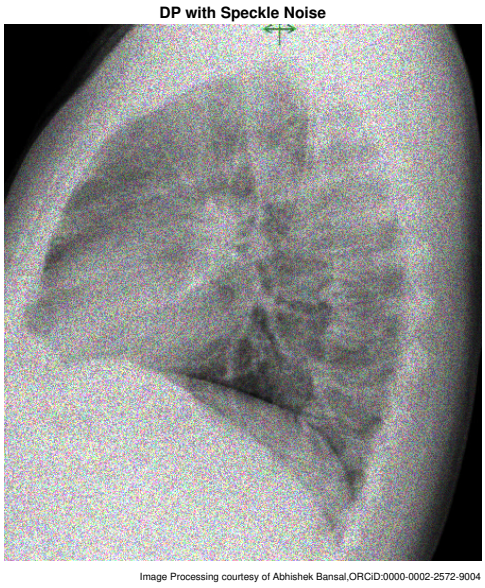

(c) Speckle Noise

Fig. 3: Noises Added to Double Precision

(a) Sobel Method

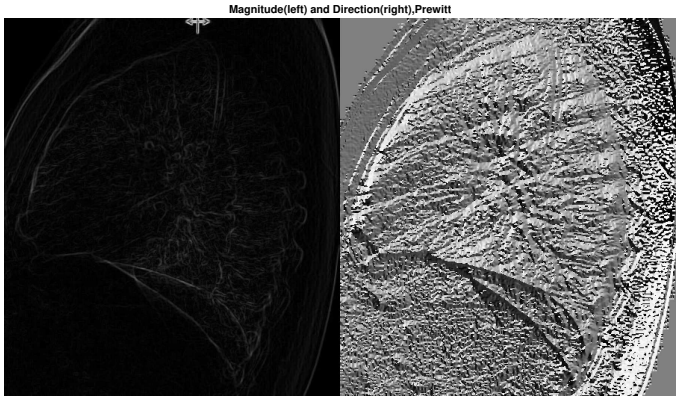

(b) Prewitt Method

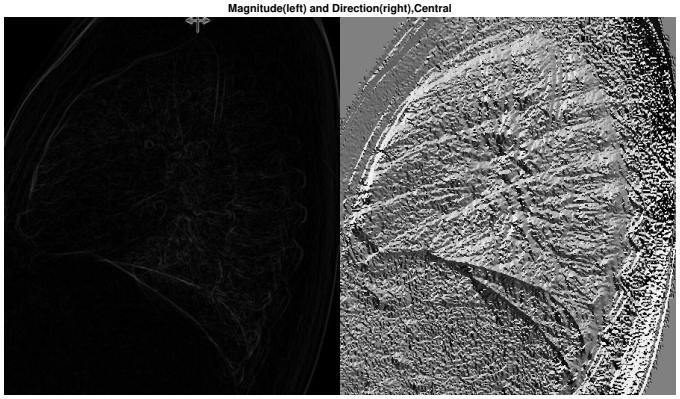

(c) Central Difference

(d) Intermediate Difference

Fig. 4: X-Ray Gradient Magnitude and Direction

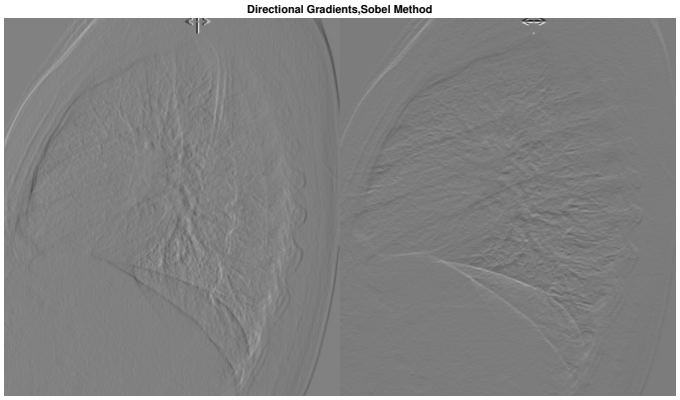

(a) Sobel Method

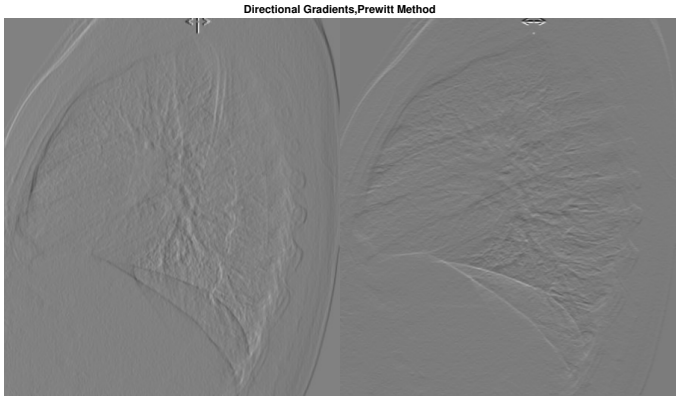

(b) Prewitt Method

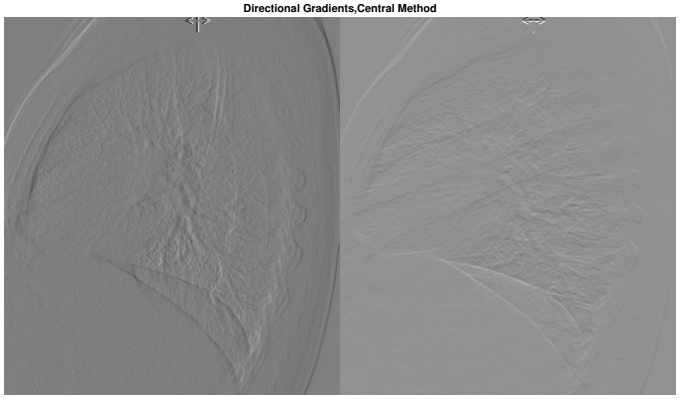

(c) Central Difference

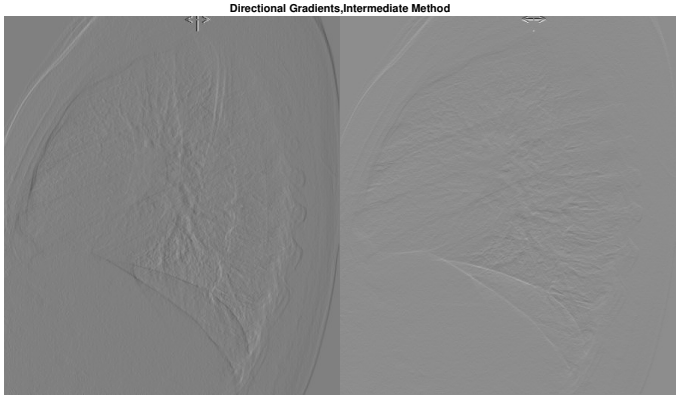

(d) Intermediate Difference

Fig. 5: Directional Gradients

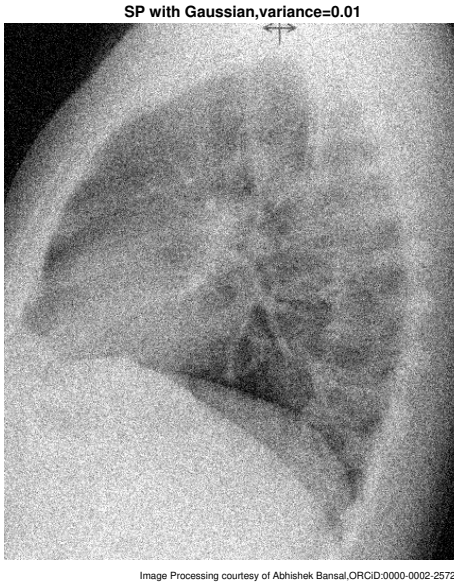

(a) Gaussian Variance = 0.01

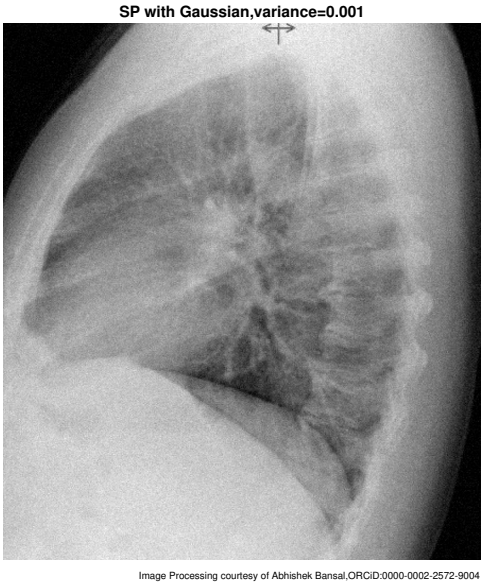

(b) Gaussian Variance = 0.001

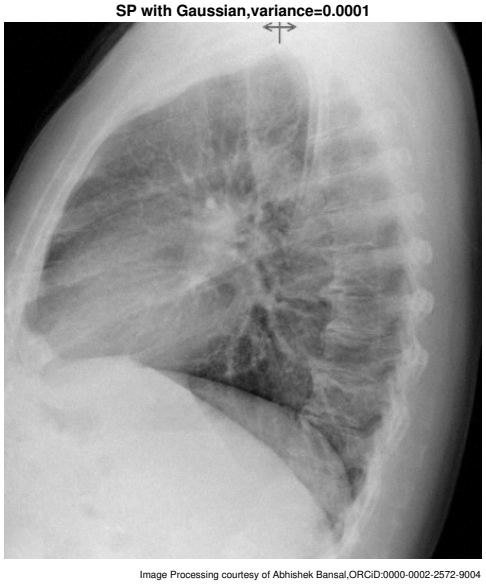

(c) Gaussian Variance = 0.0001

Fig. 6: Gaussian White Noise added to Image

(a) Gaussian Variance = 0.01

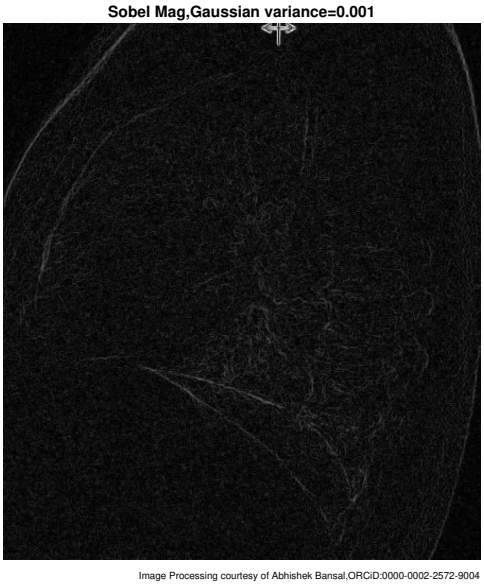

(b) Gaussian Variance = 0.001

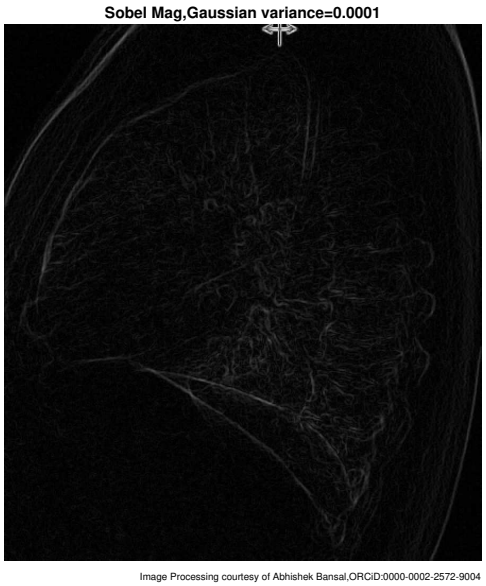

(c) Gaussian Variance = 0.0001

Fig. 7: Gradient of Noisy X-Ray using Sobel Method

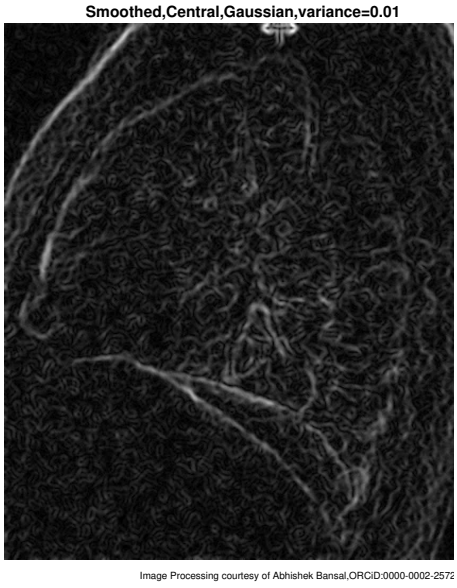

(a) Gaussian Variance = 0.01

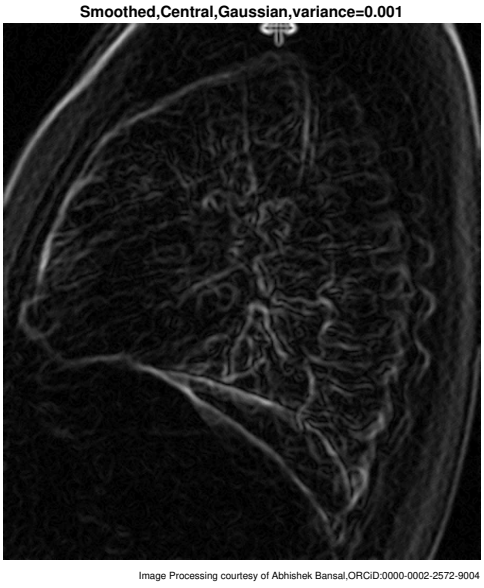

(b) Gaussian Variance = 0.001

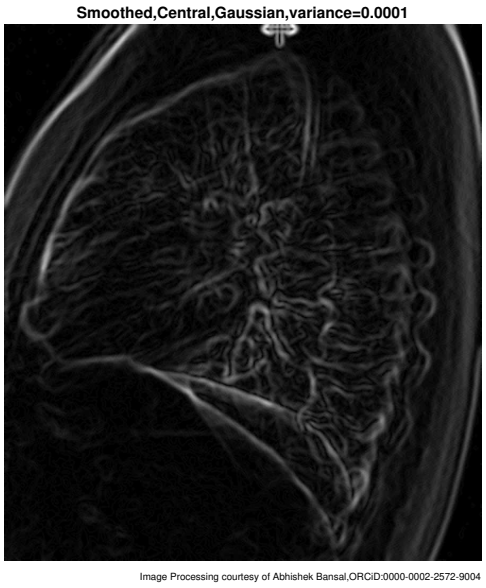

(c) Gaussian Variance = 0.0001

Fig. 8: Gaussian smoothing & central difference gradient

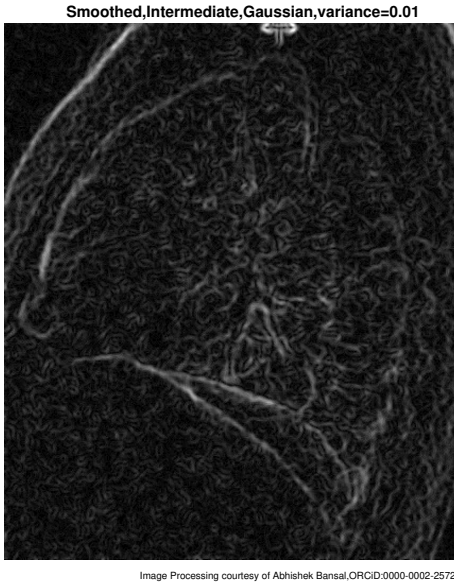

(a) Gaussian Variance = 0.01

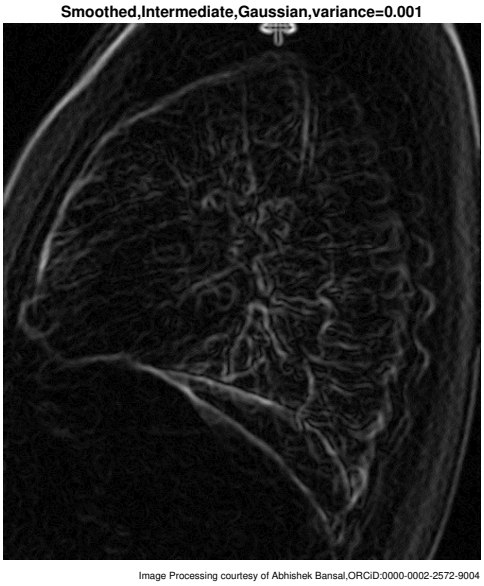

(b) Gaussian Variance = 0.001

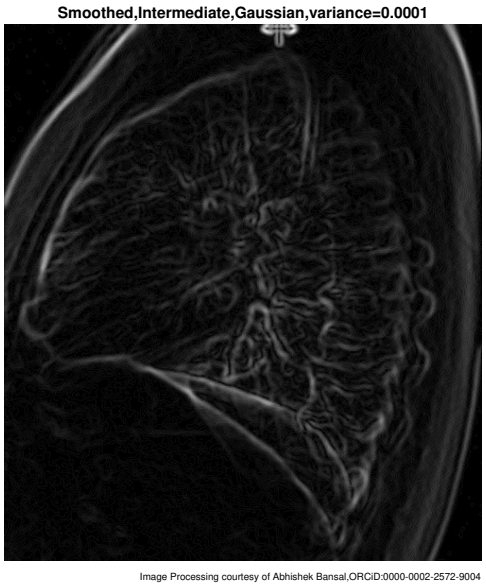

(c) Gaussian Variance = 0.0001

Fig. 9: Gaussian smoothing & intermediate difference gradient

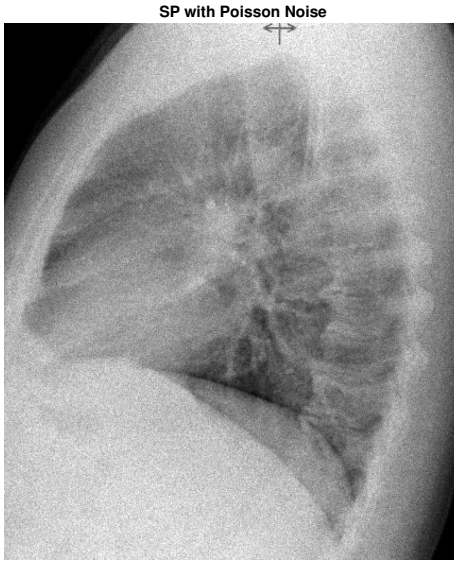

(a) Poisson Noise added

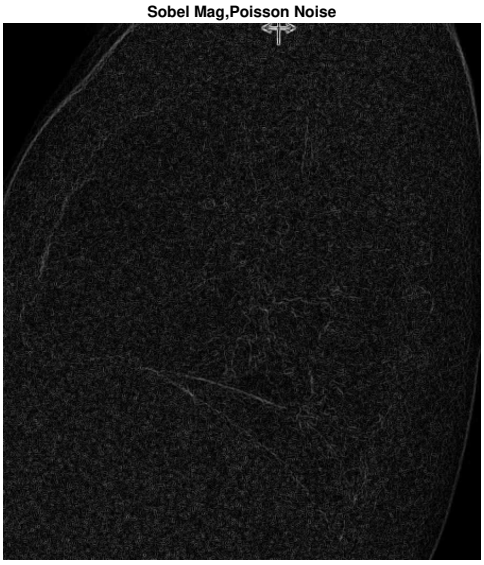

(b) Sobel Gradient Magnitude

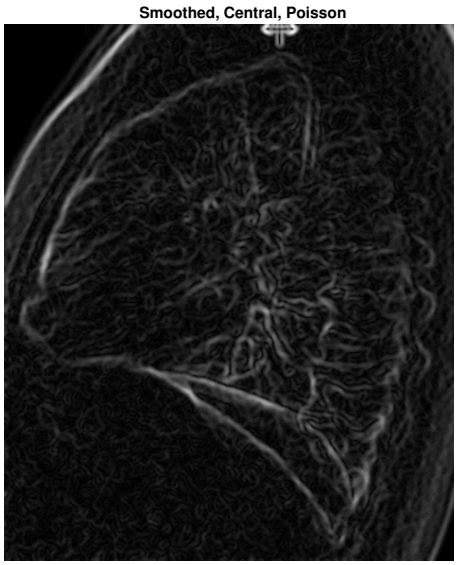

(c) Smoothed by Central Difference

(d) Smoothed by Intermediate Difference

Fig. 10: Poisson Noise & Gradient Magnitude

(a) Speckle Variance = 0.05

(b) Speckle Variance = 0.01

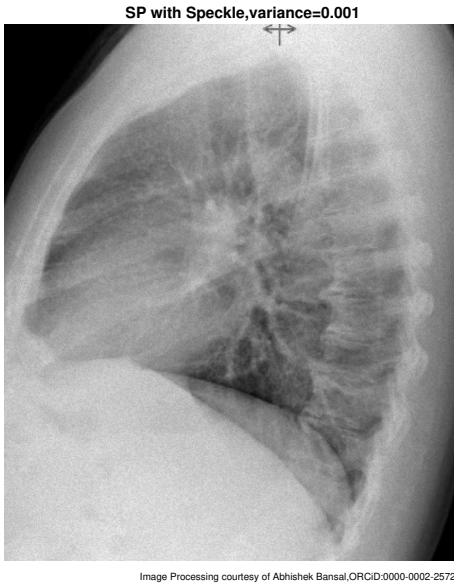

(c) Speckle Variance = 0.001

(d) Speckle Variance = 0.1

Fig. 11: Speckle Noise added to Image

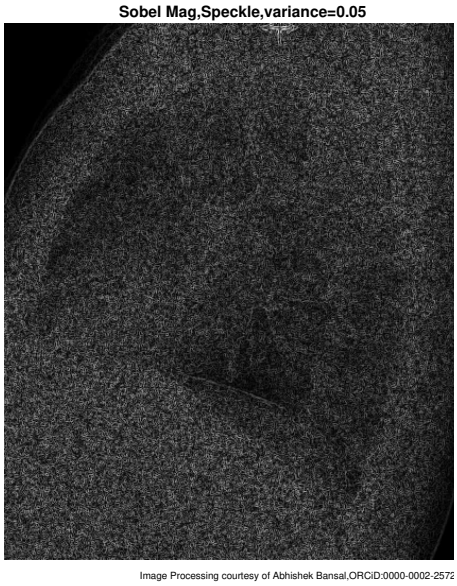

(a) Speckle Variance = 0.05

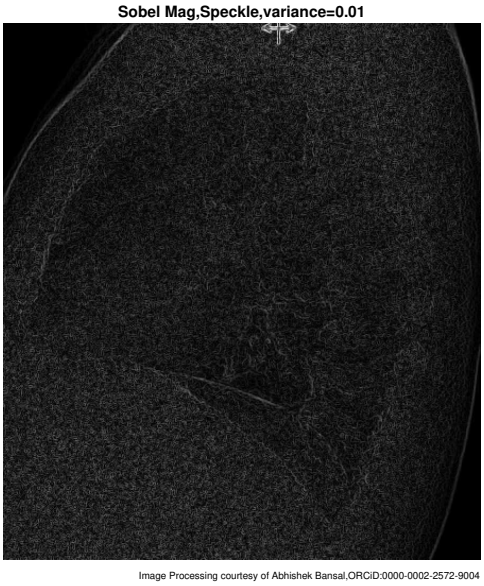

(b) Speckle Variance = 0.01

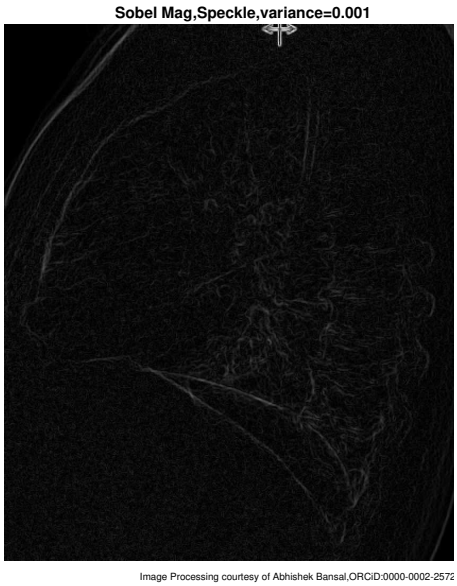

(c) Speckle Variance = 0.001

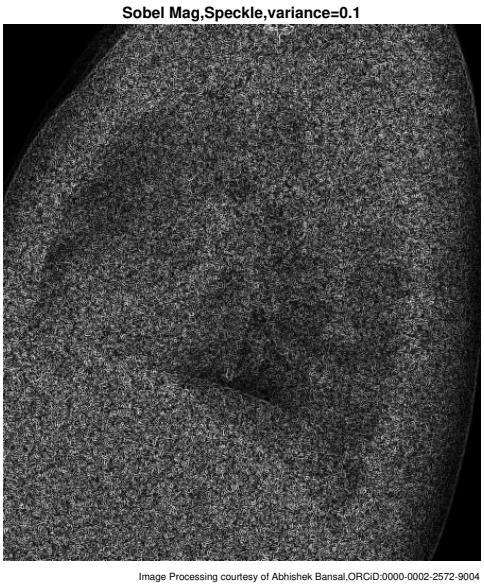

(d) Speckle Variance = 0.1

Fig. 12: Gradient of Noisy X-Ray using Sobel Method

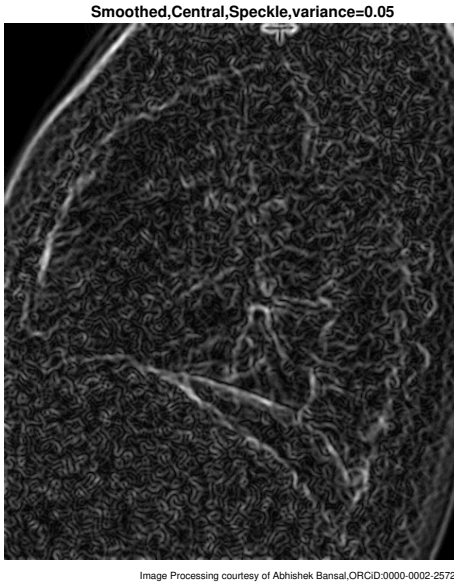

(a) Speckle Variance = 0.05

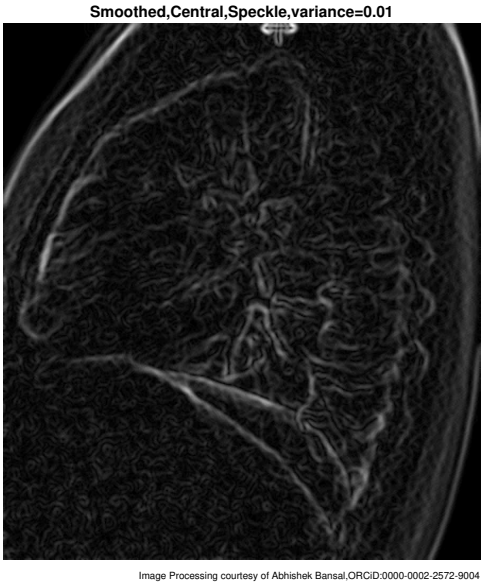

(b) Speckle Variance = 0.01

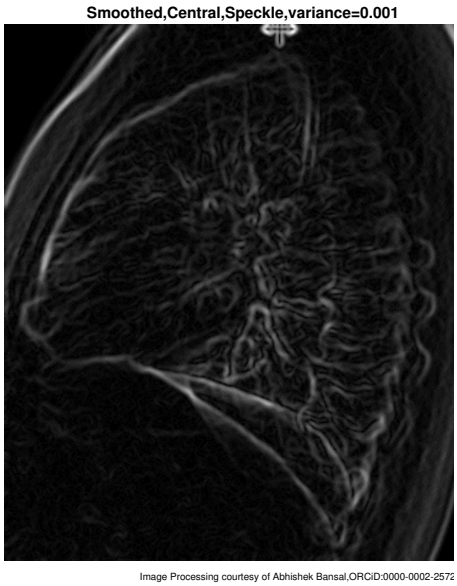

(c) Speckle Variance = 0.001

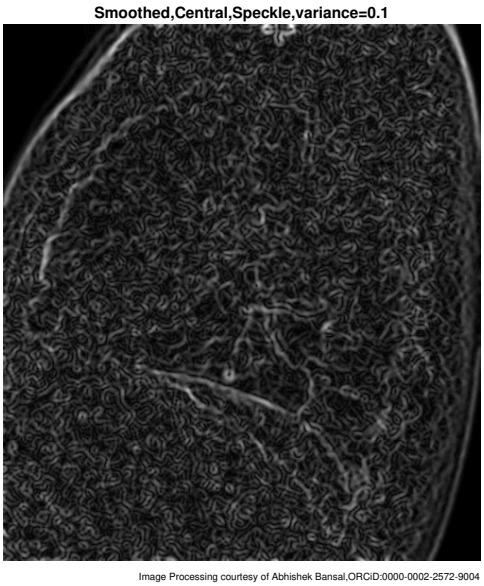

(d) Speckle Variance = 0.1

Fig. 13: Gaussian smoothing & central difference gradient

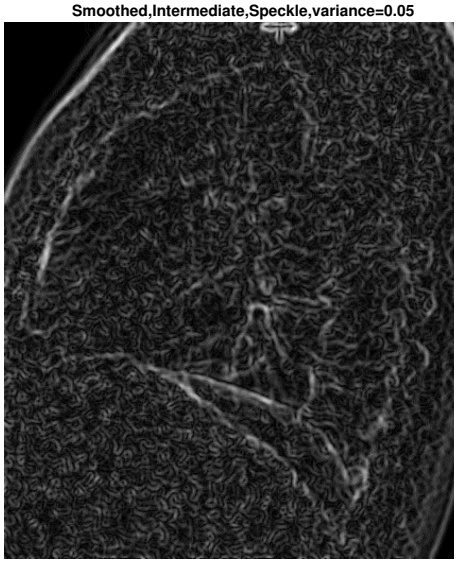

(a) Speckle Variance = 0.05

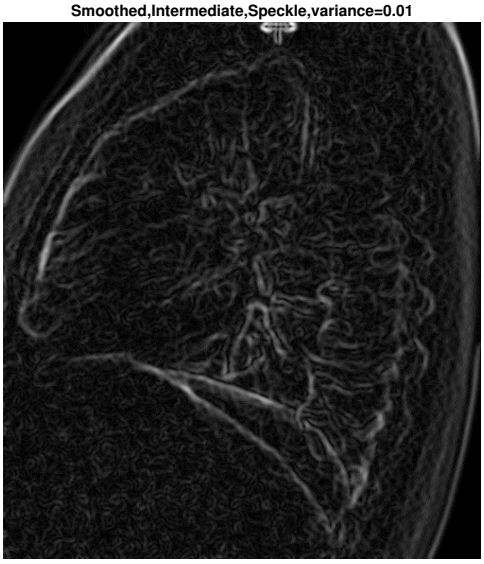

(b) Speckle Variance = 0.01

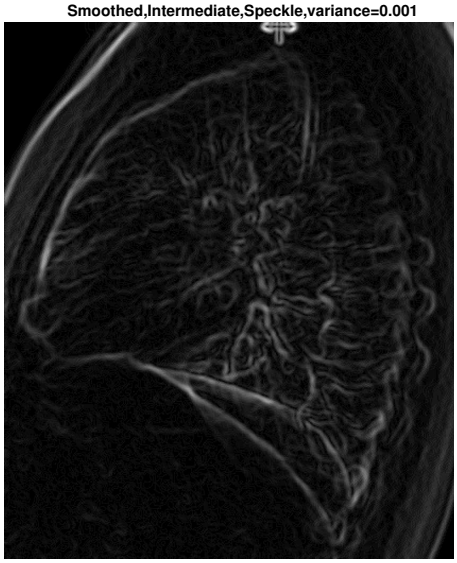

(c) Speckle Variance = 0.001

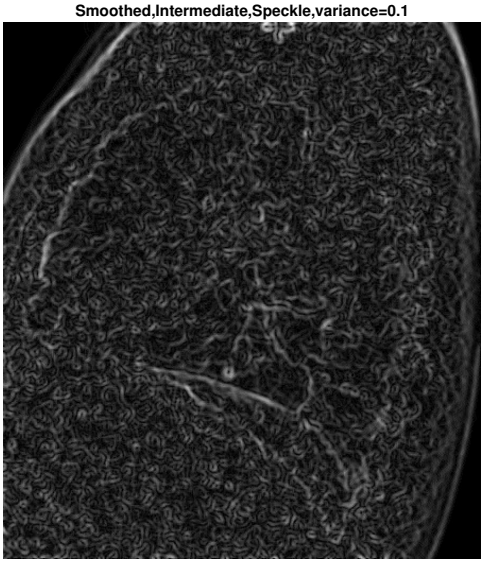

(d) Speckle Variance = 0.1

Fig. 14: Gaussian smoothing & intermediate difference gradient

(a) X-Ray Contrast Improved

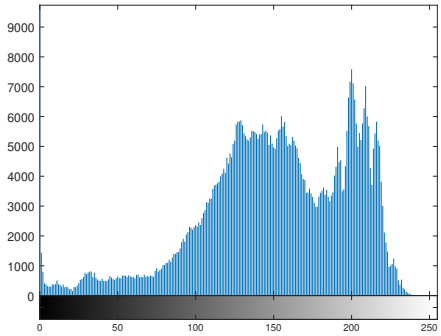

(b) Distribution of Pixel Intensities

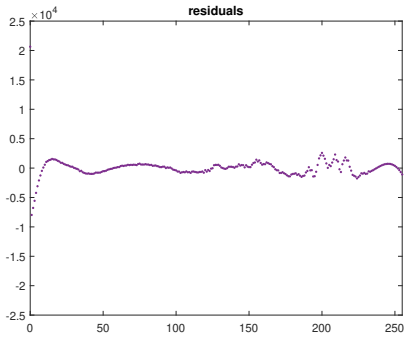

(c) Error Estimation Plot

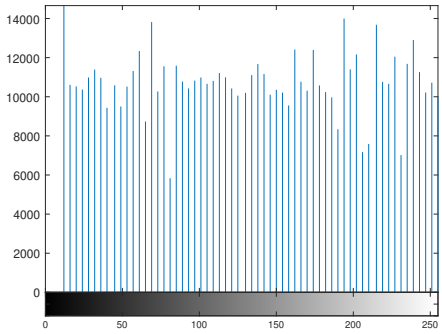

(d) X-Ray Histogram Equalization

Fig. 15: Distribution of Pixel Intensities in X-Ray

(a) X-Ray Contrast Improved 2

(b) X-Ray Contrast Improved 3

(c) X-Ray Contrast Improved 4

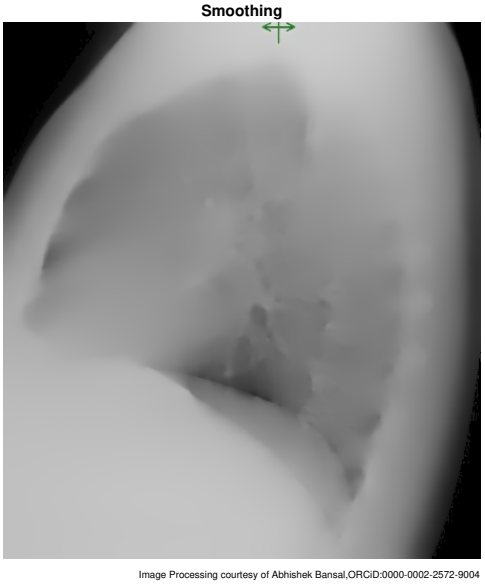

(d) X-Ray Contrast Improved & Smoothed

Fig. 16: X-Ray Contrast Improved with Five Local Luminances

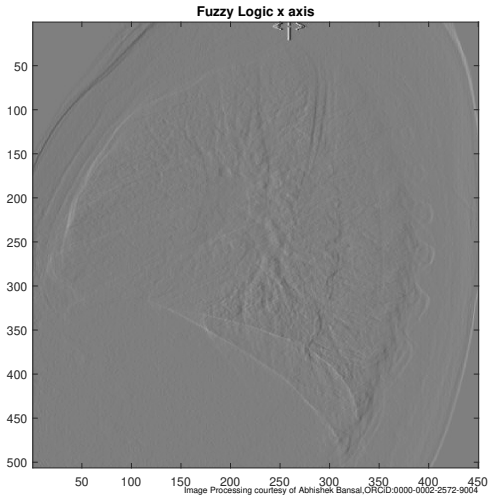

(a) x axis

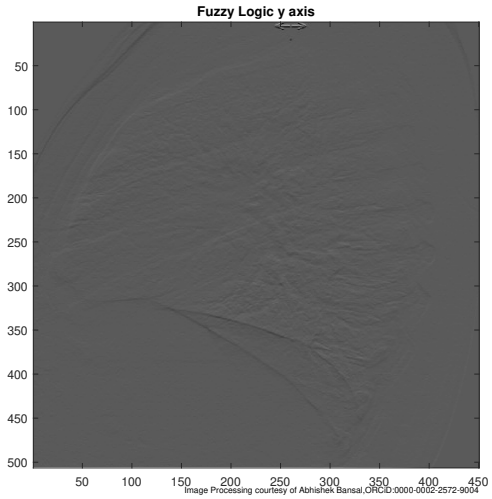

(b) y axis

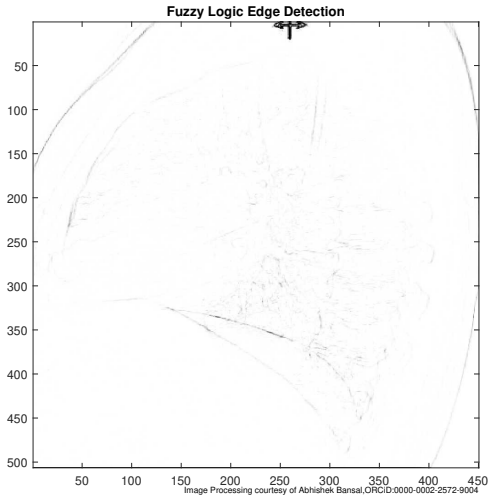

(c) Edge Detection

Fig. 17: Fuzzy Logic

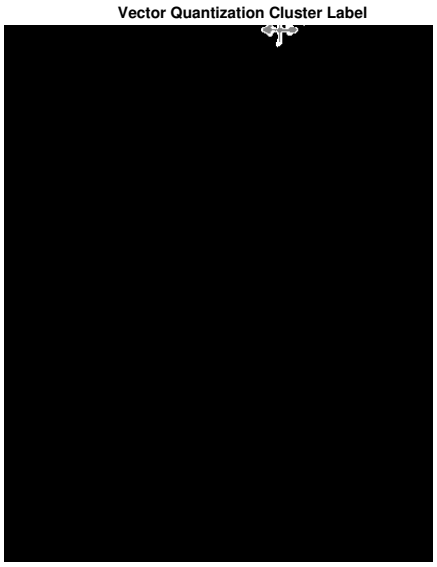

(a) Vector Quantization Cluster Lab

(b) Cluster 1

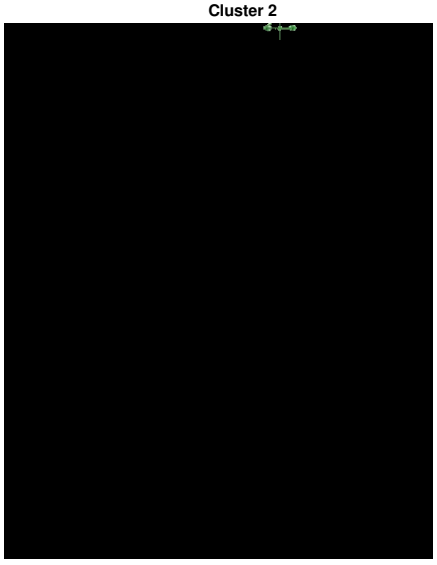

(c) Cluster 2

(d) Cluster 3

Fig. 18: Vector Quantization,K-means Clustering

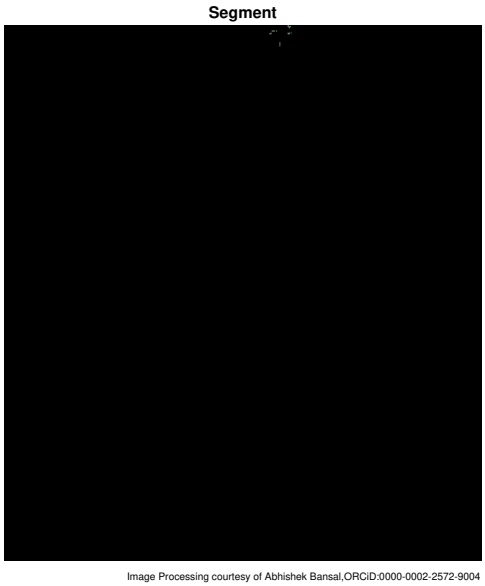

(a) Segmentation

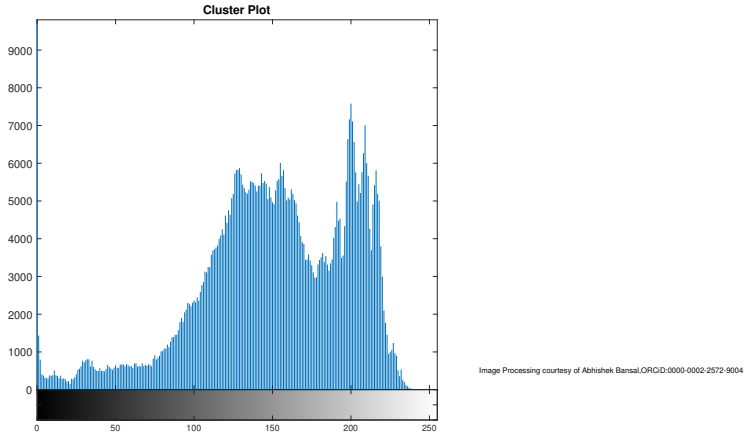

(b) Cluster Plot

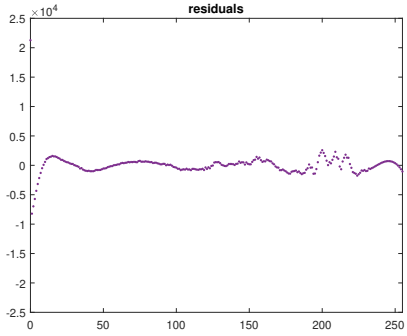

(c) Cluster Plot Residuals

Fig. 19: Clustering Plot and Segment

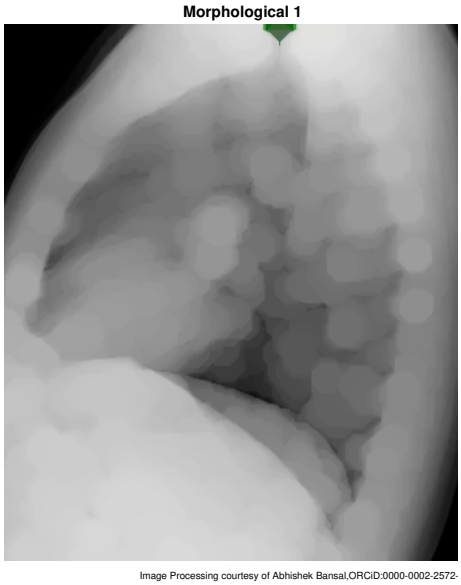

(a) Morphological Opening 1

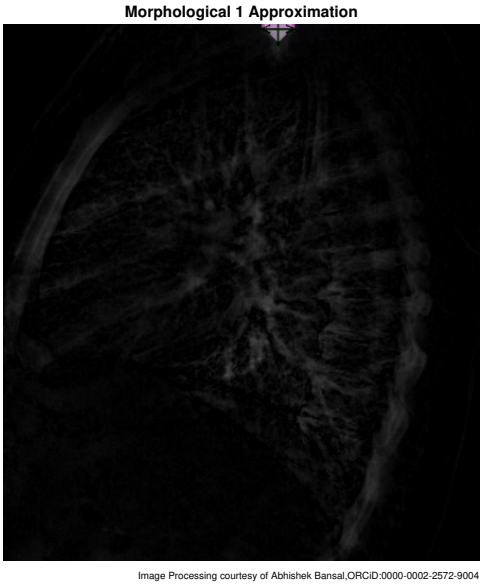

(b) Background Approximation Removed from Fig. 19(a)

(c) [Morphological Opening 2

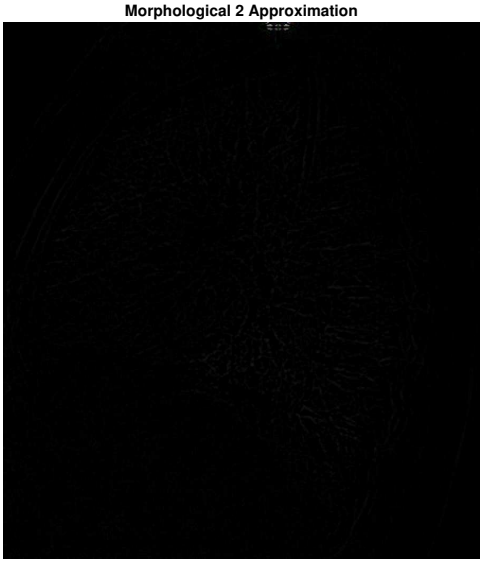

(d) Background Approximation Removed from Fig. 19(c)

Fig. 20: Morphological Segmentation

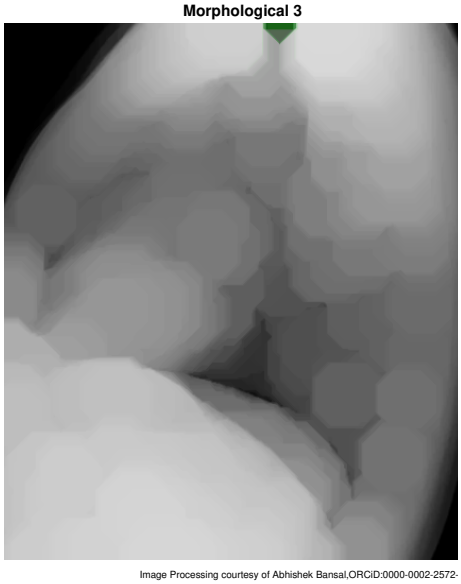

(a) Morphological Opening 3

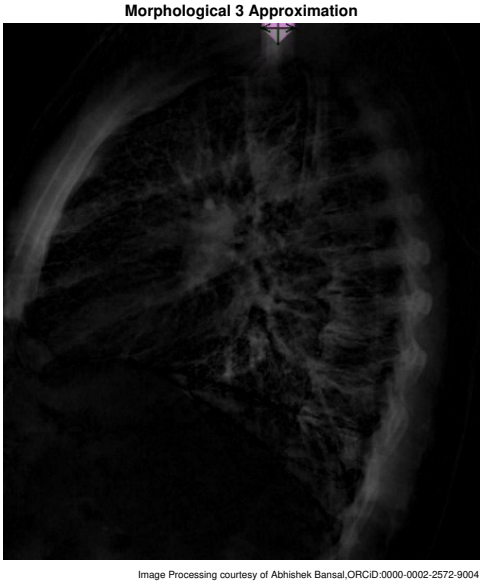

(b) Background Approximation Removed from Fig. 20(a)

Fig. 21: Morphological Segmentation

(a) X-Ray Inverted & Illuminated

(b) Hazing Reduction Algorithm

(c) Dehazing Algorithm

(d) Dehazing Algorithm

Fig. 22: Dehazing Algorithm

(a) Dehazing Algorithm

(b) Dehazing Algorithm

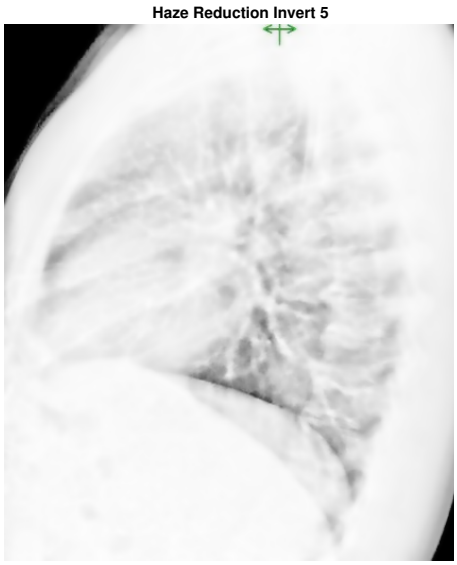

(c) Dehazing Algorithm

(d) Dehazing Algorithm

Fig. 23: Dehazing Algorithm

IV Results : Day 0, PA

1 X-Ray Converted

In this subsection, X-Ray(PA) of Day 0 is converted to single precision grayscale and double precision,on which all further image processings will be done. These are shown in Fig. 24.

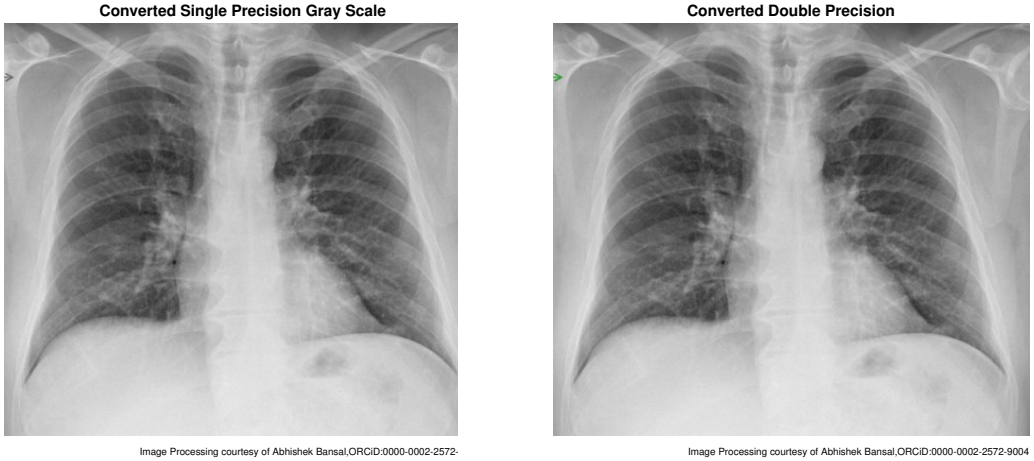

(a) Single Precision (b) Double Precision

Fig. 24: Converted to Single Precision & Double Precision

2 Double Precision Noise Addition

In this subsection, the double precision X-Ray of Day 0 (Fig 24(b)) of the previous subsection is subjected to noises namely Gaussian with variance 0.01, Poisson Noise and speckle noise with variance 0.05. These are shown in Fig. 25.

3 Gradient Magnitude and Direction

In this subsection, the gradient of the single precision X-Ray of Day 0 (Fig 24(a)) is obtained and its magnitude and direction is plotted using methods of Sobel, Prewitt, central difference and intermediate difference. These are shown in Fig. 26.

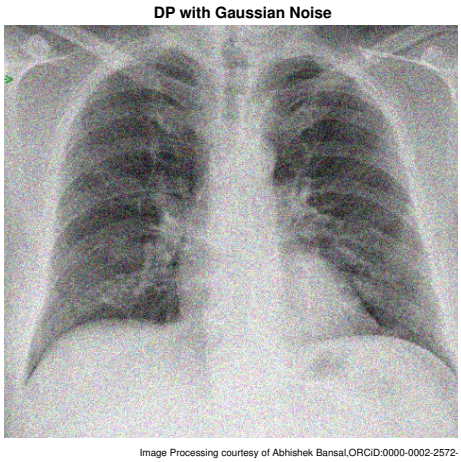

(a) Gaussian Noise

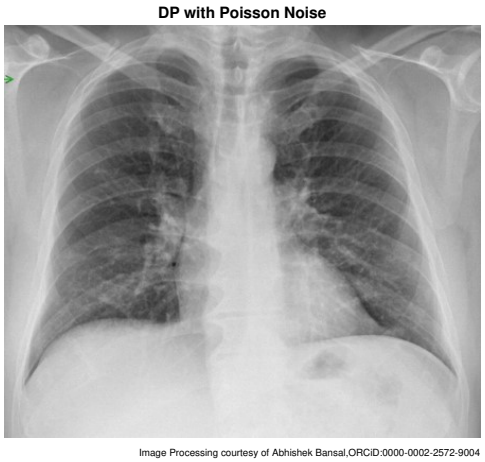

(b) Poisson Noise

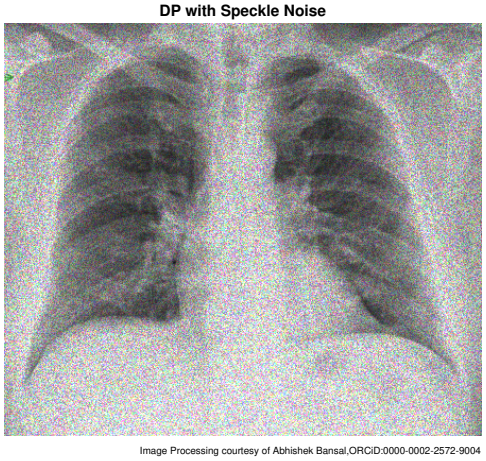

(c) Speckle Noise

Fig. 25: Noises Added to Double Precision

4 *Directional Gradients*

In this subsection, the directional gradient of the single precision X-Ray of Day 0 (Fig 24(a)) is plotted using methods of Sobel, Prewitt, central difference and intermediate difference. These are shown in Fig. 27.

5 Gaussian Noises & Sobel Gradient

In this subsection, the single precision X-Ray of Day 0 (Fig 24(a)) is subjected to Gaussian noise with three variances of 0.01, 0.001 and 0.0001. These are shown in Fig. 28. The gradient magnitude of these noisy X-Rays are plotted using Sobel method, which are shown in Fig. 29. The figures of gradient magnitude of Fig. 29 are further smoothed using 2-D Gaussian smoothing. The Gaussian smoothing and central difference gradient are shown in Fig. 30. The Gaussian smoothing and intermediate difference gradient are shown in Fig. 31.

6 Poisson Noise & Sobel Gradient

In this subsection, the single precision X-Ray of Day 0 (Fig 24(a)) is subjected to Poisson Noise,Fig. 32(a). The gradient magnitude of Poisson noise X-Ray is plotted using Sobel method, which are shown in Fig. 32(b). This is further smoothed using 2-D Gaussian smoothing and central difference gradient in Fig. 32(c); and 2-D Gaussian smoothing and intermediate difference gradient in Fig. 32(d).

7 Speckle Noise & Sobel Gradient

In this subsection, the single precision X-Ray of Day 0 (Fig 24(a)) is subjected to Speckle noise with four variances of 0.05, 0.01, 0.001 and 0.1. These are shown in Fig. 33[a-d]. The gradient magnitude of these noisy X-Rays are plotted using Sobel method, which are shown in Fig. 34. These are further smoothed using 2-D Gaussian smoothing. The Gaussian smoothing and central difference gradient are shown in Fig. 35. The Gaussian smoothing and intermediate difference gradient are shown in Fig. 36.

8 Pixel Intensities & Contrast

In this subsection, the original X-Ray (without converting to single precision or double precision) is contrasted for study and analysis.

Let the center fit $z = \frac{(x - 127.5)}{74.05}$, then from polynomial regression

$y = 68.38 \times z^9 + 79.92 \times z^8 + 508.3 \times z^7 + 211.7 \times z^6 - 3969 \times z^5 - 2424 \times z^4 + 5591 \times z^3 + 2489 \times z^2 + 45.89 \times z + 2385$

Let $\bar{y}$ be the mean of y, $\hat{y}$ the calculated values of y, then the coefficient of determination, $R^2 = 1 - \frac{\sum_{i=1}^{n}(y_i - \hat{y})^2}{\sum_{i=1}^{n}(y_i - \bar{y})^2} = 0.9428$

The measure of the goodness of fit given by norm of residuals is 6536. Here, the polynomial of degree 9 chosen here is the global which can be focused on the areas of interest (to be decided by infection part or researchers/doctors interest) and separate equations can be obtained for each particular area of interest. This gives insight in mathematical formulation and has been used in the Novel $\mathcal{B}$-Mathematical Modeling of Respiratory System.

The Fig.37(a) shows that X-Ray contrast is improved for analysis when compared with Fig. 1(a). Fig. 37(b) shows the distribution of X-Ray pixel intensities. Fig. 37(c) shows the error estimation plot, which is the plot of the residuals. Fig. 37(d) shows the X-Ray histogram equalization which is the spreading of the intensity values over the full range.

In Fig. 38, X-Ray Contrast is improved with five local luminances. The original Fig. 24(a) X-Ray contrast is improved with four more local luminances by varying the

TABLE III: Data Statistics for Fig. 37(b)

	X	Y
min	0	0
max	255	5996
mean	127.5	2051
median	127.5	2257
mode	0	0
std deviation	74.05	1711
range	255	5996

intensity values at low and high intensities. These are shown in Fig 38(a), Fig. 38(b) and Fig. 38(c). In Fig. 38(d), the original Fig. 24(a) X-Ray is contrasted with fifth value of improvement but smoothing technique is applied after it.

9 Fuzzy Logic

In this subsection, the images obtained using fuzzy logic edge-detection algorithm and Fuzzy Inference System (FIS) are given. Two 2-D Convolution are performed. The x-axis of directional gradient is convolved with x-axis gradients of double-precision X-Ray obtained in Fig. 24(b) and the X-Ray gradient of fuzzy logic x-axis is given in Fig. 39(a). The y-axis of directional gradient is convolved with y-axis gradients of double-precision X-Ray obtained in Fig. 24(b) and the X-Ray gradient of fuzzy logic y-axis is given in Fig. 39(b). The edge detection is shown in Fig. 39(c).

10 K-means Clustering

In this subsection, the popular vector quantization technique of K-Means clustering is applied to X-Ray. In this technique, firstly CIE XYZ tristimulus technique is

used to know the color information and thus, the information of luminosity layer 'L*', chromaticity-layer 'a*' and chromaticity-layer 'b*' is obtained. Then every pixel is clustered with its pixel label and partitioned into three clusters. The clustering obtained is shown in Fig. 40(a), Vector Quantization Cluster Label. And three clusters Cluster 1, Cluster 2 and Cluster 3 obtained are shown in Fig. 40(b), Fig. 40(c) and Fig. 40(d) respectively.

In Fig. 41(a), segmentation is applied and Fig. 41(b) and Fig. 41(c) shows respectively the cluster plot and the plot of error estimation, that is, the plot of residuals.

Moving in similar way as in the *Subsection-8* and choosing same $z = \frac{(x - 127.5)}{74.05}$, we have

$y = 60.64 \times z^9 + 87.05 \times z^8 + 551.5 \times z^7 + 176.3 \times z^6 - 4048 \times z^5 - 2370 \times z^4 + 5643 \times z^3 + 2464 \times z^2 + 36.35 \times z + 2386$

$R^2 = 0.9425$ and Norm of Residuals = 6546

TABLE IV: Data Statistics for Fig. 18(b)

	X	Y
min	0	0
max	255	5996
mean	127.5	2051
median	127.5	2256
mode	0	0
std deviation	74.05	1710
range	255	5996

11 Morphological Segmentation

In this subsection, known morphological segmentation technique is applied on X-Rays. Three morphological openings are used. The morphological opening with structuring element of disk shaped with three different radius are shown in Fig. 42(a), Fig. 42(c) and Fig. 43(a). The background approximation images of X-Ray obtained after subtracting from the original image are shown in Fig. 42(b), Fig. 42(d) and Fig. 43(b).

12 Dehazing Algorithm

In Fig. 44(a), the original Fig. 24(a) X-Ray is inverted and the low-light areas and focused and the new X-Ray is obtained. The hazing obtained in Fig. 44(a) is reduced by hazing reduction algorithm.

On the new X-Ray of Fig. 44(b), dehazing algorithm is applied and its result is in Fig. 44(c,d). Fig. 45[a-d] has four more such combinations on which dehazing algorithm is implemented.

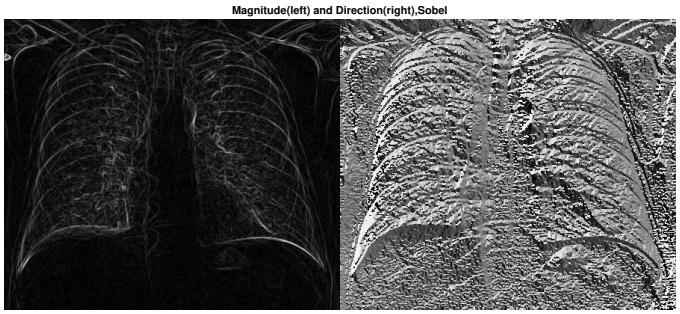

(a) Sobel Method

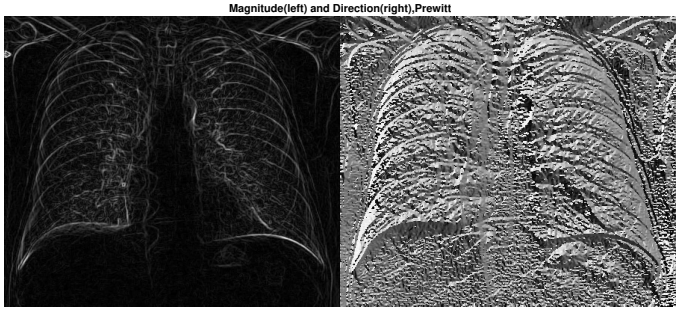

(b) Prewitt Method

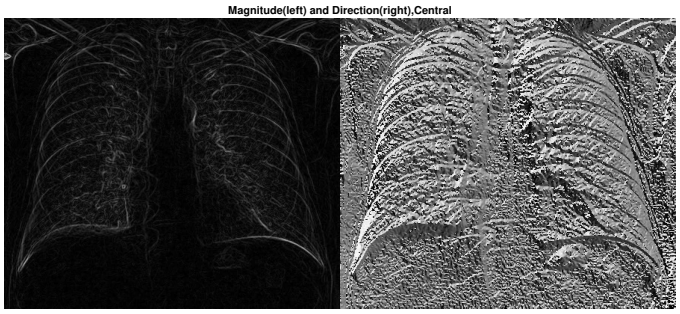

(c) Central Difference

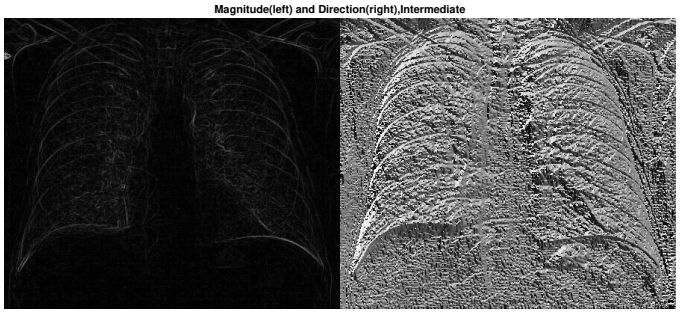

(d) Intermediate Difference

Fig. 26: X-Ray Gradient Magnitude and Direction

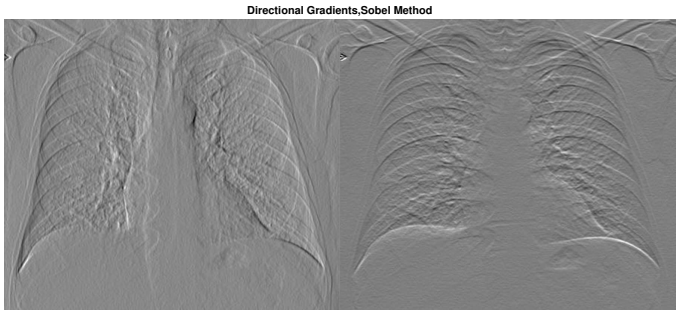

(a) Sobel Method

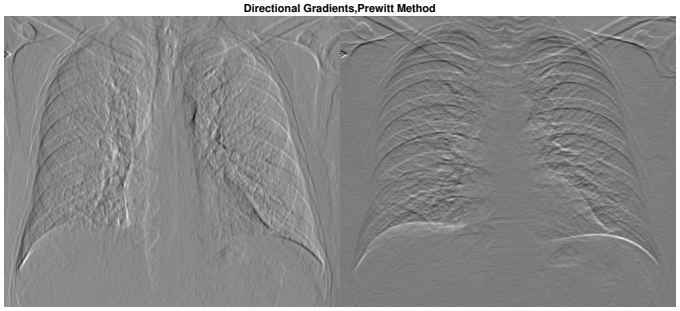

(b) Prewitt Method

(c) Central Difference

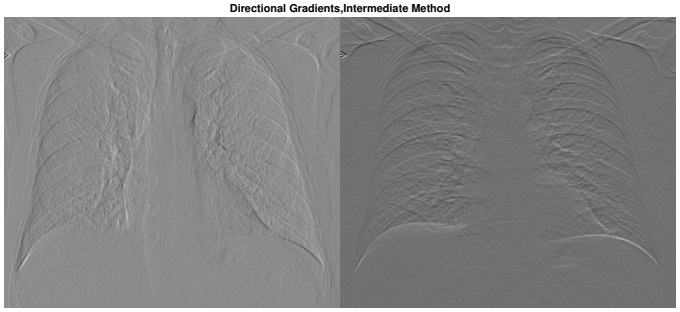

(d) Intermediate Difference

Fig. 27: Directional Gradients

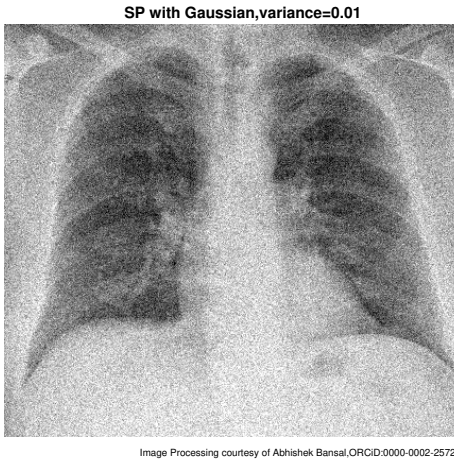

(a) Gaussian Variance = 0.01

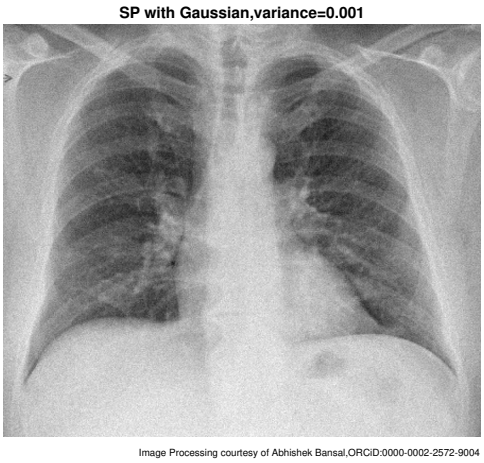

(b) Gaussian Variance = 0.001

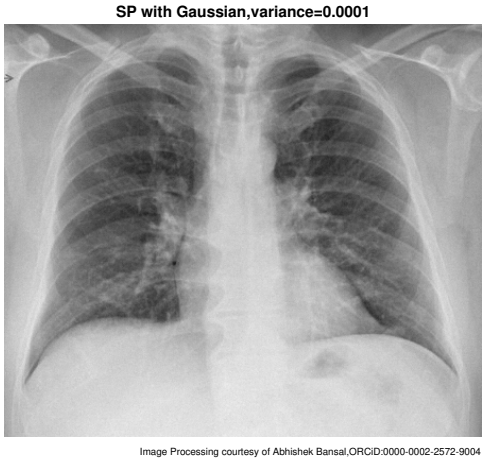

(c) Gaussian Variance = 0.0001

Fig. 28: Gaussian White Noise added to Image

(a) Gaussian Variance = 0.01

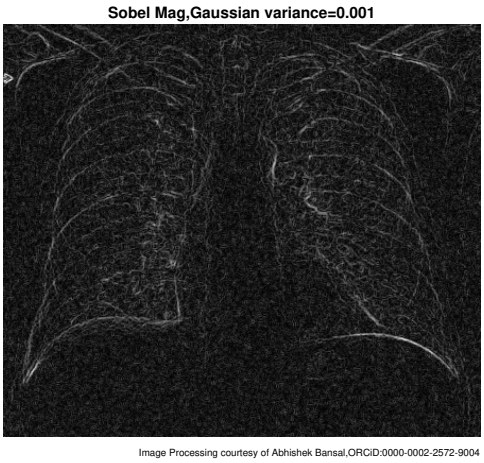

(b) Gaussian Variance = 0.001

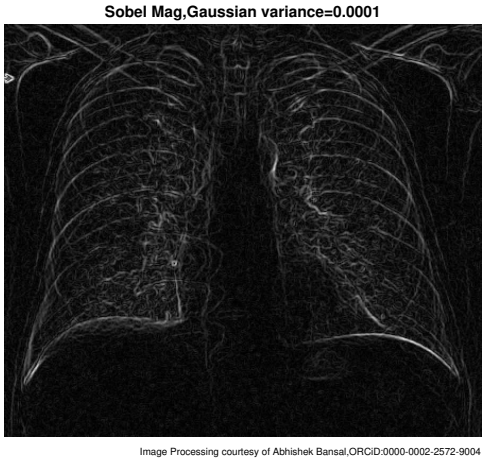

(c) Gaussian Variance = 0.0001

Fig. 29: Gradient of Noisy X-Ray using Sobel Method

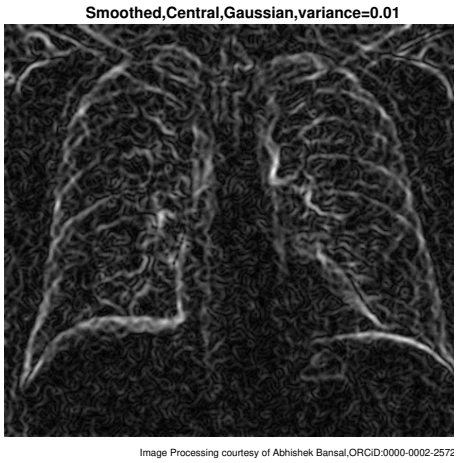

(a) Gaussian Variance = 0.01

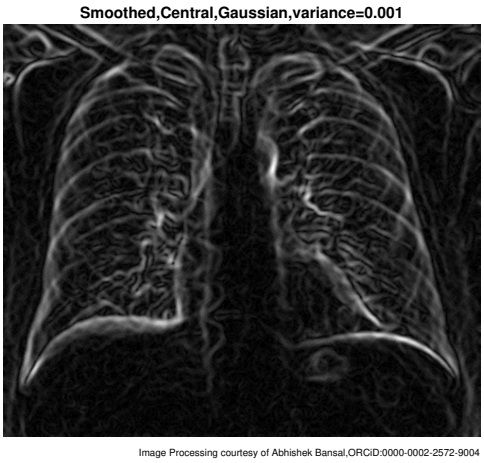

(b) Gaussian Variance = 0.001

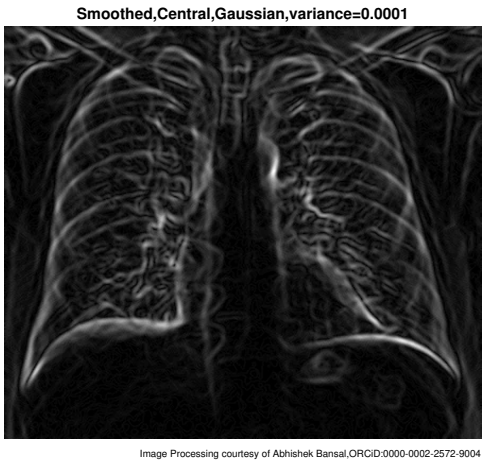

(c) Gaussian Variance = 0.0001

Fig. 30: Gaussian smoothing & central difference gradient

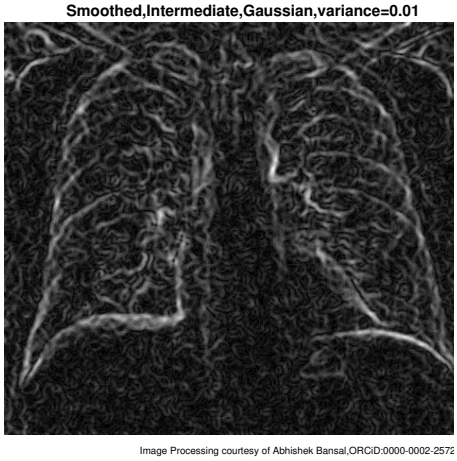

(a) Gaussian Variance = 0.01

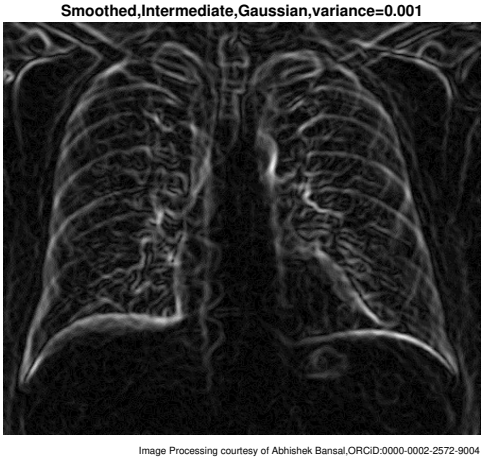

(b) Gaussian Variance = 0.001

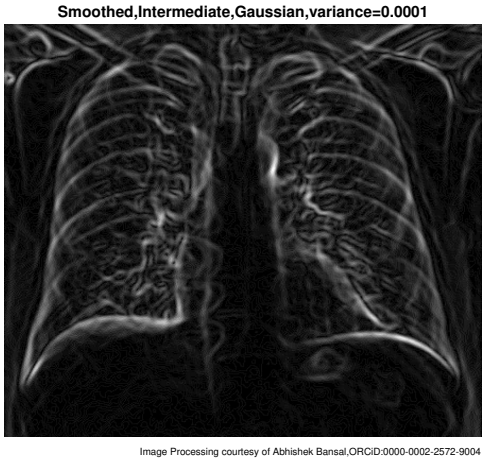

(c) Gaussian Variance = 0.0001

Fig. 31: Gaussian smoothing & intermediate difference gradient

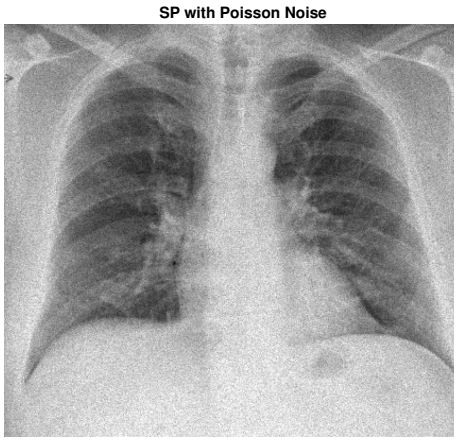

(a) Poisson Noise added

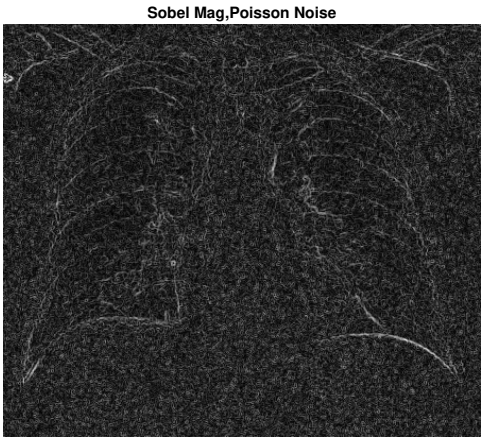

(b) Sobel Gradient Magnitude

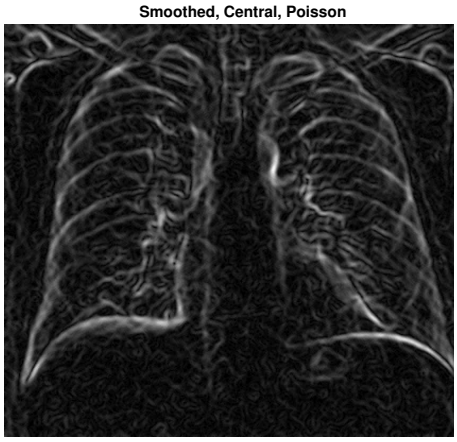

(c) Smoothed by Central Difference

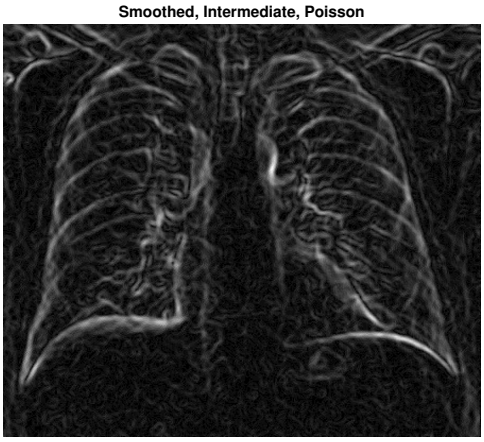

(d) Smoothed by Intermediate Difference

Fig. 32: Poisson Noise & Gradient Magnitude

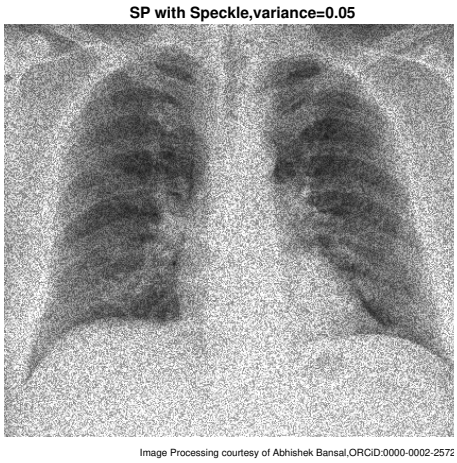

(a) Speckle Variance = 0.05

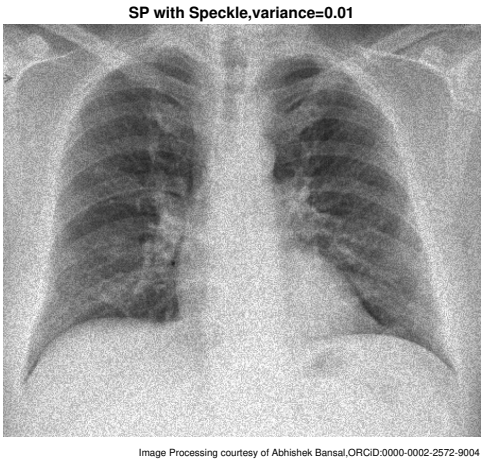

(b) Speckle Variance = 0.01

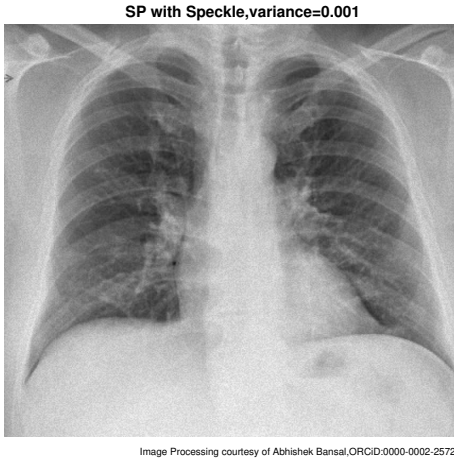

(c) Speckle Variance = 0.001

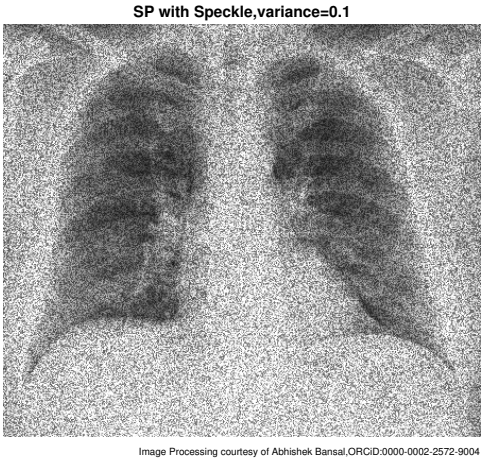

(d) Speckle Variance = 0.1

Fig. 33: Speckle Noise added to Image

(a) Speckle Variance = 0.05

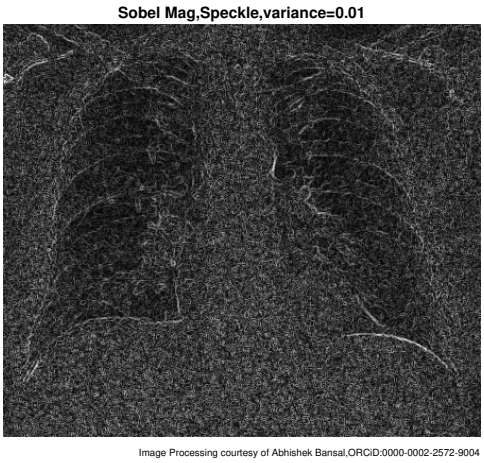

(b) Speckle Variance = 0.01

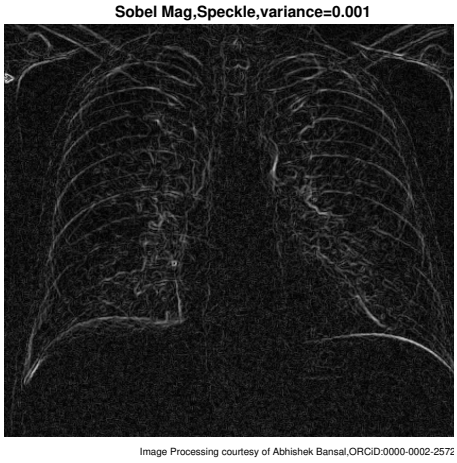

(c) Speckle Variance = 0.001

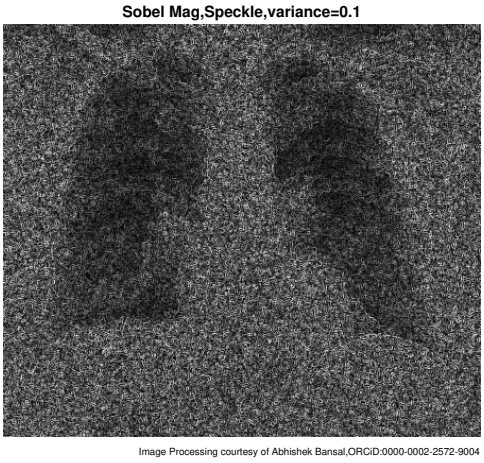

(d) Speckle Variance = 0.1

Fig. 34: Gradient of Noisy X-Ray using Sobel Method

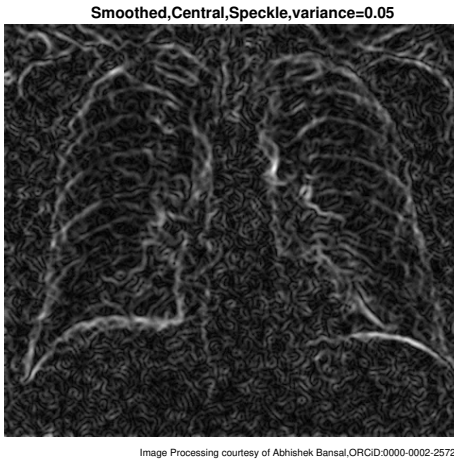

(a) Speckle Variance = 0.05

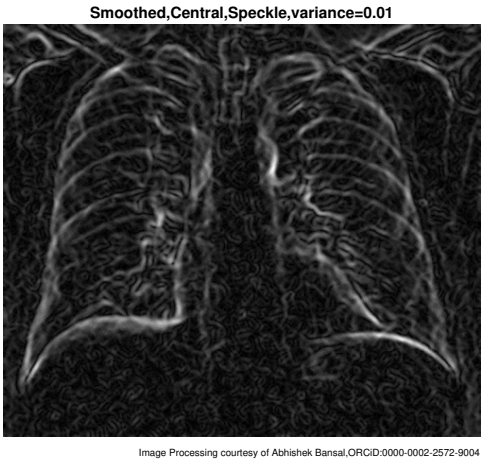

(b) Speckle Variance = 0.01

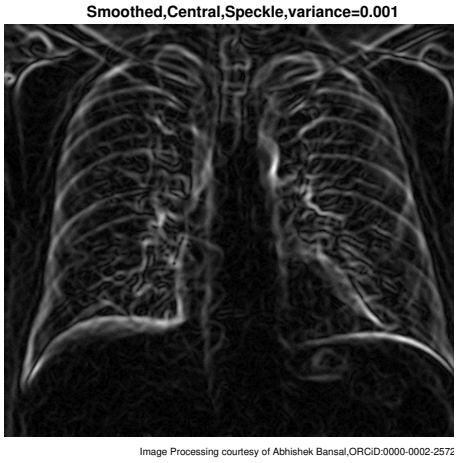

(c) Speckle Variance = 0.001

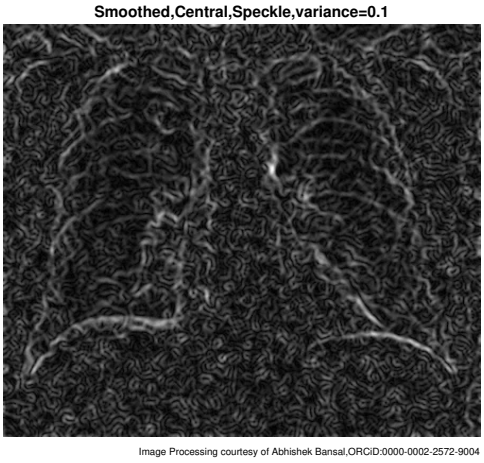

(d) Speckle Variance = 0.1

Fig. 35: Gaussian smoothing & central difference gradient

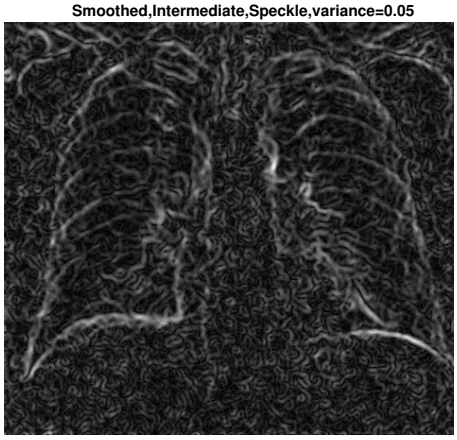

(a) Speckle Variance = 0.05

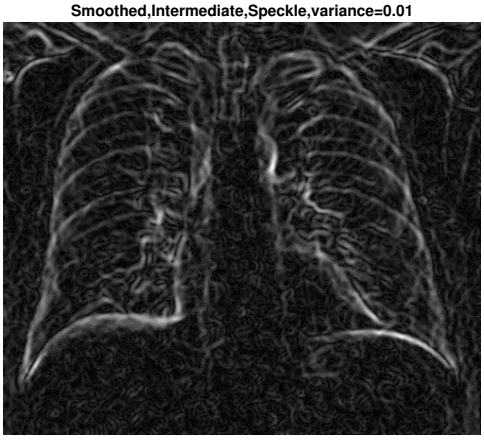

(b) Speckle Variance = 0.01

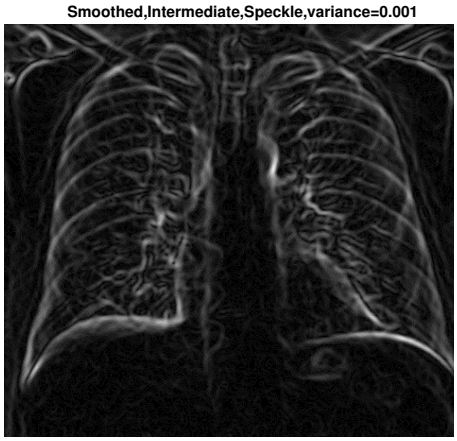

(c) Speckle Variance = 0.001

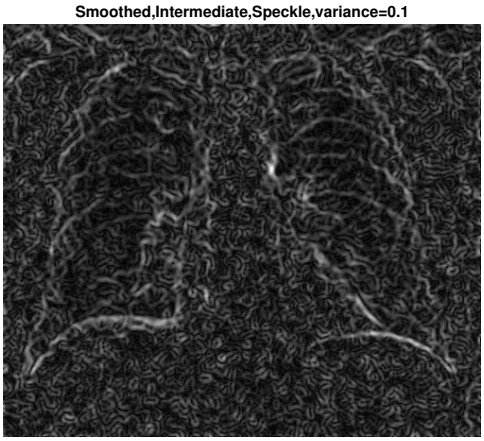

(d) Speckle Variance = 0.1

Fig. 36: Gaussian smoothing & intermediate difference gradient

(a) X-Ray Contrast Improved

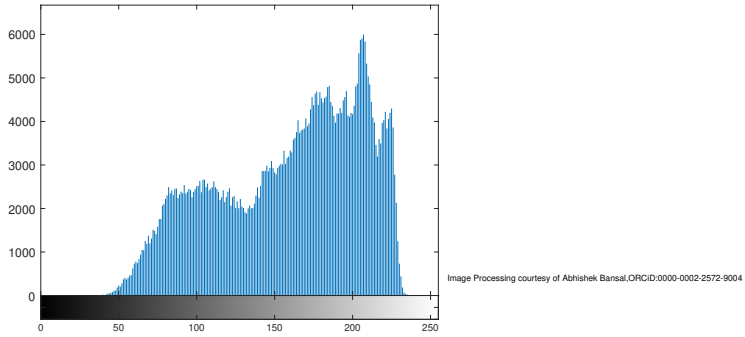

(b) Distribution of Pixel Intensities

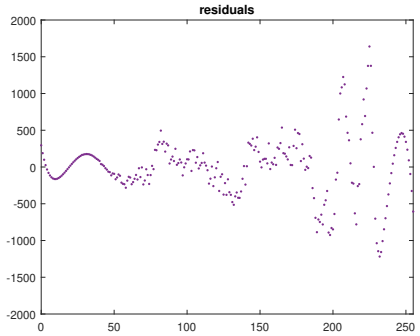

(c) Error Estimation Plot

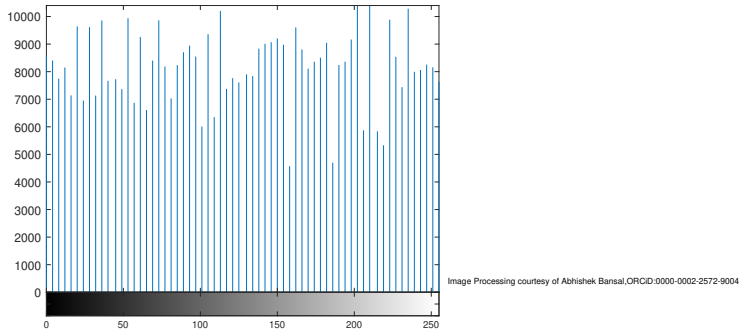

(d) X-Ray Histogram Equalization

Fig. 37: Distribution of Pixel Intensities in X-Ray

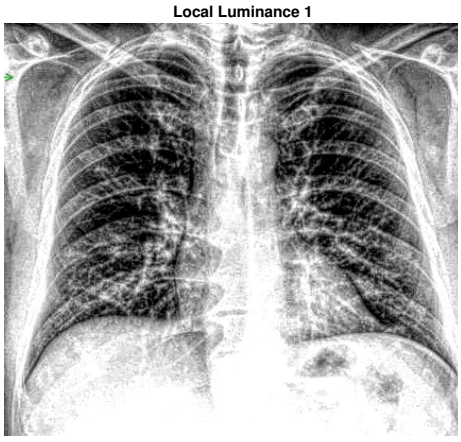

(a) X-Ray Contrast Improved 2

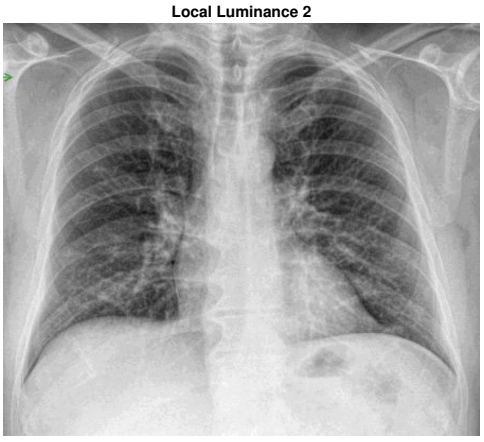

(b) X-Ray Contrast Improved 3

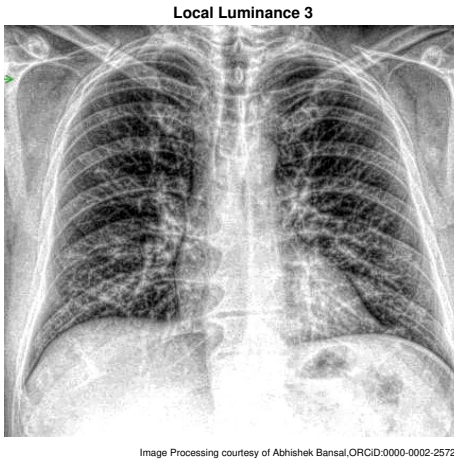

(c) X-Ray Contrast Improved 4

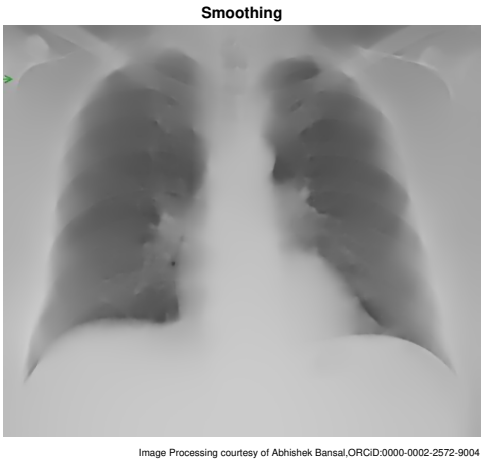

(d) X-Ray Contrast Improved & Smoothed

Fig. 38: X-Ray Contrast Improved with Five Local Luminances

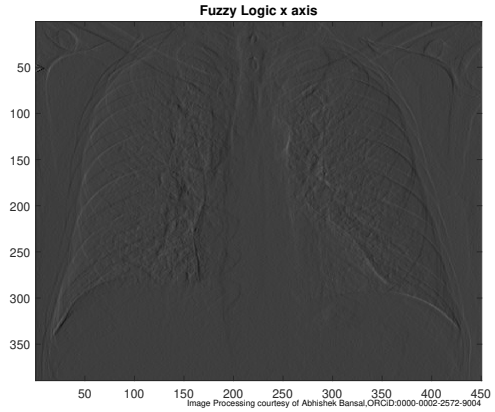

(a) x axis

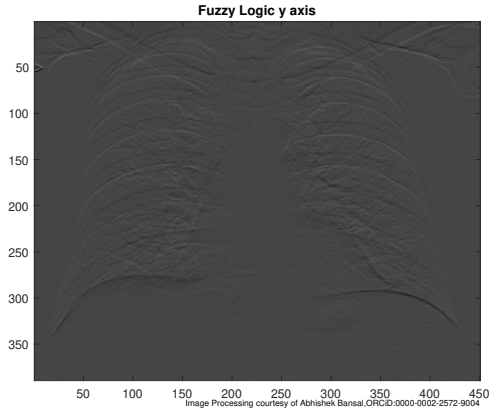

(b) y axis

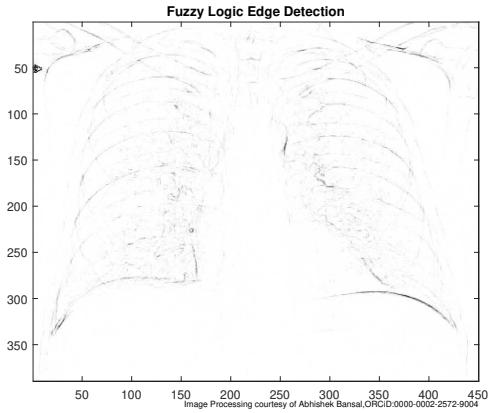

(c) Edge Detection

Fig. 39: Fuzzy Logic

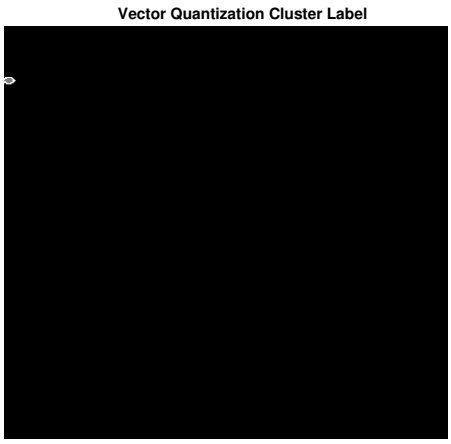

(a) Vector Quantization Cluster Label

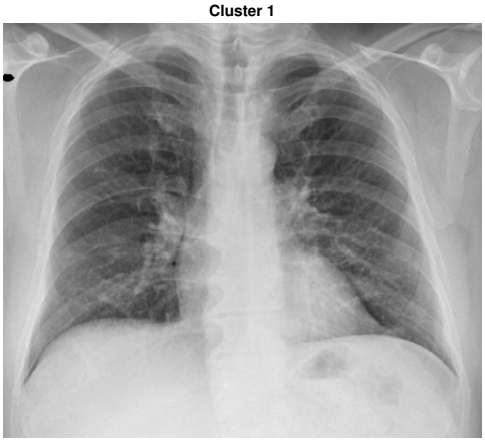

(b) Cluster 1

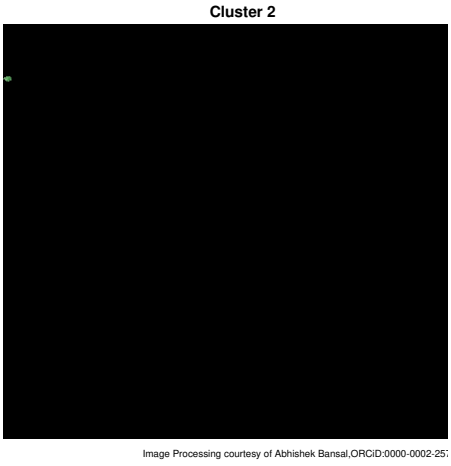

(c) Cluster 2

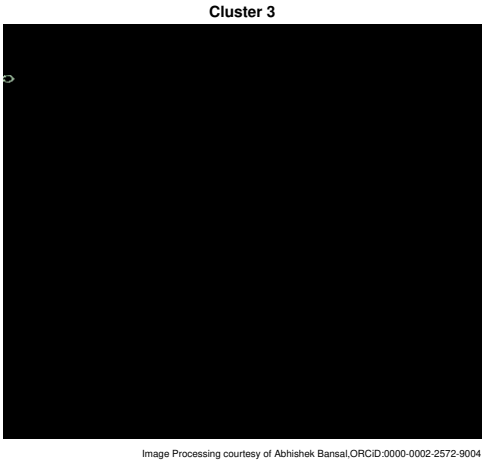

(d) Cluster 3

Fig. 40: Vector Quantization,K-means Clustering

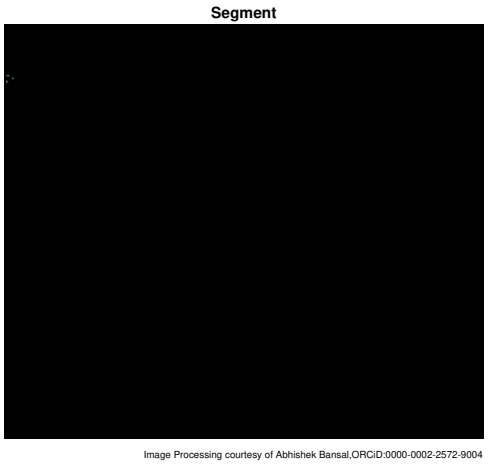

(a) Segmentation

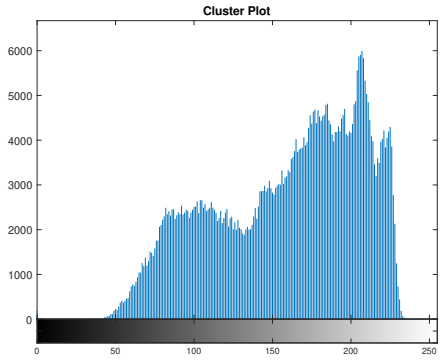

(b) Cluster Plot

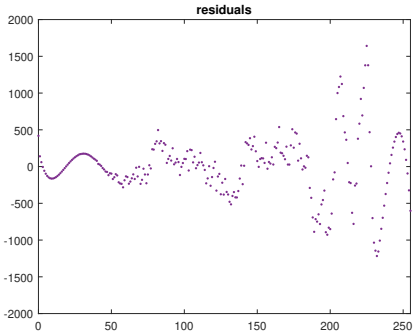

(c) Cluster Plot Residuals

Fig. 41: Clustering Plot and Segment

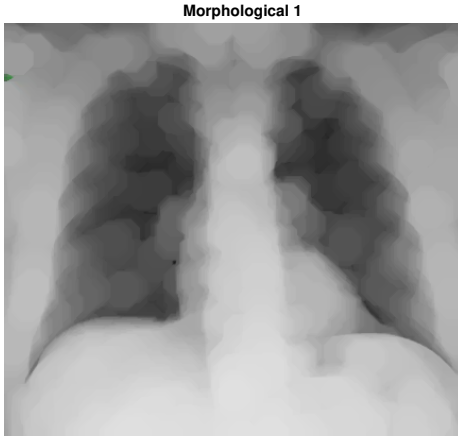

(a) Morphological Opening 1

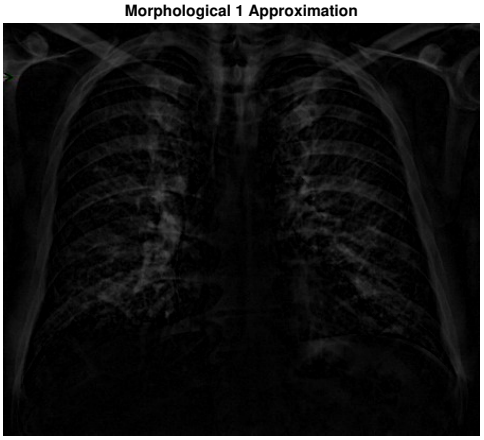

(b) Background Approximation Removed from Fig. 19(a)

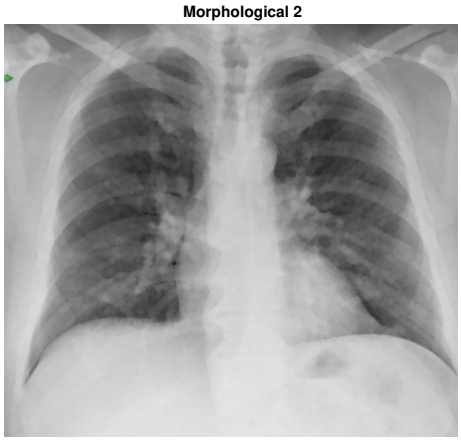

(c) [Morphological Opening 2

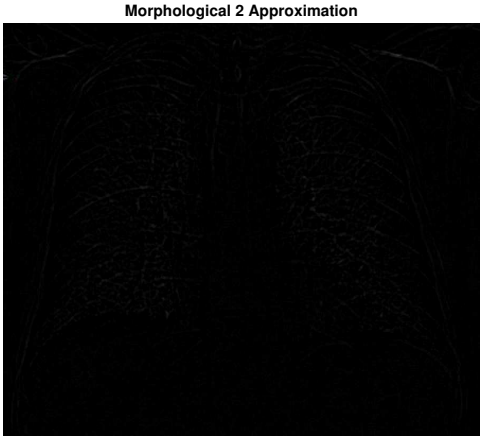

(d) Background Approximation Removed from Fig. 19(c)

Fig. 42: Morphological Segmentation

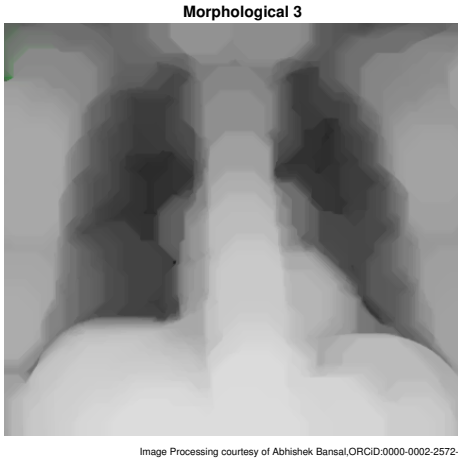

(a) Morphological Opening 3

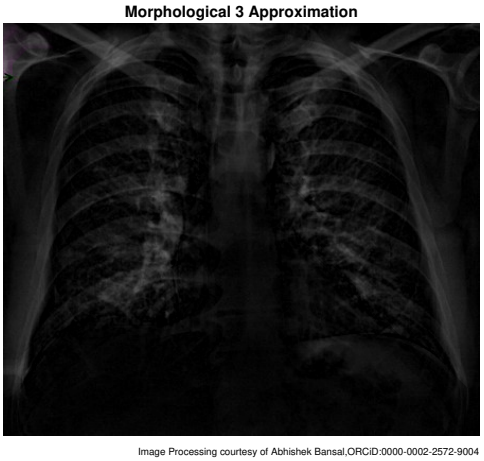

(b) Background Approximation Removed from Fig. 20(a)

Fig. 43: Morphological Segmentation

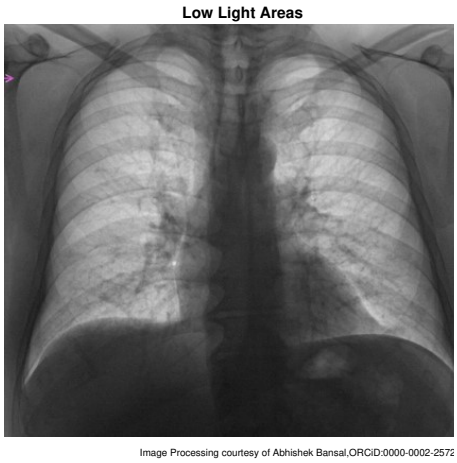

(a) X-Ray Inverted & Illuminated

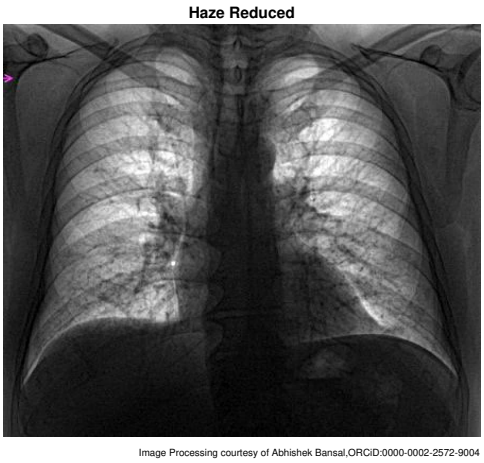

(b) Hazing Reduction Algorithm

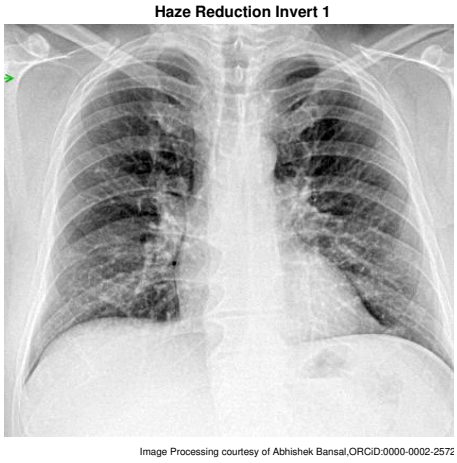

(c) Dehazing Algorithm

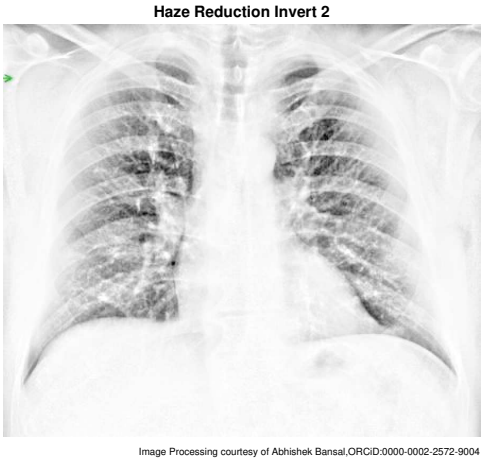

(d) Dehazing Algorithm

Fig. 44: Dehazing Algorithm

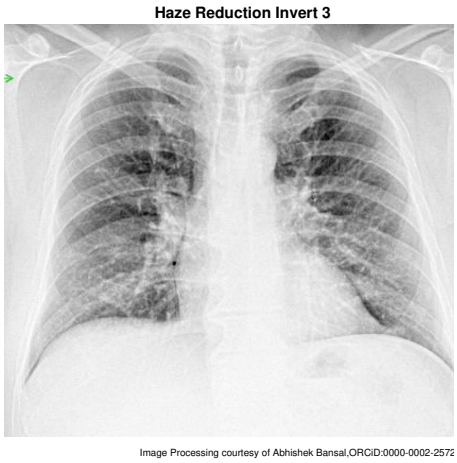

(a) Dehazing Algorithm

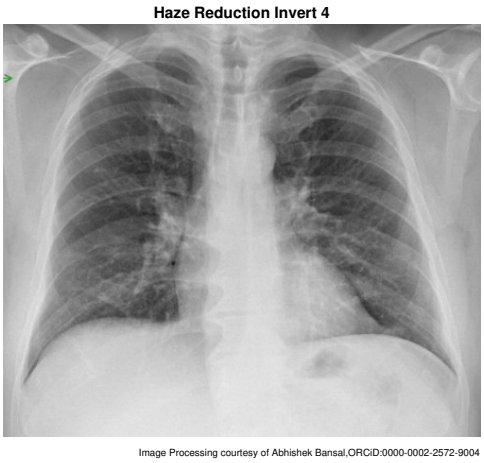

(b) Dehazing Algorithm

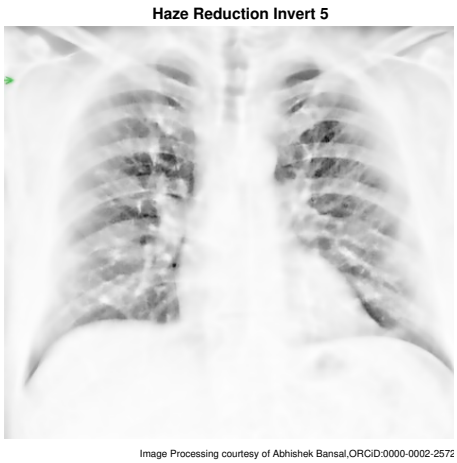

(c) Dehazing Algorithm

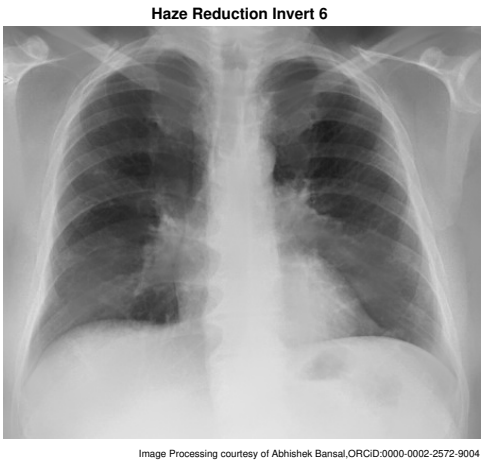

(d) Dehazing Algorithm

Fig. 45: Dehazing Algorithm

V Results : Day 3, PA

1 X-Ray Converted

In this subsection, X-Ray(PA) of Day 3 is converted to single precision grayscale and double precision,on which all further image processings will be done. These are shown in Fig. 46.

(a) Single Precision (b) Double Precision

Fig. 46: Converted to Single Precision & Double Precision,Day3

2 Double Precision Noise Addition

In this subsection, the double precision X-Ray of Day 3 (Fig 46(b)) of the previous subsection is subjected to noises namely Gaussian with variance 0.01, Poisson Noise and speckle noise with variance 0.05. These are shown in Fig. 47.

3 Gradient Magnitude and Direction

In this subsection, the gradient of the single precision X-Ray of Day 3 (Fig 46(a)) is obtained and its magnitude and direction is plotted using methods of Sobel, Prewitt, central difference and intermediate difference. These are shown in Fig. 48.

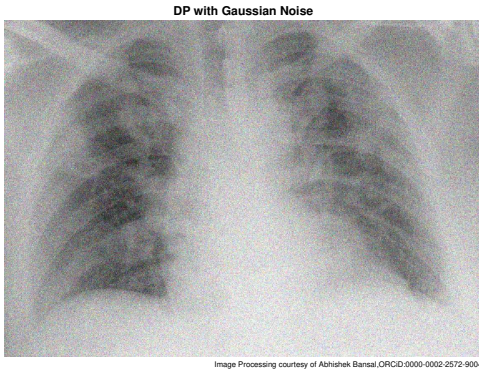

(a) Gaussian Noise

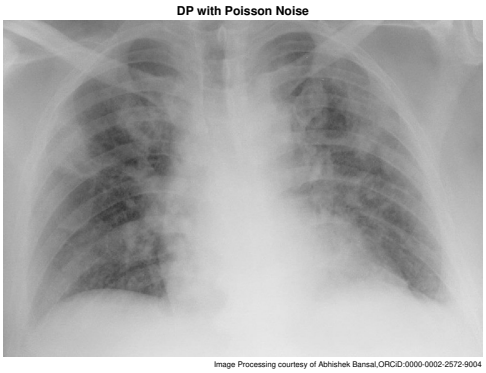

(b) Poisson Noise

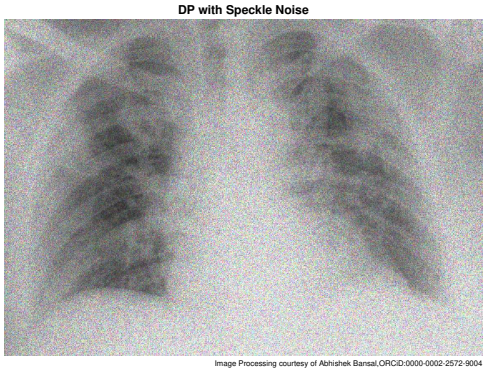

(c) Speckle Noise

Fig. 47: Noises Added to Double Precision,Day3

4 Directional Gradients

In this subsection, the directional gradient of the single precision X-Ray of Day 3 (Fig 46(a)) is plotted using methods of Sobel, Prewitt, central difference and intermediate difference. These are shown in Fig. 49.

5 Gaussian Noises & Sobel Gradient

In this subsection, the single precision X-Ray of Day 3 (Fig 46(a)) is subjected to Gaussian noise with three variances of 0.01, 0.001 and 0.0001. These are shown in Fig. 50. The gradient magnitude of these noisy X-Rays are plotted using Sobel method, which

are shown in Fig. 51. The figures of gradient magnitude of Fig. 50 are further smoothed using 2-D Gaussian smoothing. The Gaussian smoothing and central difference gradient are shown in Fig. 52. The Gaussian smoothing and intermediate difference gradient are shown in Fig. 53.

6 Poisson Noise & Sobel Gradient

In this subsection, the single precision X-Ray of Day 3 (Fig 46(a)) is subjected to Poisson Noise,Fig. 54(a). The gradient magnitude of Poisson noise X-Ray is plotted using Sobel method, which are shown in Fig. 54(b). This is further smoothed using 2-D Gaussian smoothing and central difference gradient in Fig. 54(c); and 2-D Gaussian smoothing and intermediate difference gradient in Fig. 54(d).

7 Speckle Noise & Sobel Gradient

In this subsection, the single precision X-Ray of Day 3 (Fig 46(a)) is subjected to Speckle noise with four variances of 0.05, 0.01, 0.001 and 0.1. These are shown in Fig. 55[a-d]. The gradient magnitude of these noisy X-Rays are plotted using Sobel method, which are shown in Fig. 56. These are further smoothed using 2-D Gaussian smoothing. The Gaussian smoothing and central difference gradient are shown in Fig. 57. The Gaussian smoothing and intermediate difference gradient are shown in Fig. 58.

8 Pixel Intensities & Contrast

In this subsection, the original X-Ray (without converting to single precision or double precision) is contrasted for study and analysis.

Let the center fit $z = \frac{(x - 127.5)}{74.05}$, then from polynomial regression

$y = 1911 \times z^9 + 949.3 \times z^8 - 1.239 \times 10^4 \times z^7 - 5847 \times z^6 + 2.778 \times 10^4 \times z^5 + 1.157 \times 10^4 \times z^4 - 2.885 \times 10^4 \times z^3 - 1.135 \times 10^4 \times z^2 + 1.716 \times 10^4 \times z + 1.064 \times 10^4$

Let $\bar{y}$ be the mean of y, $\hat{y}$ the calculated values of y, then the coefficient of determination, $R^2 = 1 - \frac{\sum_{i=1}^{n}(y_i - \hat{y})^2}{\sum_{i=1}^{n}(y_i - \bar{y})^2} = 0.8837$

The measure of the goodness of fit given by norm of residuals is 3.244×10^4. Here, the polynomial of degree 9 chosen here is the global which can be focused on the areas of interest (to be decided by infection part or researchers/doctors interest) and separate equations can be obtained for each particular area of interest. This gives insight in mathematical formulation and has been used in the Novel $\mathcal{B}$-Mathematical Modeling of Respiratory System.

TABLE V: Data Statistics for Fig. 15(b)

	X	Y
min	0	0
max	255	1.929×10^4
mean	127.5	6111
median	127.5	5199
mode	0	0
std deviation	74.05	5956
range	255	1.929×10^4

The Fig.59(a) shows that X-Ray contrast is improved for analysis when compared with Fig. 1(a). Fig. 59(b) shows the distribution of X-Ray pixel intensities. Fig. 59(c) shows

the error estimation plot, which is the plot of the residuals. Fig. 59(d) shows the X-Ray histogram equalization which is the spreading of the intensity values over the full range.

In Fig. 60, X-Ray Contrast is improved with five local luminances. The original Fig. 46(a) X-Ray contrast is improved with four more local luminances by varying the intensity values at low and high intensities. These are shown in Fig 60(a), Fig. 60(b) and Fig. 60(c). In Fig. 60(d), the original Fig. 46(a) X-Ray is contrasted with fifth value of improvement but smoothing technique is applied after it.

9 Fuzzy Logic

In this subsection, the images obtained using fuzzy logic edge-detection algorithm and Fuzzy Inference System (FIS) are given. Two 2-D Convolution are performed. The x-axis of directional gradient is convolved with x-axis gradients of double-precision X-Ray obtained in Fig. 46(b) and the X-Ray gradient of fuzzy logic x-axis is given in Fig. 61(a). The y-axis of directional gradient is convolved with y-axis gradients of double-precision X-Ray obtained in Fig. 46(b) and the X-Ray gradient of fuzzy logic y-axis is given in Fig. 61(b). The edge detection is shown in Fig. 61(c).

10 K-means Clustering

In this subsection, the popular vector quantization technique of K-Means clustering is applied to X-Ray. In this technique, firstly CIE XYZ tristimulus technique is used to know the color information and thus, the information of luminosity layer 'L*', chromaticity-layer 'a*' and chromaticity-layer 'b*' is obtained. Then every pixel is clustered with its pixel label and partitioned into three clusters. The clustering obtained

is shown in Fig. 62(a), Vector Quantization Cluster Label. And three clusters Cluster 1, Cluster 2 and Cluster 3 obtained are shown in Fig. 62(b), Fig. 62(c) and Fig. 62(d) respectively.

In Fig. 63(a), segmentation is applied and Fig. 63(b) and Fig. 63(c) shows respectively the cluster plot and the plot of error estimation, that is, the plot of residuals.

Moving in similar way as in the *Subsection-8* and choosing same $z = \frac{(x - 127.5)}{74.05}$, we have

$y = -1.369 \times 10^4 \times z^9 + 1.246 \times 10^4 \times z^8 + 7.594 \times 10^4 \times z^7 - 6.079 \times 10^4 \times z^6 - 1.358 \times 10^5 \times z^5 + 9.016 \times 10^4 \times z^4 + 8.192 \times 10^4 \times z^3 - 4.42 \times 10^4 \times z^2 - 4723 \times z + 1.049 \times 10^4$

$R^2 = 0.3119$ and Norm of Residuals $= 2.907 \times 10^5$

TABLE VI: Data Statistics for Fig. 18(b)

	X	Y
min	0	0
max	255	3.434×10^5
mean	127.5	6111
median	127.5	955.5
mode	0	0
std deviation	74.05	2.194×10^4
range	255	3.434×10^5

11 Morphological Segmentation

In this subsection, known morphological segmentation technique is applied on X-Rays. Three morphological openings are used. The morphological opening with structuring element of disk shaped with three different radius are shown in Fig. 64(a), Fig.

64(c) and Fig. 65(a). The background approximation images of X-Ray obtained after subtracting from the original image are shown in Fig. 64(b), Fig. 64(d) and Fig. 65(b).

12 Dehazing Algorithm

In Fig. 66(a), the original Fig. 46(a) X-Ray is inverted and the low-light areas and focused and the new X-Ray is obtained. The hazing obtained in Fig. 66(a) is reduced by hazing reduction algorithm.

On the new X-Ray of Fig. 66(b), dehazing algorithm is applied and its result is in Fig.66(c,d). Fig. 67[a-d] has four more such combinations on which dehazing algorithm is implemented.

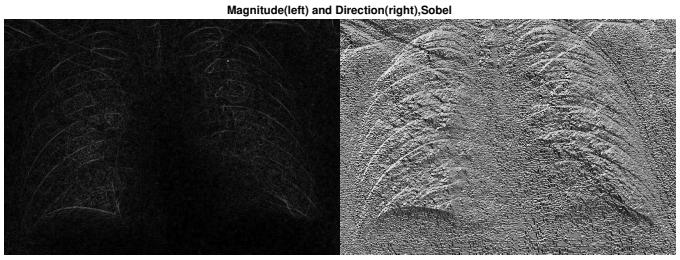

(a) Sobel Method

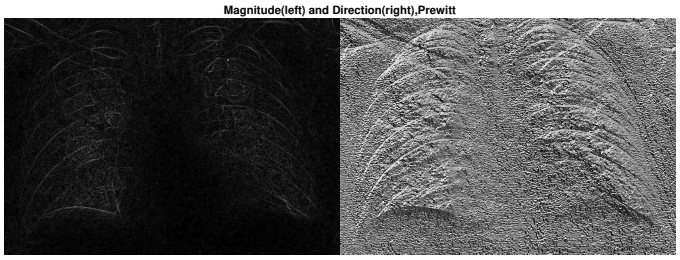

(b) Prewitt Method

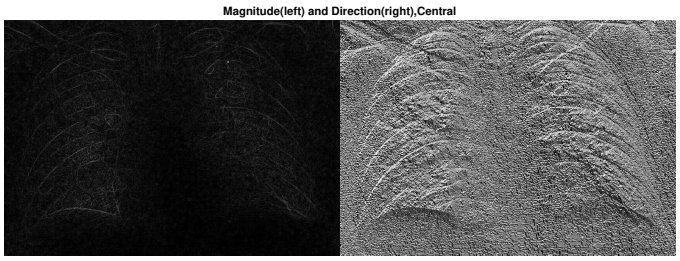

(c) Central Difference

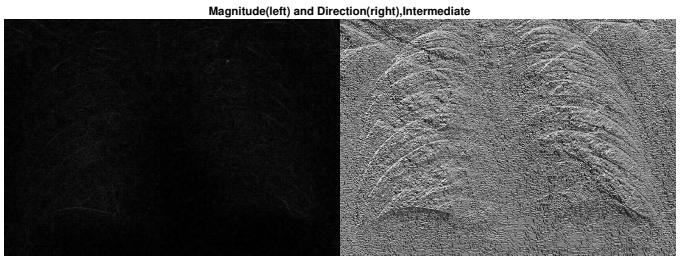

(d) Intermediate Difference

Fig. 48: X-Ray Gradient Magnitude and Direction,Day3

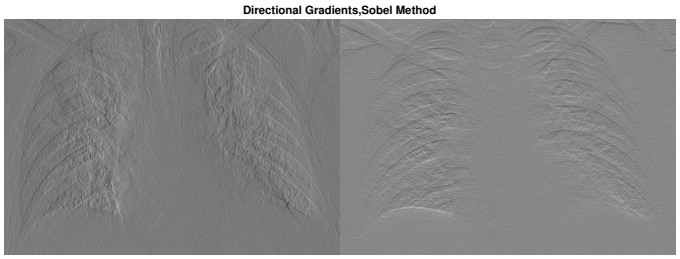

(a) Sobel Method

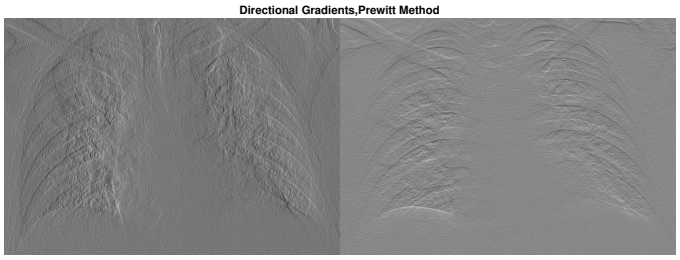

(b) Prewitt Method

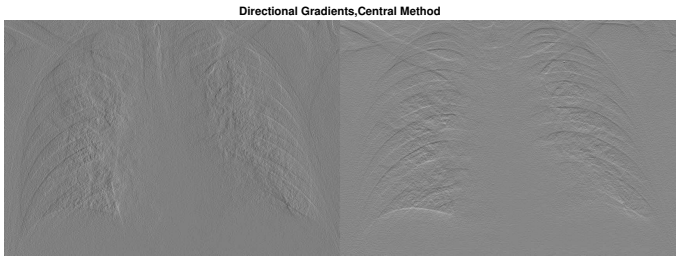

(c) Central Difference

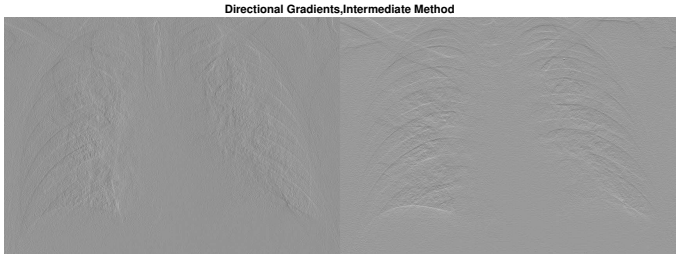

(d) Intermediate Difference

Fig. 49: Directional Gradients,Day3

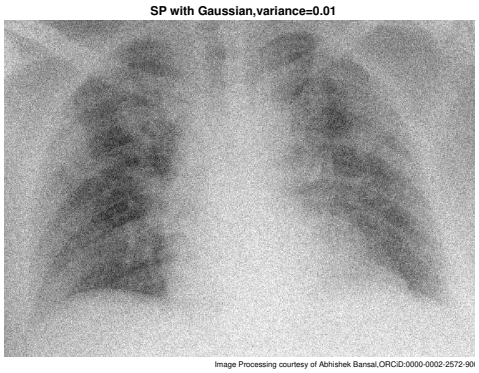

(a) Gaussian Variance = 0.01

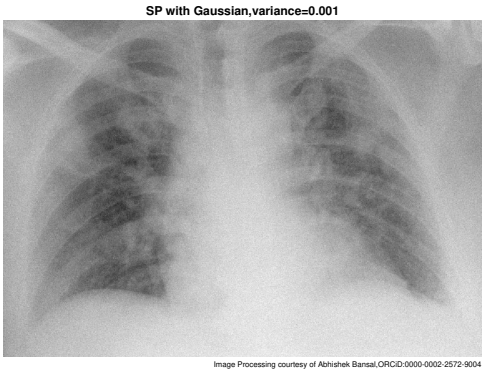

(b) Gaussian Variance = 0.001

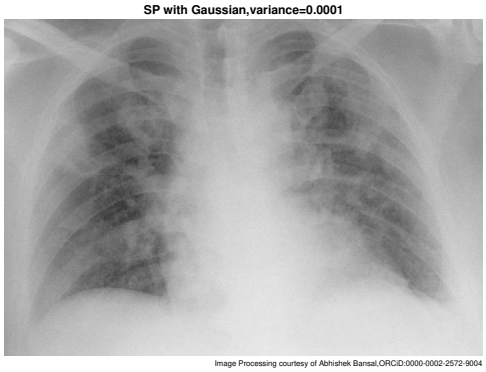

(c) Gaussian Variance = 0.0001

Fig. 50: Gaussian White Noise added to Image,Day3

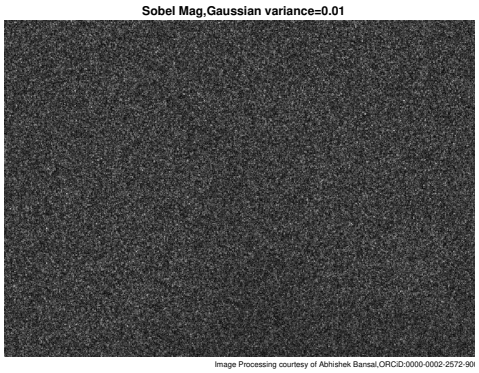

(a) Gaussian Variance = 0.01

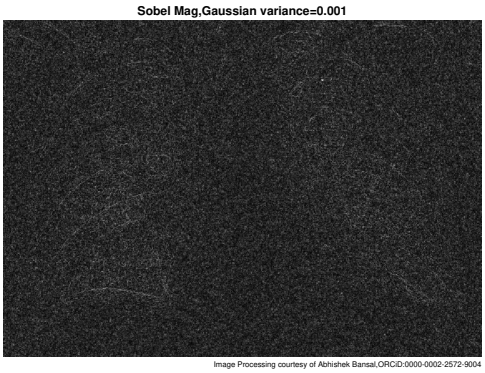

(b) Gaussian Variance = 0.001

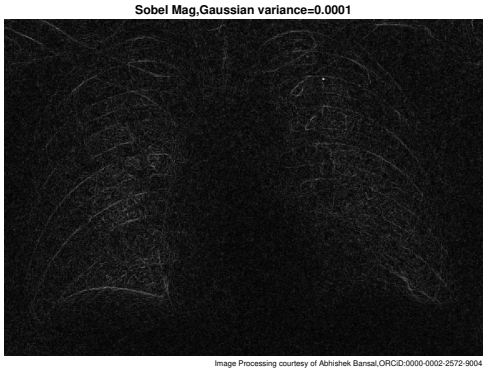

(c) Gaussian Variance = 0.0001

Fig. 51: Gradient of Noisy X-Ray using Sobel Method,Day3

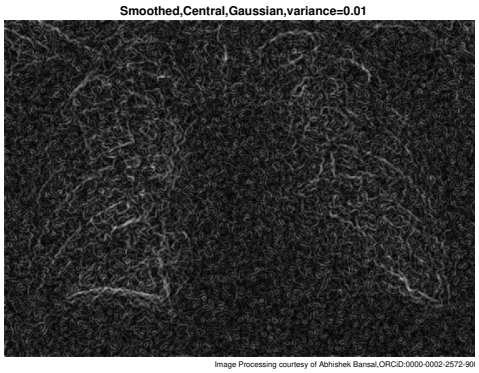

(a) Gaussian Variance = 0.01

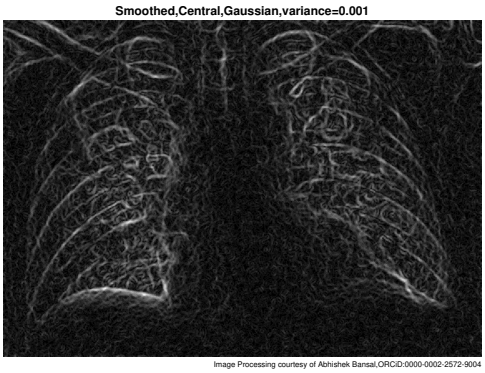

(b) Gaussian Variance = 0.001

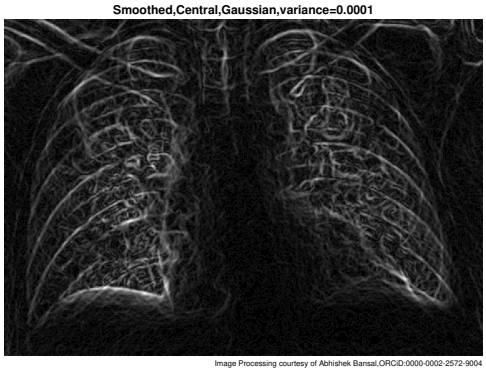

(c) Gaussian Variance = 0.0001

Fig. 52: Gaussian smoothing & central difference gradient,Day3

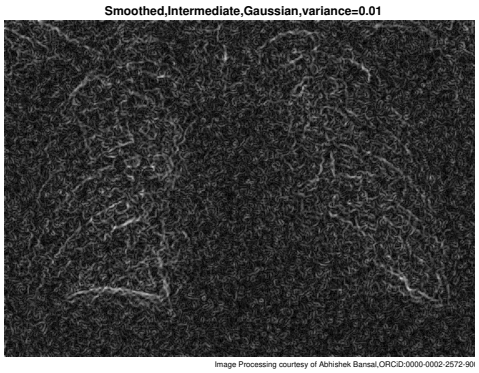

(a) Gaussian Variance = 0.01

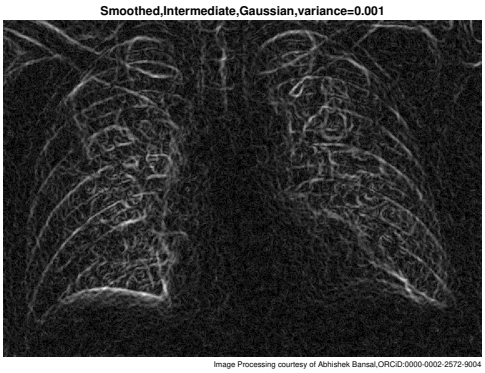

(b) Gaussian Variance = 0.001

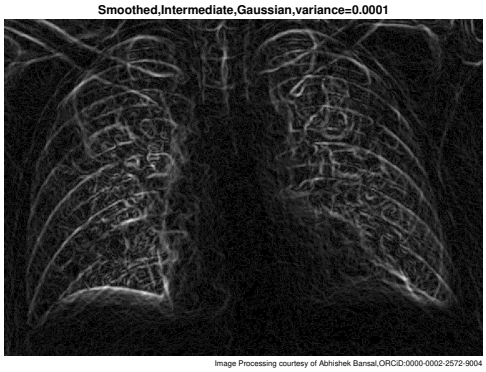

(c) Gaussian Variance = 0.0001

Fig. 53: Gaussian smoothing & intermediate difference gradient,Day3

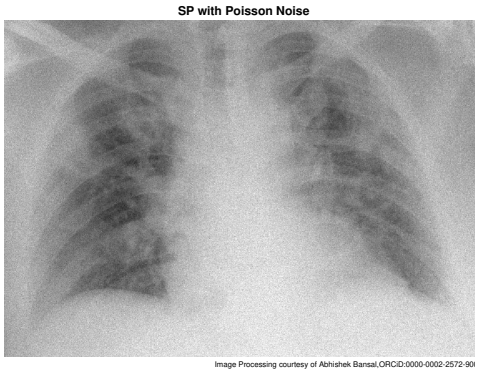

(a) Poisson Noise added

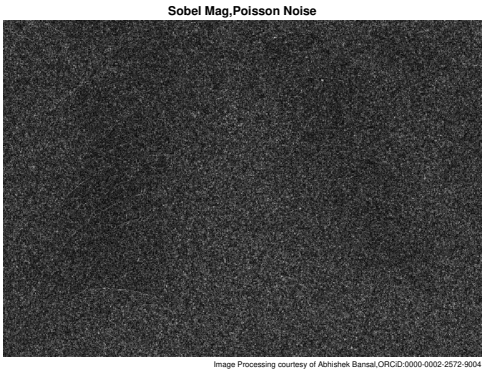

(b) Sobel Gradient Magnitude

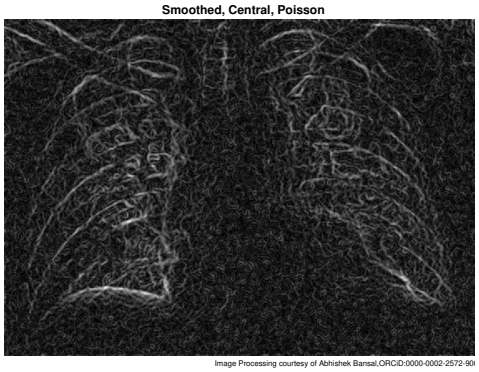

(c) Smoothed by Central Difference

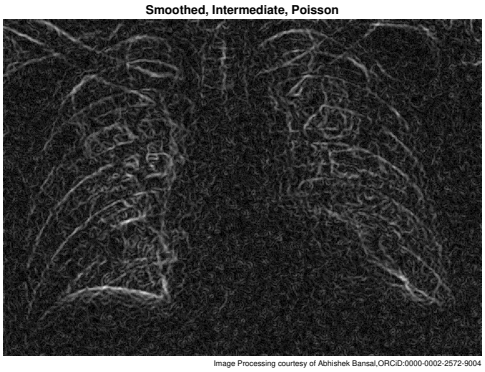

(d) Smoothed by Intermediate Difference

Fig. 54: Poisson Noise & Gradient Magnitude,Day3

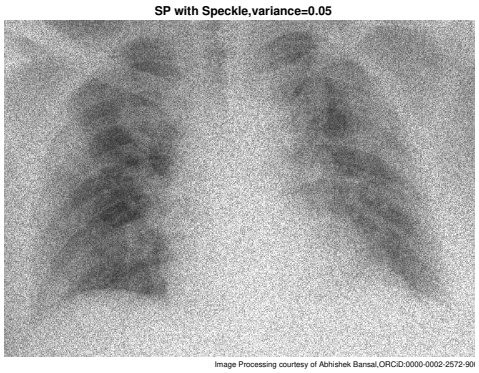

(a) Speckle Variance = 0.05

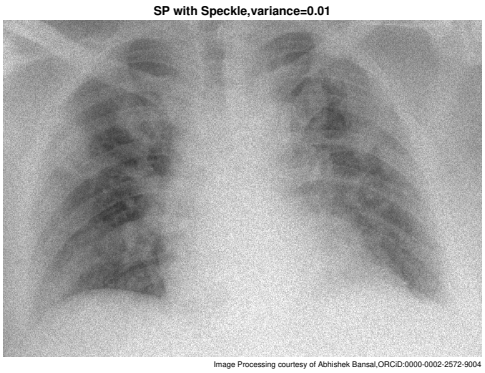

(b) Speckle Variance = 0.01

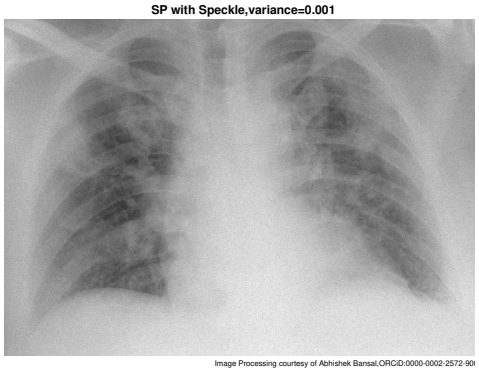

(c) Speckle Variance = 0.001

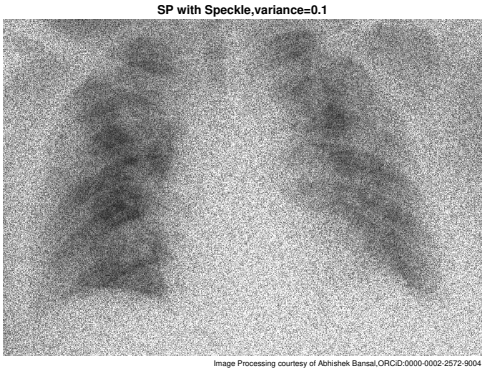

(d) Speckle Variance = 0.1

Fig. 55: Speckle Noise added to Image,Day3

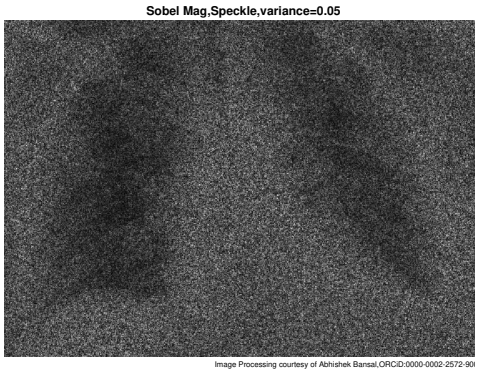

(a) Speckle Variance = 0.05

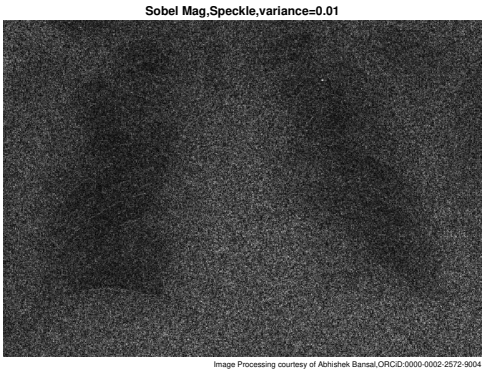

(b) Speckle Variance = 0.01

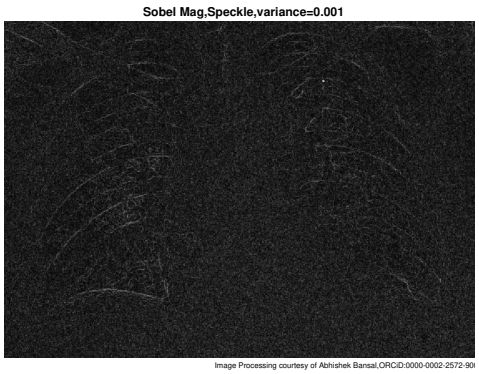

(c) Speckle Variance = 0.001

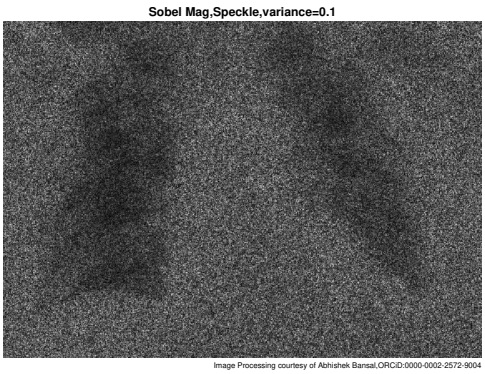

(d) Speckle Variance = 0.1

Fig. 56: Gradient of Noisy X-Ray using Sobel Method,Day3

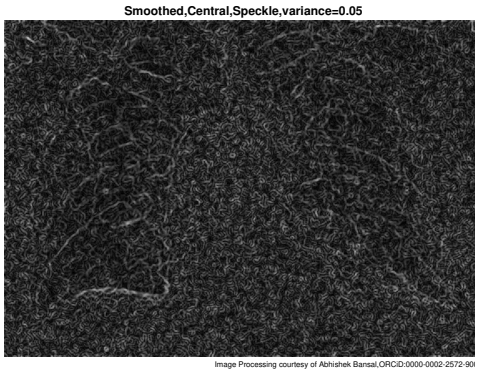

(a) Speckle Variance = 0.05

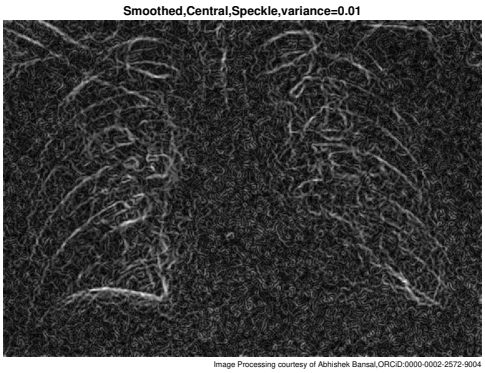

(b) Speckle Variance = 0.01

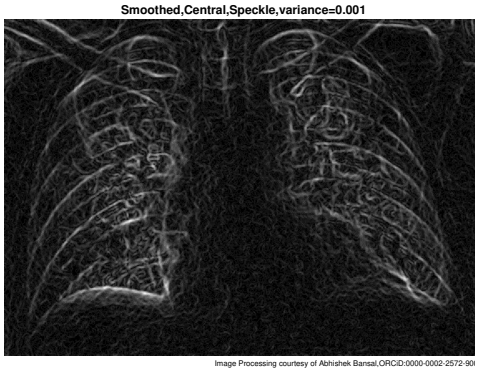

(c) Speckle Variance = 0.001

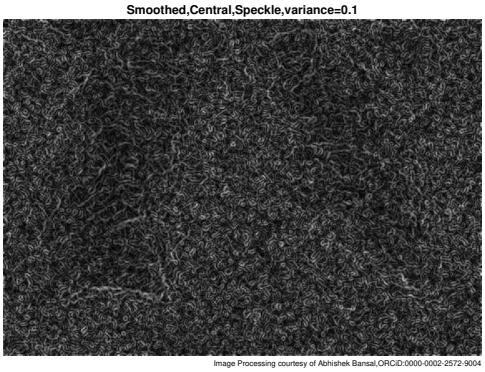

(d) Speckle Variance = 0.1

Fig. 57: Gaussian smoothing & central difference gradient,Day3

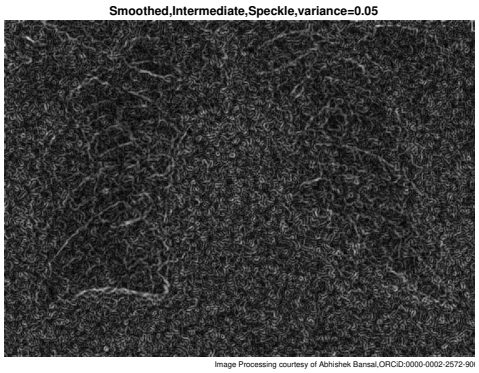

(a) Speckle Variance = 0.05

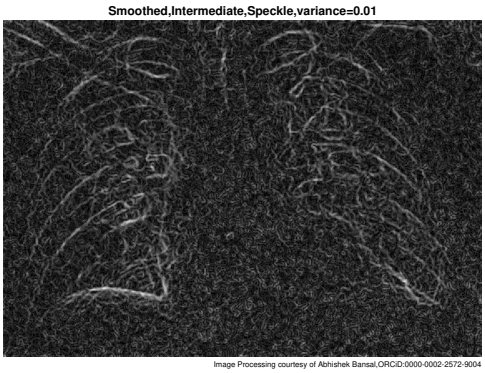

(b) Speckle Variance = 0.01

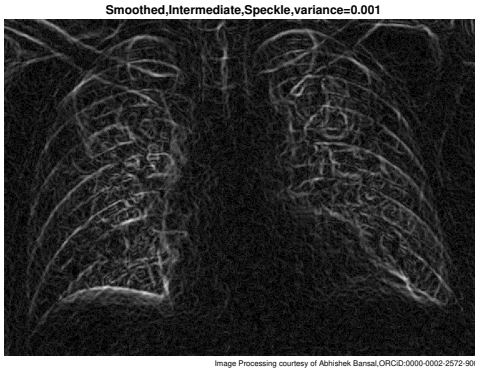

(c) Speckle Variance = 0.001

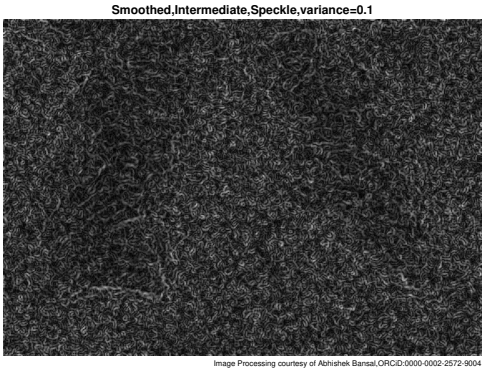

(d) Speckle Variance = 0.1

Fig. 58: Gaussian smoothing & intermediate difference gradient,Day3

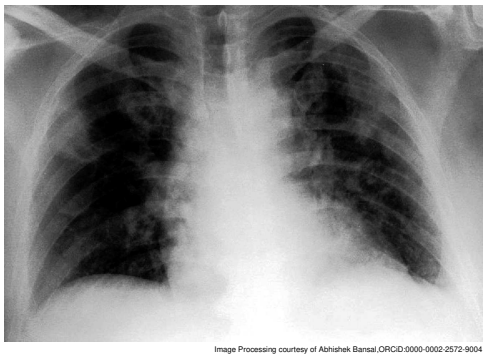

(a) X-Ray Contrast Improved

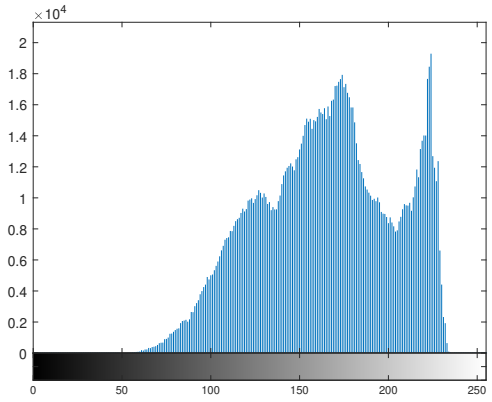

(b) Distribution of Pixel Intensities

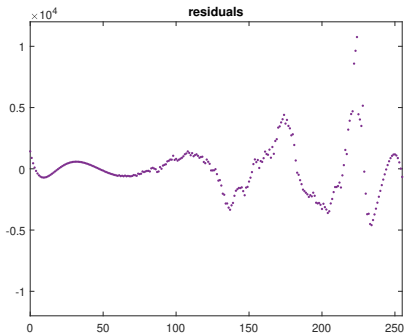

(c) Error Estimation Plot

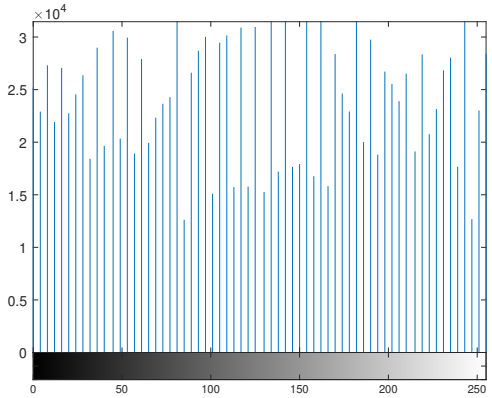

(d) X-Ray Histogram Equalization

Fig. 59: Distribution of Pixel Intensities in X-Ray,Day3

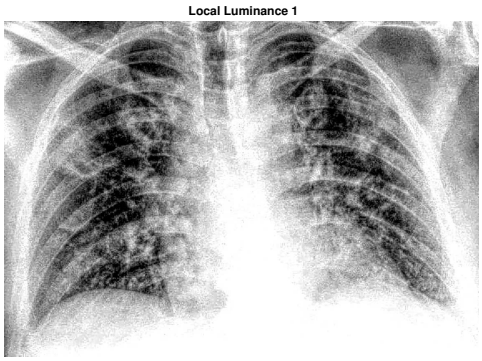

(a) X-Ray Contrast Improved 2

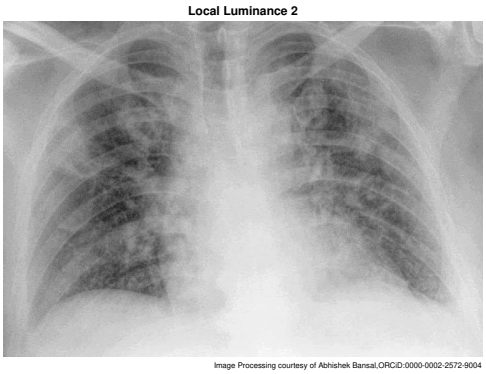

(b) X-Ray Contrast Improved 3

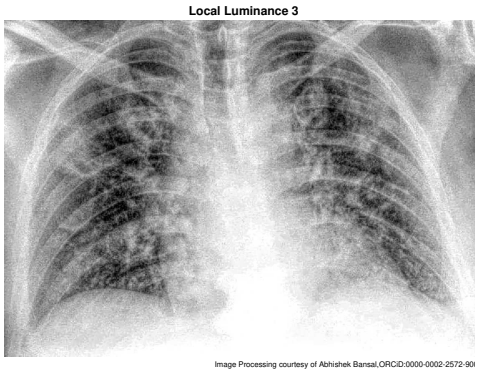

(c) X-Ray Contrast Improved 4

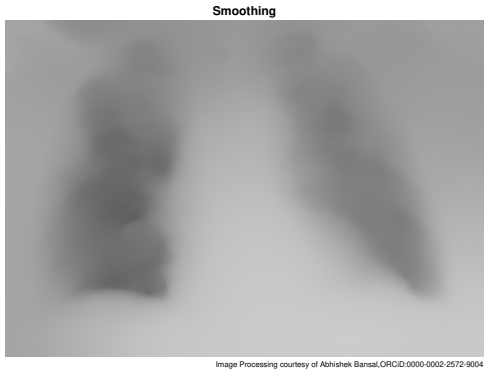

(d) X-Ray Contrast Improved & Smoothed

Fig. 60: X-Ray Contrast Improved with Five Local Luminances,Day3

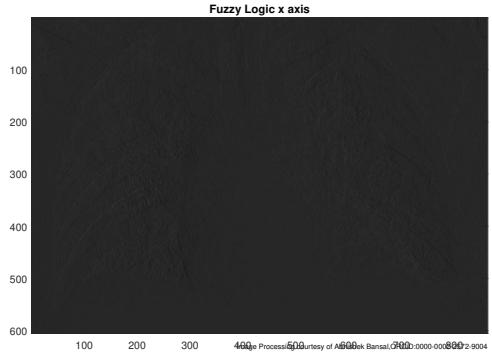

(a) x axis

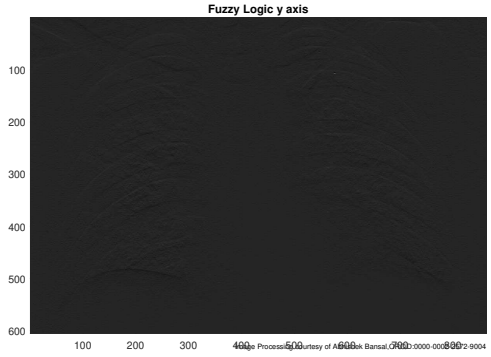

(b) y axis

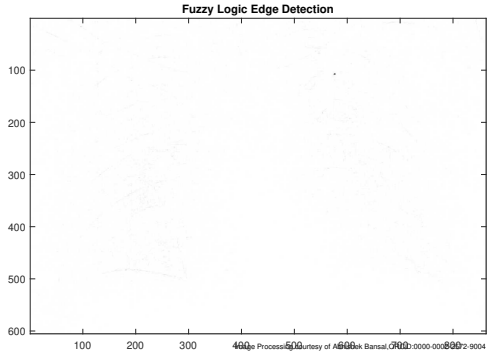

(c) Edge Detection

Fig. 61: Fuzzy Logic,Day3

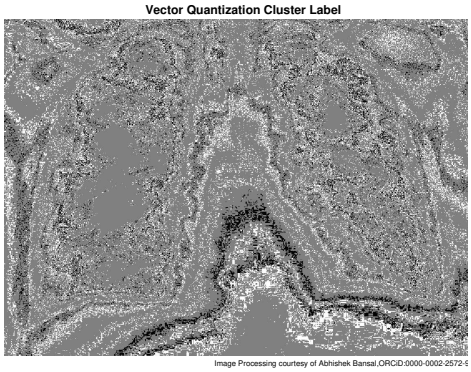

(a) Vector Quantization Cluster Label

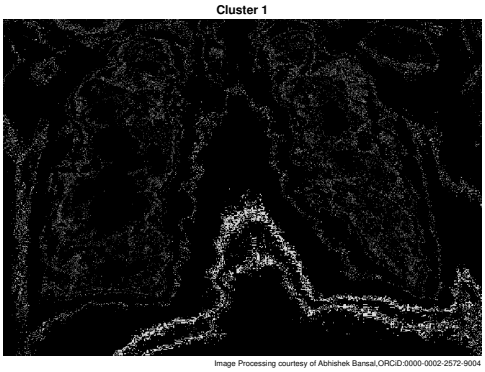

(b) Cluster 1

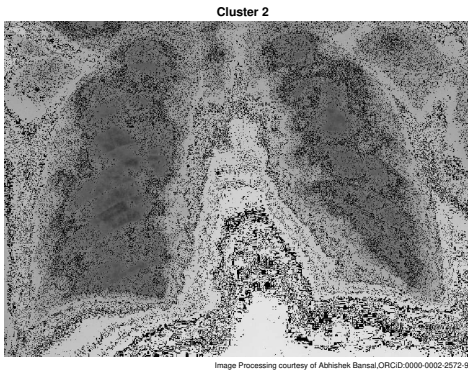

(c) Cluster 2

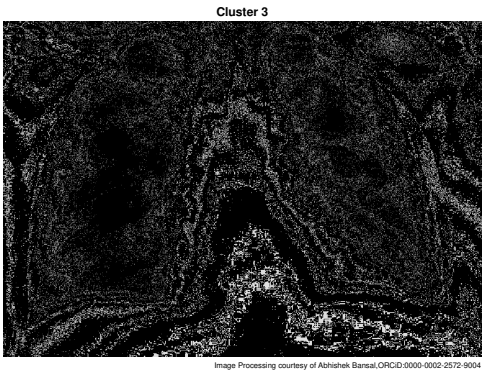

(d) Cluster 3

Fig. 62: Vector Quantization,K-means Clustering,Day3

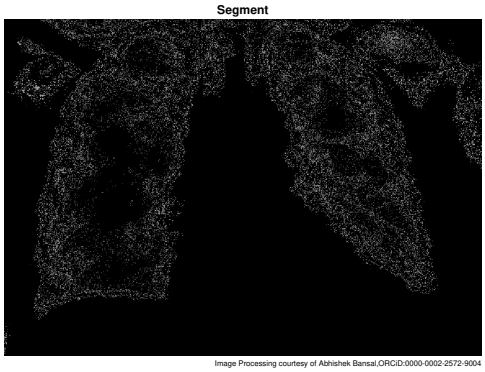

(a) Segmentation

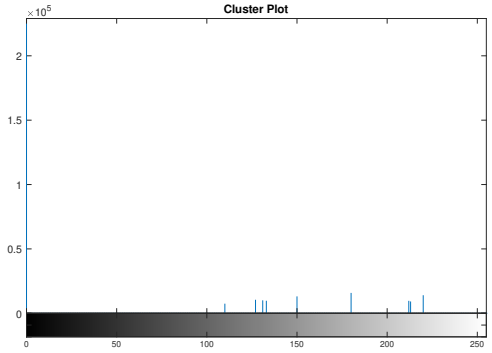

(b) Cluster Plot

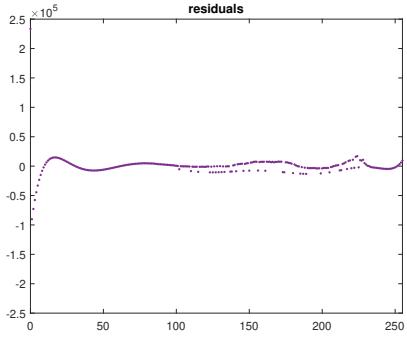

(c) Cluster Plot Residuals

Fig. 63: Clustering Plot and Segment,Day3

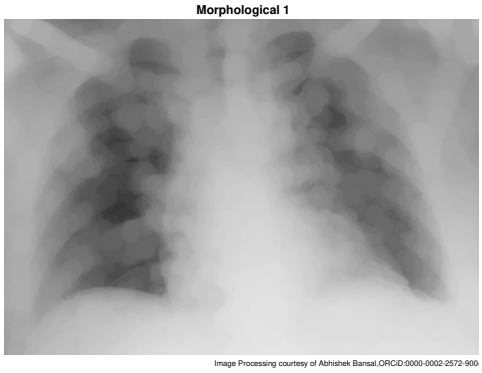

(a) Morphological Opening 1

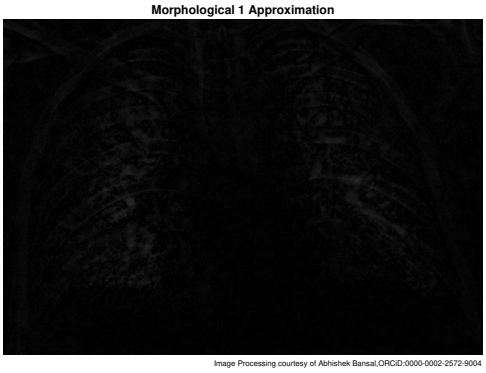

(b) Background Approximation Removed from Fig. 19(a)

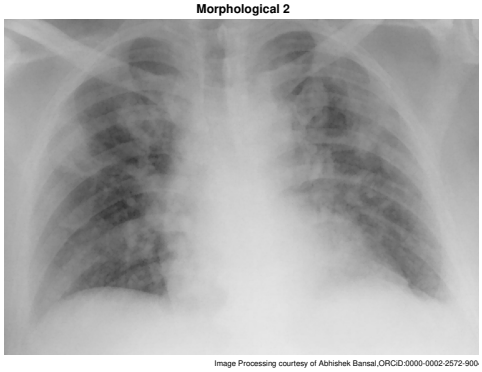

(c) [Morphological Opening 2

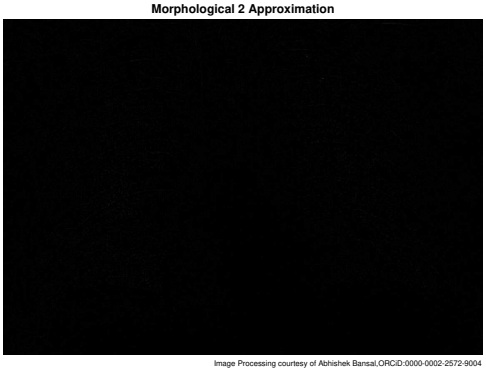

(d) Background Approximation Removed from Fig. 19(c)

Fig. 64: Morphological Segmentation,Day3

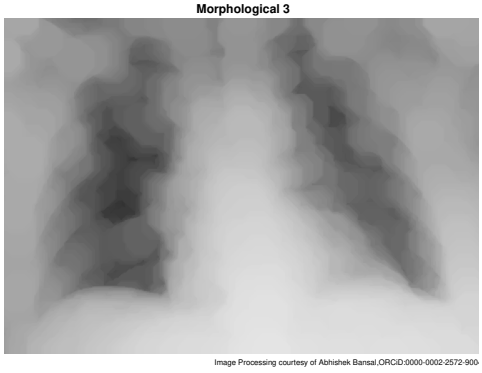

(a) Morphological Opening 3

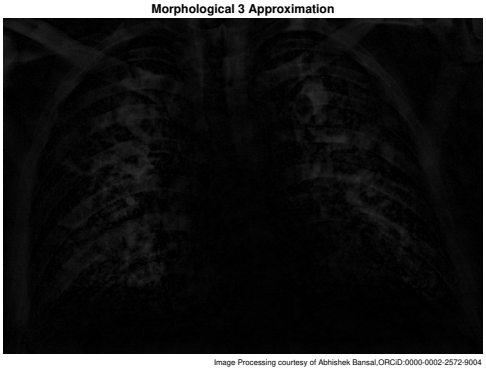

(b) Background Approximation Removed from Fig. 20(a)

Fig. 65: Morphological Segmentation,Day3

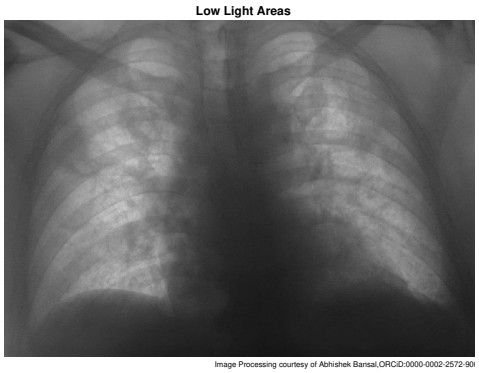

(a) X-Ray Inverted & Illuminated

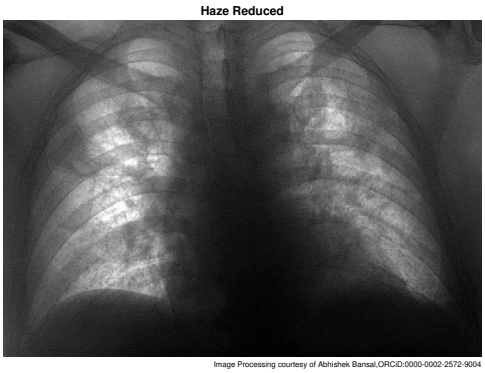

(b) Hazing Reduction Algorithm

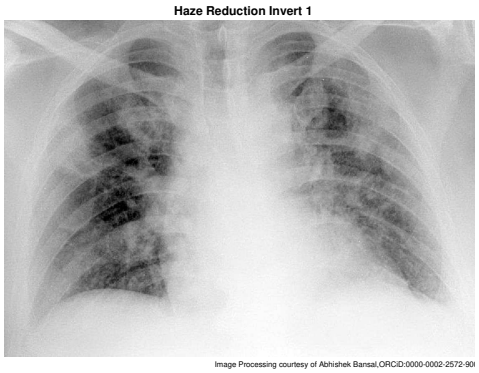

(c) Dehazing Algorithm

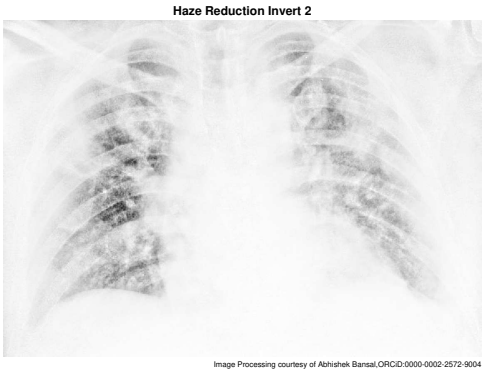

(d) Dehazing Algorithm

Fig. 66: Dehazing Algorithm,Day3

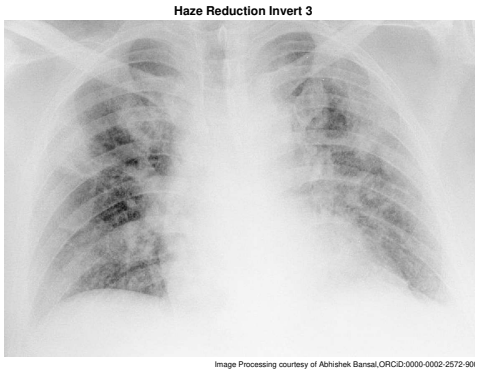

(a) Dehazing Algorithm

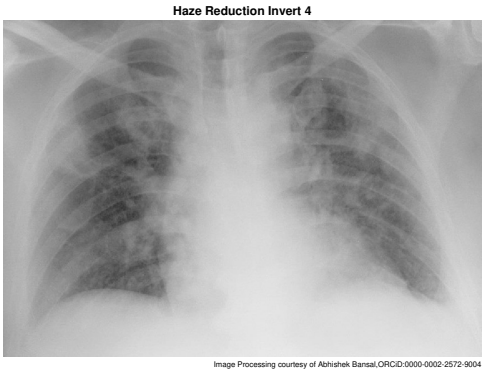

(b) Dehazing Algorithm

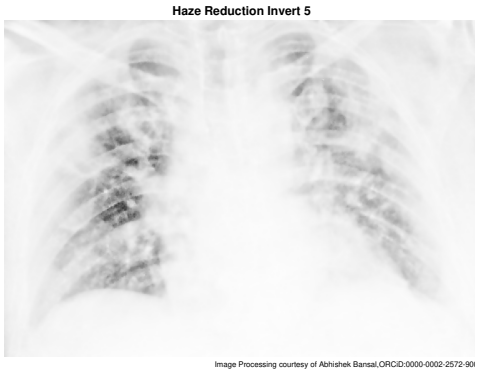

(c) Dehazing Algorithm

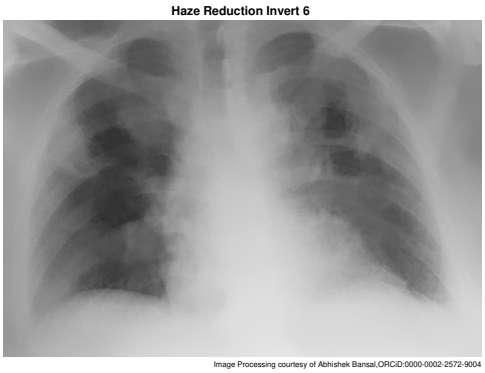

(d) Dehazing Algorithm

Fig. 67: Dehazing Algorithm,Day3

VI Results : Day 4, PA

1 X-Ray Converted

In this subsection, X-Ray(PA) of Day 4 is converted to single precision grayscale and double precision,on which all further image processings will be done. These are shown in Fig. 68.

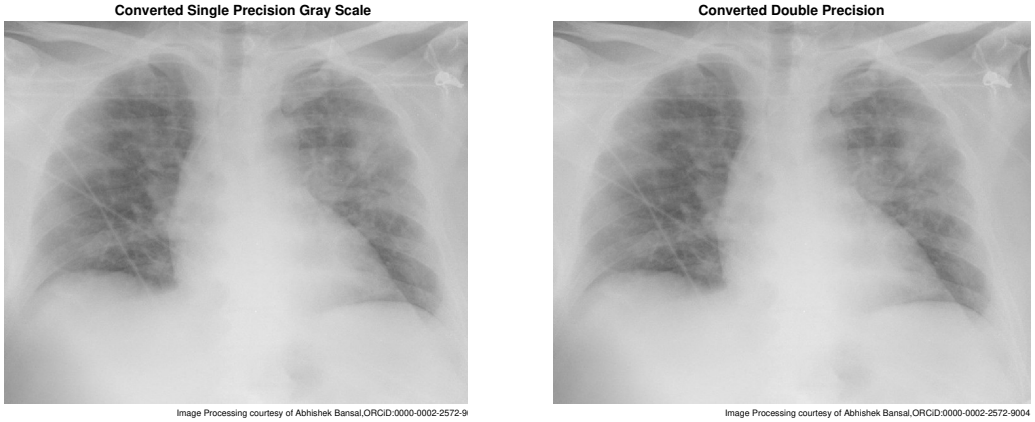

(a) Single Precision (b) Double Precision

Fig. 68: Converted to Single Precision & Double Precision,Day4

2 Double Precision Noise Addition

In this subsection, the double precision X-Ray of Day 4 (Fig 68(b)) of the previous subsection is subjected to noises namely Gaussian with variance 0.01, Poisson Noise and speckle noise with variance 0.05. These are shown in Fig. 69.

3 Gradient Magnitude and Direction

In this subsection, the gradient of the single precision X-Ray of Day 4 (Fig 68(a)) is obtained and its magnitude and direction is plotted using methods of Sobel, Prewitt, central difference and intermediate difference. These are shown in Fig. 70.

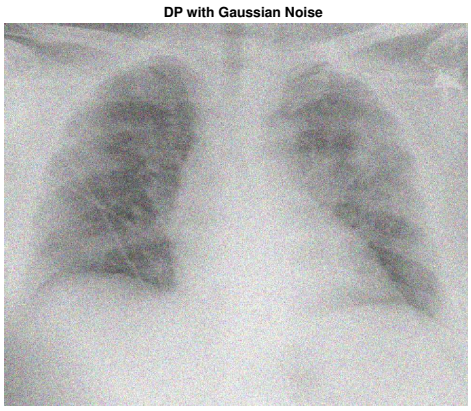

(a) Gaussian Noise

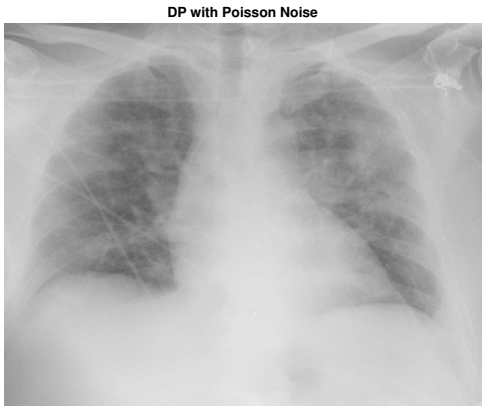

(b) Poisson Noise

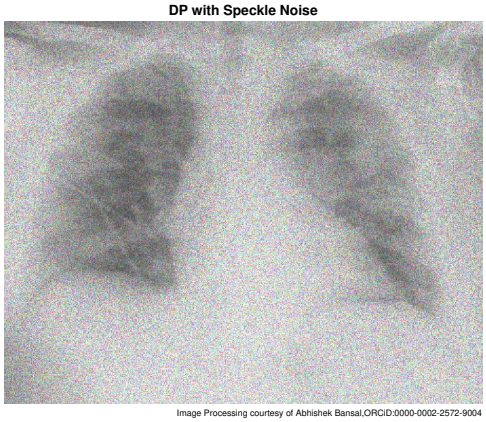

(c) Speckle Noise

Fig. 69: Noises Added to Double Precision,Day4

4 Directional Gradients

In this subsection, the directional gradient of the single precision X-Ray of Day 4 (Fig 68(a)) is plotted using methods of Sobel, Prewitt, central difference and intermediate difference. These are shown in Fig. 71.

5 Gaussian Noises & Sobel Gradient

In this subsection, the single precision X-Ray of Day 4 (Fig 68(a)) is subjected to Gaussian noise with three variances of 0.01, 0.001 and 0.0001. These are shown in Fig.

72. The gradient magnitude of these noisy X-Rays are plotted using Sobel method, which are shown in Fig. 73. The figures of gradient magnitude of Fig. 73 are further smoothed using 2-D Gaussian smoothing. The Gaussian smoothing and central difference gradient are shown in Fig. 74. The Gaussian smoothing and intermediate difference gradient are shown in Fig. 75.

6 Poisson Noise & Sobel Gradient

In this subsection, the single precision X-Ray of Day 4 (Fig 68(a)) is subjected to Poisson Noise,Fig. 76(a). The gradient magnitude of Poisson noise X-Ray is plotted using Sobel method, which are shown in Fig. 76(b). This is further smoothed using 2-D Gaussian smoothing and central difference gradient in Fig. 76(c); and 2-D Gaussian smoothing and intermediate difference gradient in Fig. 76(d).

7 Speckle Noise & Sobel Gradient

In this subsection, the single precision X-Ray of Day 4 (Fig 68(a)) is subjected to Speckle noise with four variances of 0.05, 0.01, 0.001 and 0.1. These are shown in Fig. 77[a-d]. The gradient magnitude of these noisy X-Rays are plotted using Sobel method, which are shown in Fig. 78. These are further smoothed using 2-D Gaussian smoothing. The Gaussian smoothing and central difference gradient are shown in Fig. 79. The Gaussian smoothing and intermediate difference gradient are shown in Fig. 80.

8 Pixel Intensities & Contrast

In this subsection, the original X-Ray (without converting to single precision or double precision) is contrasted for study and analysis.

Let the center fit $z = \frac{(x - 137.5)}{74.05}$, then from polynomial regression

$y = -456.5 \times z^9 + 2091 \times z^8 + 5796 \times z^7 - 9125 \times z^6 - 1.939 \times 10^4 \times z^5 + 6667 \times z^4 + 1.607 \times 10^4 \times z^3 + 5324 \times z^2 + 7713 \times z + 4413$

Let $\bar{y}$ be the mean of y, $\hat{y}$ the calculated values of y, then the coefficient of determination, $R^2 = 1 - \frac{\sum_{\iota=1}^{n}(y_i - \hat{y})^2}{\sum_{\iota=1}^{n}(y_i - \bar{y})^2} = 0.9513$

The measure of the goodness of fit given by norm of residuals is 2.42×10^4. Here, the polynomial of degree 9 chosen here is the global which can be focused on the areas of interest (to be decided by infection part or researchers/doctors interest) and separate equations can be obtained for each particular area of interest. This gives insight in mathematical formulation and has been used in the Novel $\mathcal{B}$-Mathematical Modeling of Respiratory System.

TABLE VII: Data Statistics for Fig. 15(b)

	X	Y
min	0	0
max	255	2.192×10^4
mean	137.5	5360
median	137.5	616.5
mode	0	0
std deviation	74.05	6870
range	255	2.192×10^4

The Fig.81(a) shows that X-Ray contrast is improved for analysis when compared with

Fig. 1(a). Fig. 81(b) shows the distribution of X-Ray pixel intensities. Fig. 81(c) shows the error estimation plot, which is the plot of the residuals. Fig. 81(d) shows the X-Ray histogram equalization which is the spreading of the intensity values over the full range.

In Fig. 82, X-Ray Contrast is improved with five local luminances. The original Fig. 68(a) X-Ray contrast is improved with four more local luminances by varying the intensity values at low and high intensities. These are shown in Fig 82(a), Fig. 82(b) and Fig. 82(c). In Fig. 82(d), the original Fig. 68(a) X-Ray is contrasted with fifth value of improvement but smoothing technique is applied after it.

9 Fuzzy Logic

In this subsection, the images obtained using fuzzy logic edge-detection algorithm and Fuzzy Inference System (FIS) are given. Two 2-D Convolution are performed. The x-axis of directional gradient is convolved with x-axis gradients of double-precision X-Ray obtained in Fig. 68(b) and the X-Ray gradient of fuzzy logic x-axis is given in Fig. 83(a). The y-axis of directional gradient is convolved with y-axis gradients of double-precision X-Ray obtained in Fig. 68(b) and the X-Ray gradient of fuzzy logic y-axis is given in Fig. 83(b). The edge detection is shown in Fig. 83(c).

10 K-means Clustering

In this subsection, the popular vector quantization technique of K-Means clustering is applied to X-Ray. In this technique, firstly CIE XYZ tristimulus technique is used to know the color information and thus, the information of luminosity layer 'L*', chromaticity-layer 'a*' and chromaticity-layer 'b*' is obtained. Then every pixel is

clustered with its pixel label and partitioned into three clusters. The clustering obtained is shown in Fig. 84(a), Vector Quantization Cluster Label. And three clusters Cluster 1, Cluster 2 and Cluster 3 obtained are shown in Fig. 84(b), Fig. 84(c) and Fig. 84(d) respectively.

In Fig. 85(a), segmentation is applied and Fig. 85(b) and Fig. 85(c) shows respectively the cluster plot and the plot of error estimation, that is, the plot of residuals.

Moving in similar way as in the *Subsection-8* and choosing same $z = \frac{(x - 137.5)}{74.05}$, we have

$y = -1.465 \times 10^4 \times z^9 + 1.29 \times 10^4 \times z^8 + 8.51 \times 10^4 \times z^7 - 6.144 \times 10^4 \times z^6 - 1.632 \times 10^5 \times z^5 + 8.416 \times 10^4 \times z^4 + 1.101 \times 10^5 \times z^3 - 3.07 \times 10^4 \times z^2 - 1.052 \times 10^4 \times z + 5573$

$R^2 = 0.3442$ and Norm of Residuals $= 2.704 \times 10^5$

TABLE VIII: Data Statistics for Fig. 18(b)

	X	Y
min	0	0
max	255	3.225×10^5
mean	137.5	5360
median	137.5	0
mode	0	0
std deviation	74.05	2.091×10^4
range	255	3.225×10^5

11 Morphological Segmentation

In this subsection, known morphological segmentation technique is applied on X-Rays. Three morphological openings are used. The morphological opening with structuring element of disk shaped with three different radius are shown in Fig. 86(a), Fig.

86(c) and Fig. 87(a). The background approximation images of X-Ray obtained after subtracting from the original image are shown in Fig. 86(b), Fig. 86(d) and Fig. 87(b).

12 Dehazing Algorithm

In Fig. 88(a), the original Fig. 68(a) X-Ray is inverted and the low-light areas and focused and the new X-Ray is obtained. The hazing obtained in Fig. 88(a) is reduced by hazing reduction algorithm.

On the new X-Ray of Fig. 88(b), dehazing algorithm is applied and its result is in Fig. 88(c,d). Fig. 89[a-d] has four more such combinations on which dehazing algorithm is implemented.

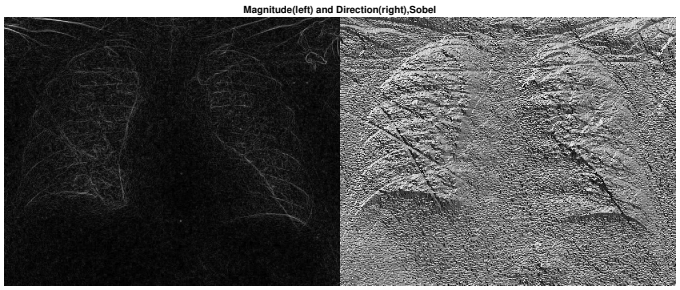

(a) Sobel Method

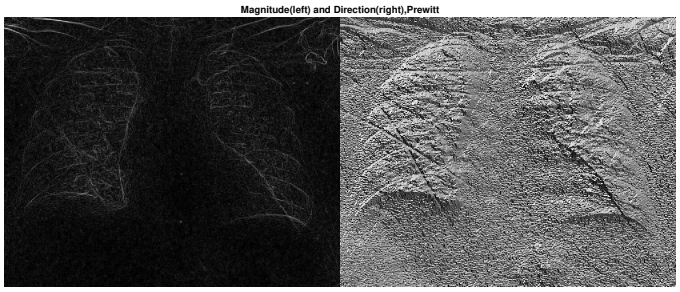

(b) Prewitt Method

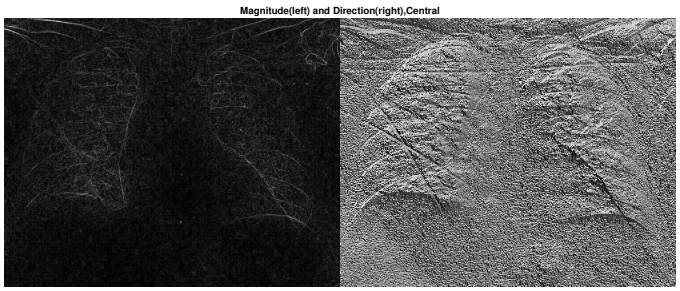

(c) Central Difference

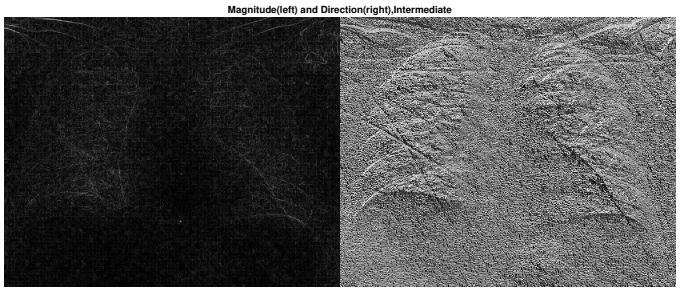

(d) Intermediate Difference

Fig. 70: X-Ray Gradient Magnitude and Direction,Day4

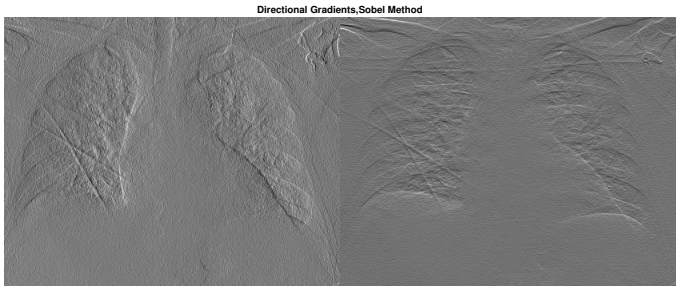

(a) Sobel Method

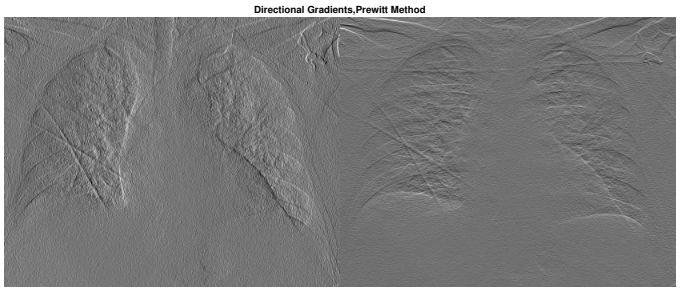

(b) Prewitt Method

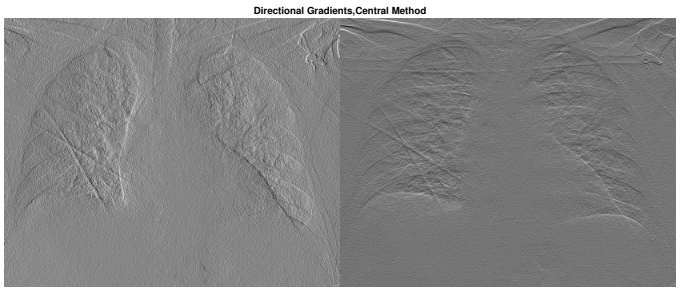

(c) Central Difference

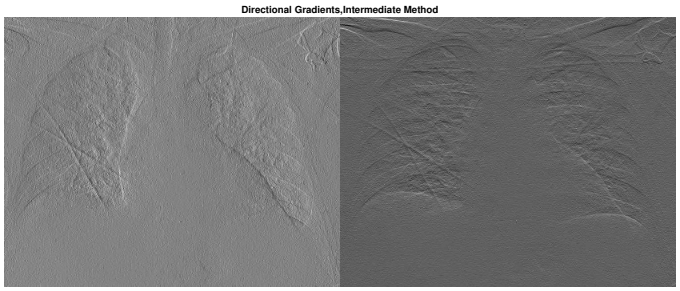

(d) Intermediate Difference

Fig. 71: Directional Gradients,Day4

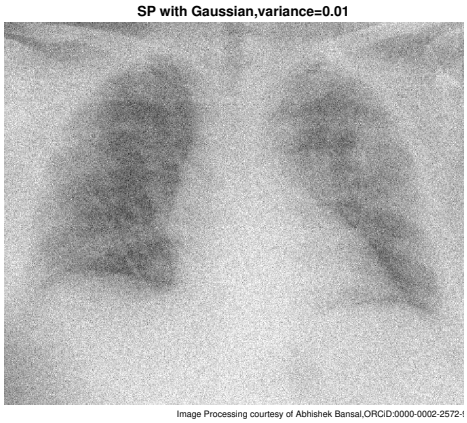

(a) Gaussian Variance = 0.01

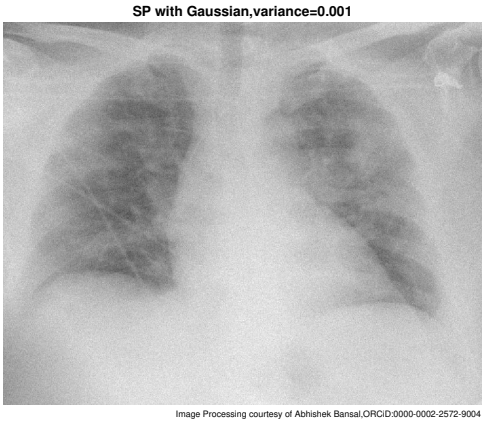

(b) Gaussian Variance = 0.001

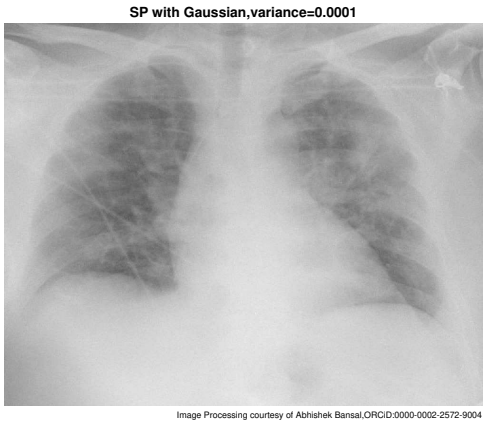

(c) Gaussian Variance = 0.0001

Fig. 72: Gaussian White Noise added to Image,Day4

(a) Gaussian Variance = 0.01

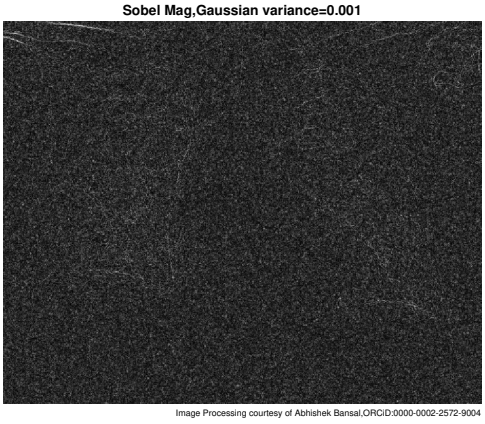

(b) Gaussian Variance = 0.001

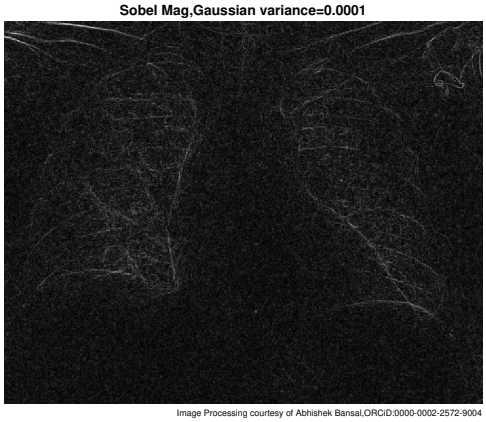

(c) Gaussian Variance = 0.0001

Fig. 73: Gradient of Noisy X-Ray using Sobel Method,Day4

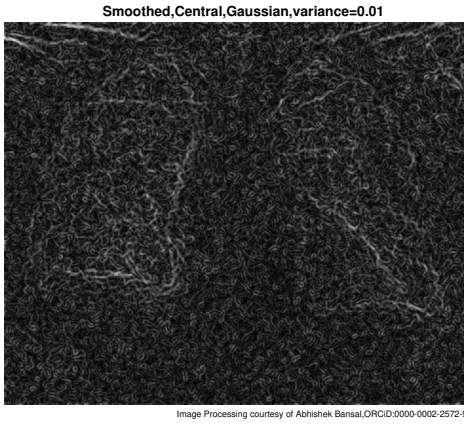

(a) Gaussian Variance = 0.01

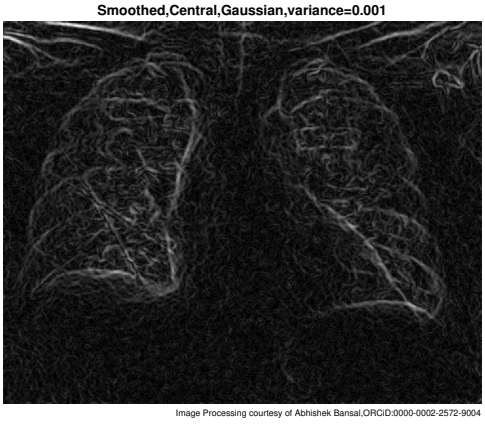

(b) Gaussian Variance = 0.001

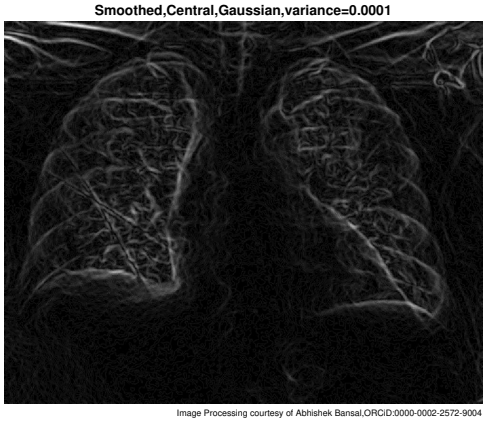

(c) Gaussian Variance = 0.0001

Fig. 74: Gaussian smoothing & central difference gradient,Day4

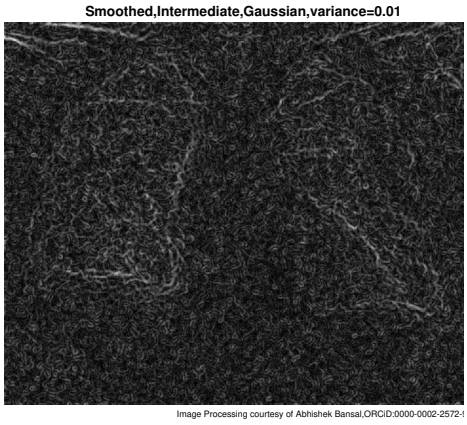

(a) Gaussian Variance = 0.01

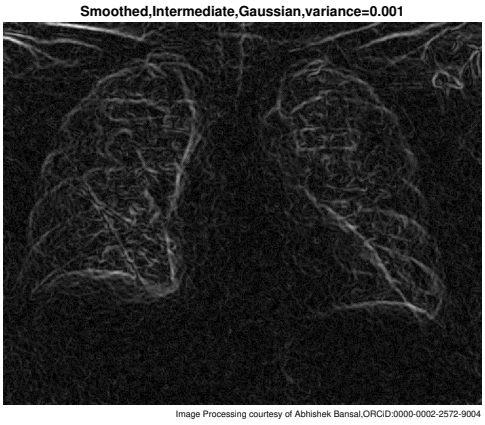

(b) Gaussian Variance = 0.001

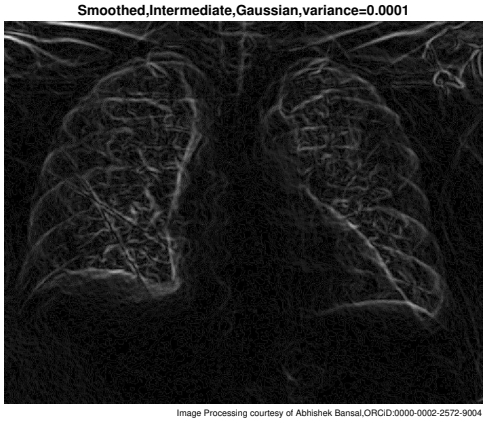

(c) Gaussian Variance = 0.0001

Fig. 75: Gaussian smoothing & intermediate difference gradient,Day4

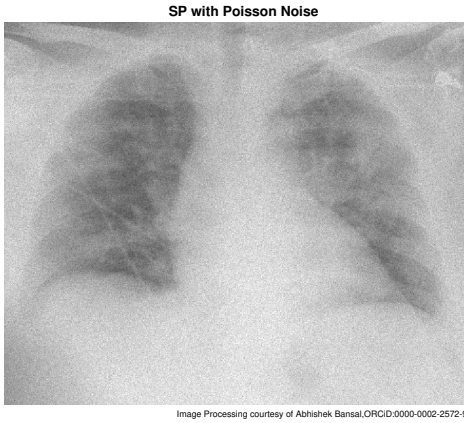

(a) Poisson Noise added

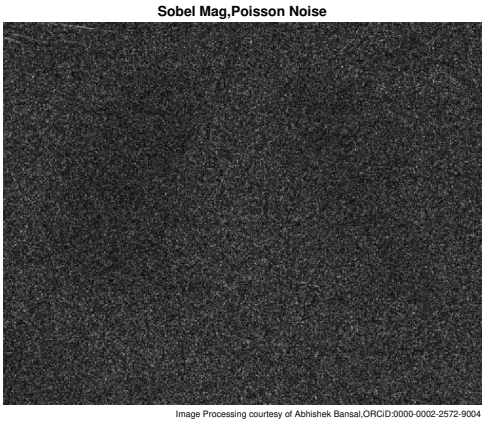

(b) Sobel Gradient Magnitude

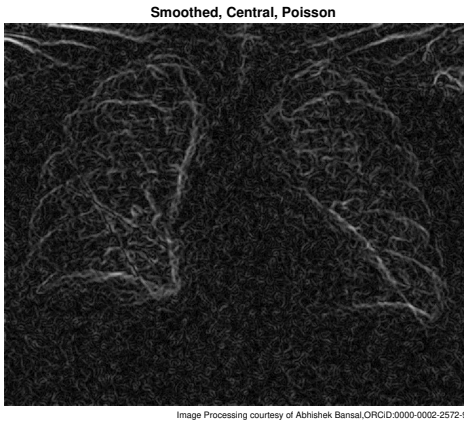

(c) Smoothed by Central Difference

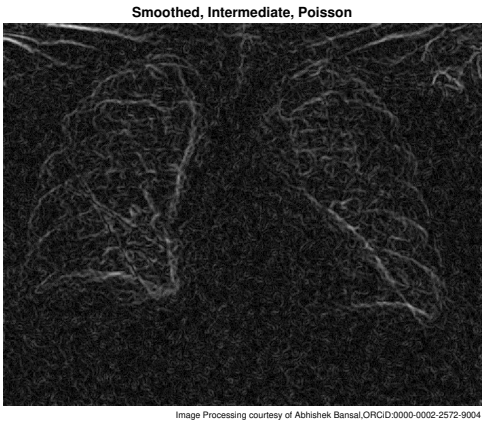

(d) Smoothed by Intermediate Difference

Fig. 76: Poisson Noise & Gradient Magnitude,Day4

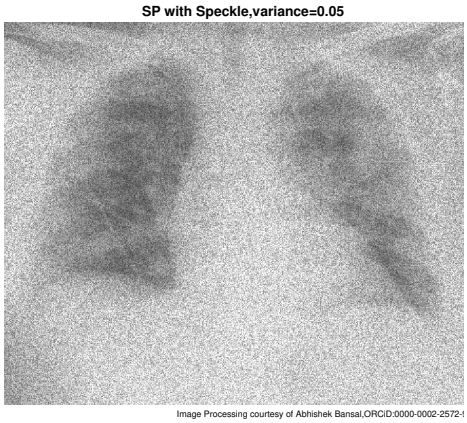

(a) Speckle Variance = 0.05

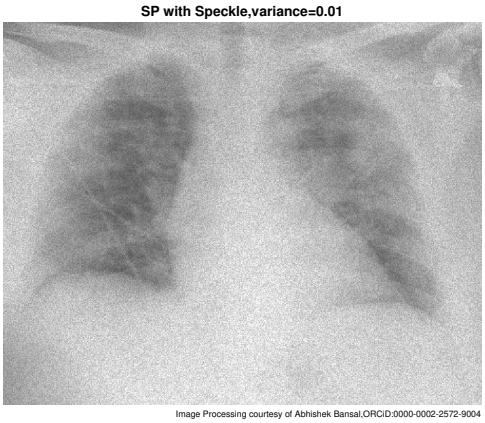

(b) Speckle Variance = 0.01

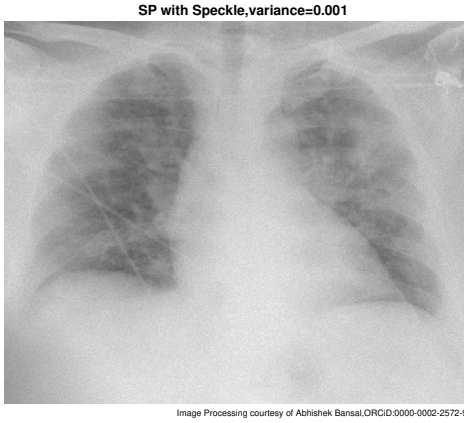

(c) Speckle Variance = 0.001

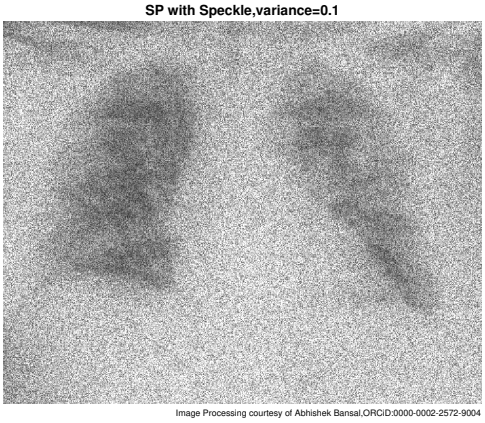

(d) Speckle Variance = 0.1

Fig. 77: Speckle Noise added to Image,Day4

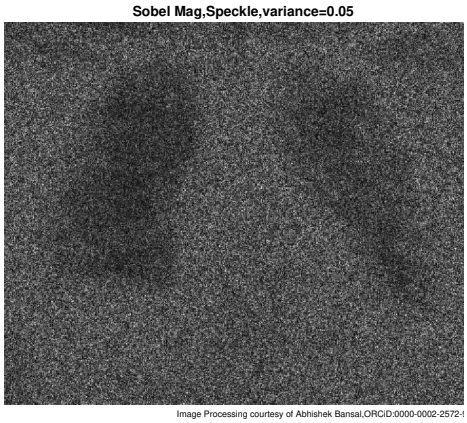

(a) Speckle Variance = 0.05

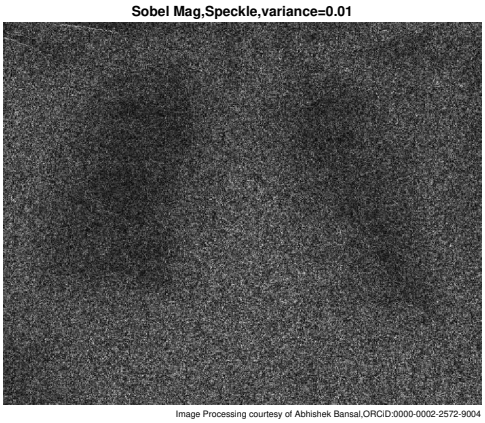

(b) Speckle Variance = 0.01

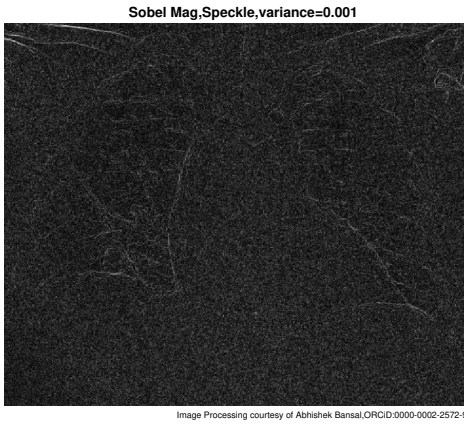

(c) Speckle Variance = 0.001

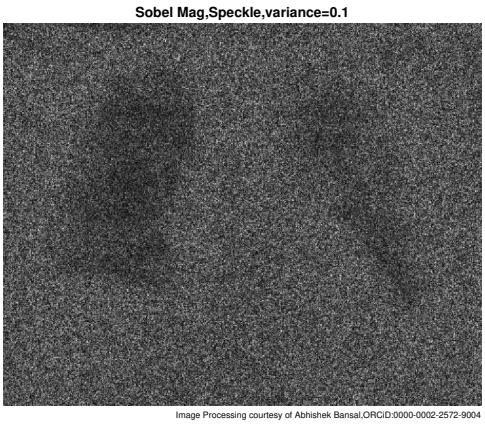

(d) Speckle Variance = 0.1

Fig. 78: Gradient of Noisy X-Ray using Sobel Method,Day4

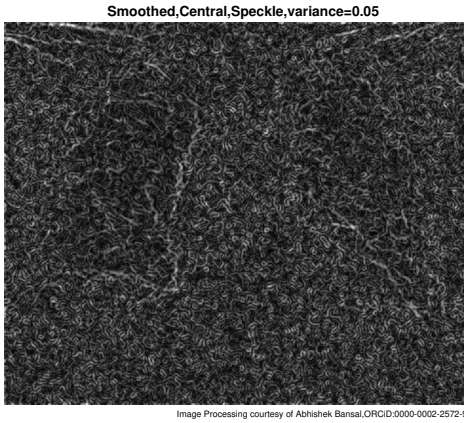

(a) Speckle Variance = 0.05

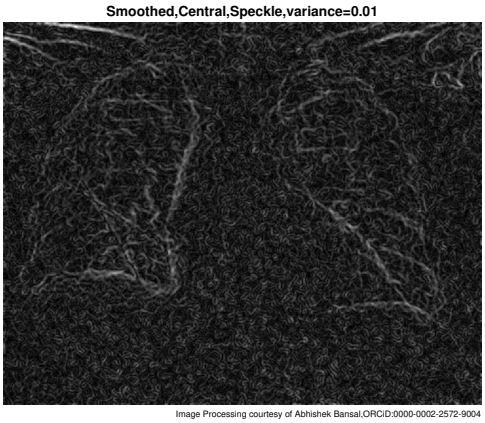

(b) Speckle Variance = 0.01

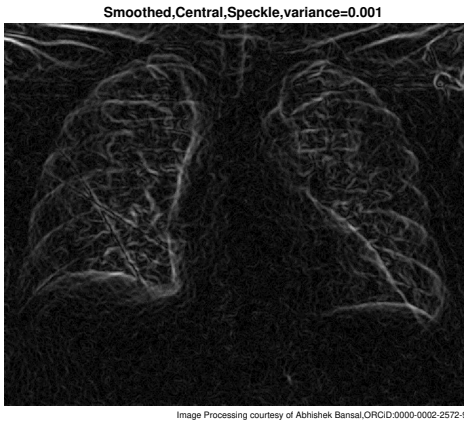

(c) Speckle Variance = 0.001

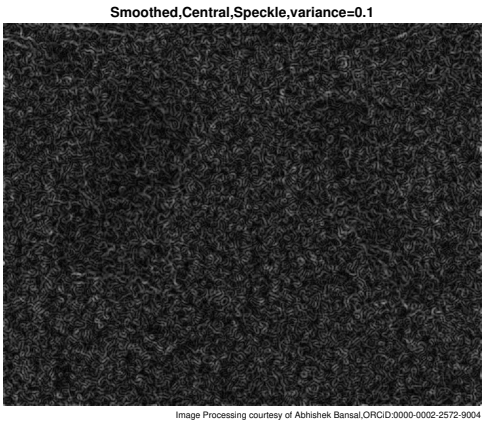

(d) Speckle Variance = 0.1

Fig. 79: Gaussian smoothing & central difference gradient,Day4

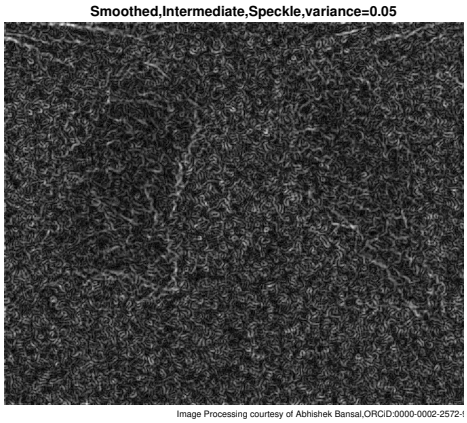

(a) Speckle Variance = 0.05

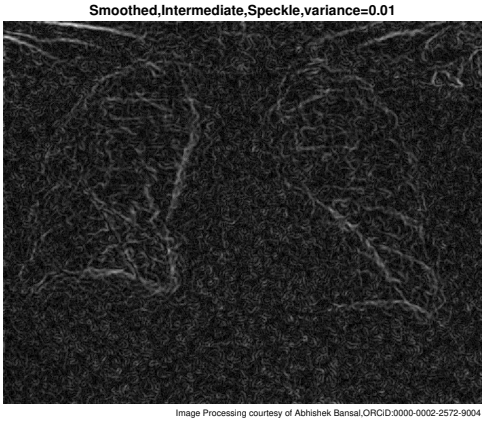

(b) Speckle Variance = 0.01

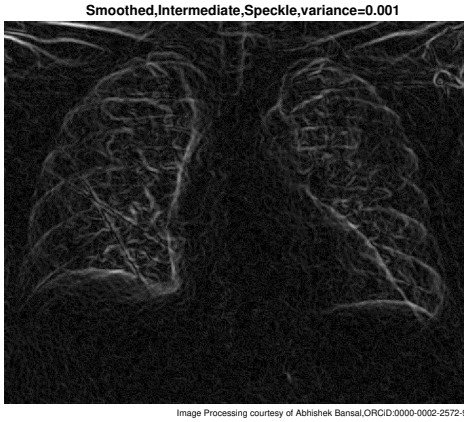

(c) Speckle Variance = 0.001

(d) Speckle Variance = 0.1

Fig. 80: Gaussian smoothing & intermediate difference gradient,Day4

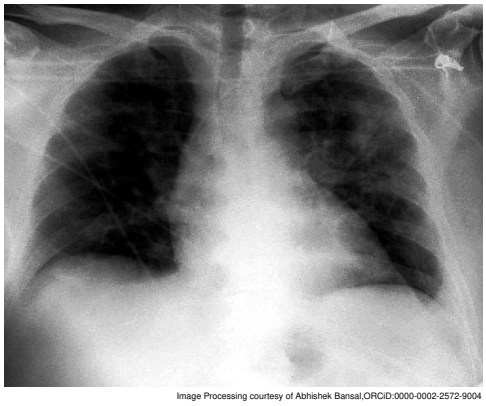

(a) X-Ray Contrast Improved

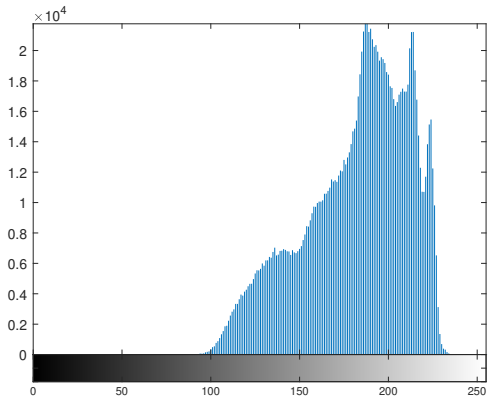

(b) Distribution of Pixel Intensities

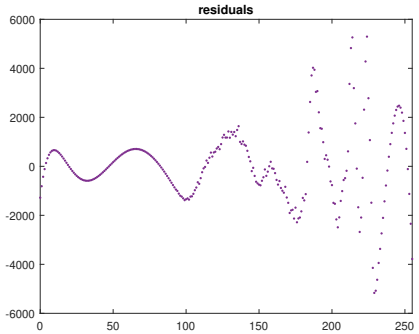

(c) Error Estimation Plot

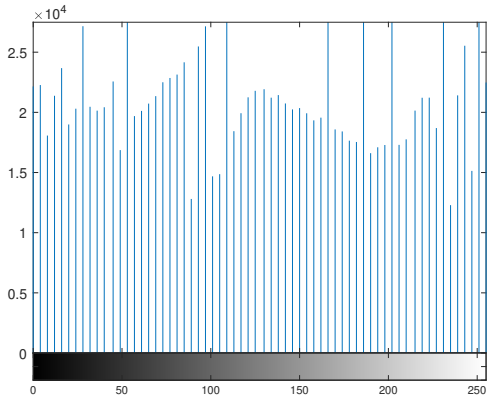

(d) X-Ray Histogram Equalization

Fig. 81: Distribution of Pixel Intensities in X-Ray,Day4

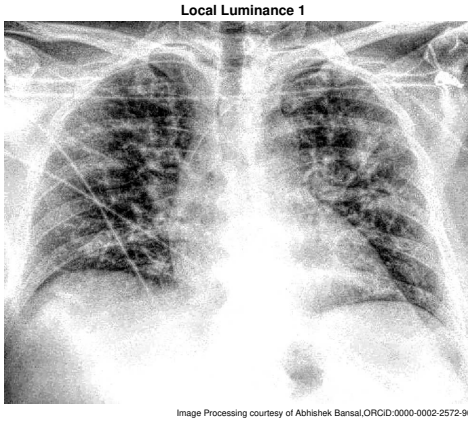

(a) X-Ray Contrast Improved 2

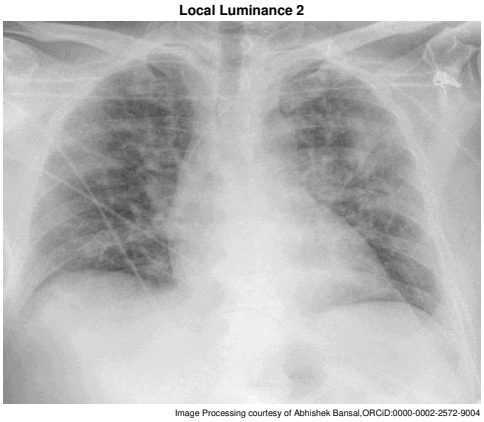

(b) X-Ray Contrast Improved 3

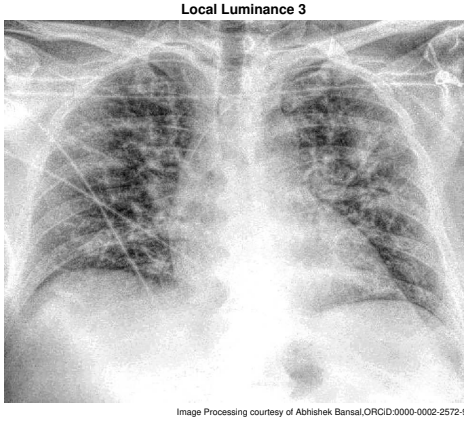

(c) X-Ray Contrast Improved 4

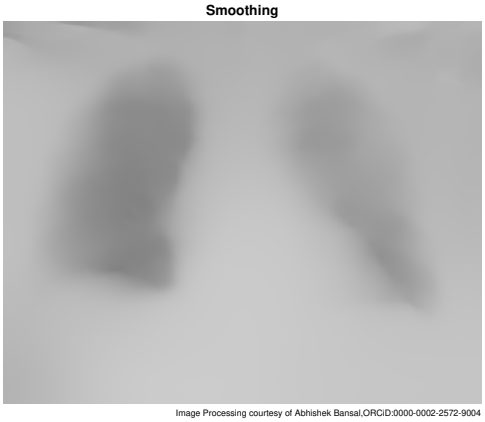

(d) X-Ray Contrast Improved & Smoothed

Fig. 82: X-Ray Contrast Improved with Five Local Luminances,Day4

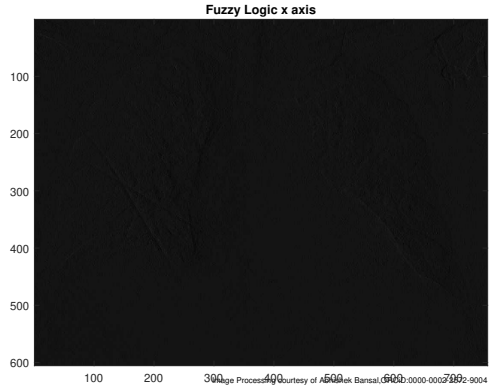

(a) x axis

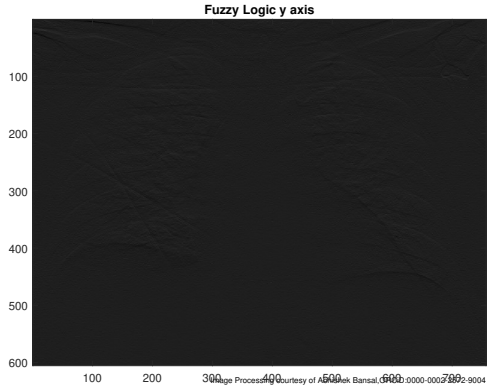

(b) y axis

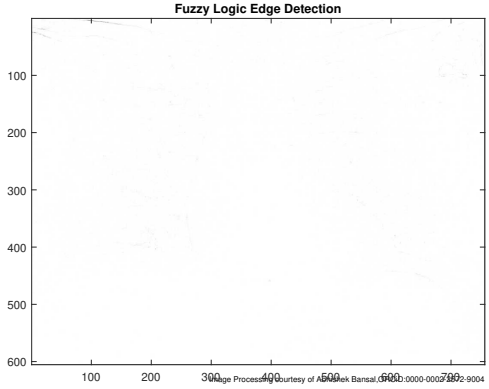

(c) Edge Detection

Fig. 83: Fuzzy Logic,Day4

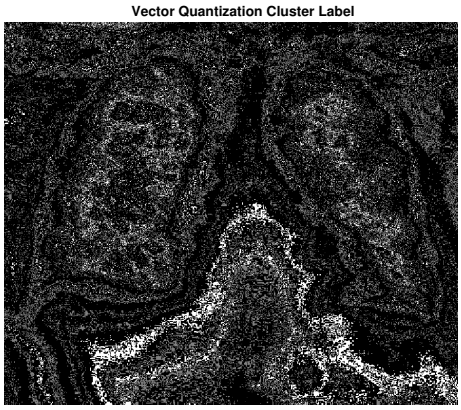

(a) Vector Quantization Cluster Label

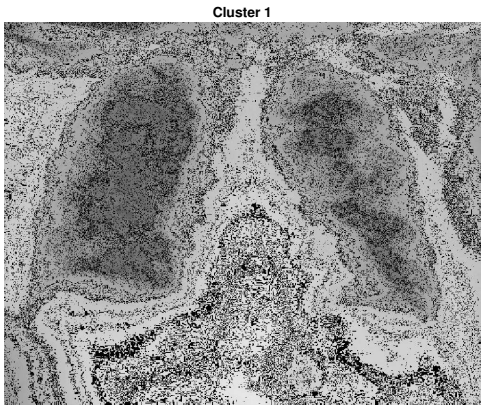

(b) Cluster 1

(c) Cluster 2

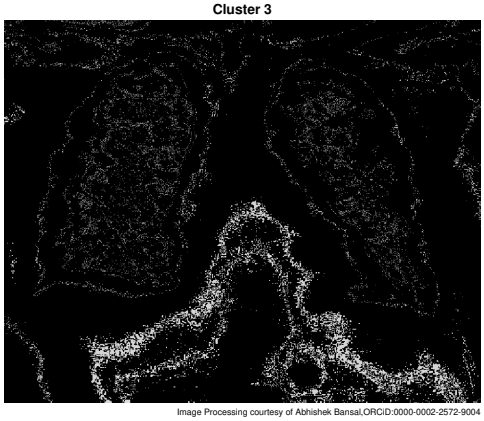

(d) Cluster 3

Fig. 84: Vector Quantization,K-means Clustering,Day4

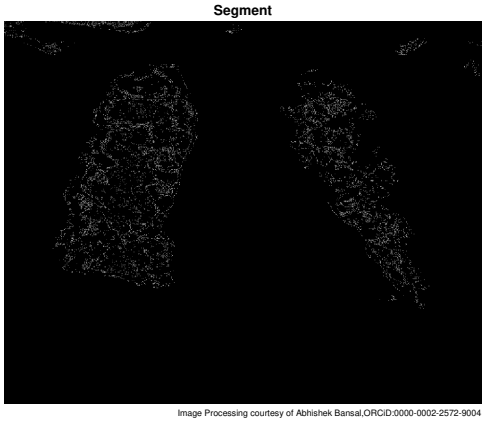

(a) Segmentation

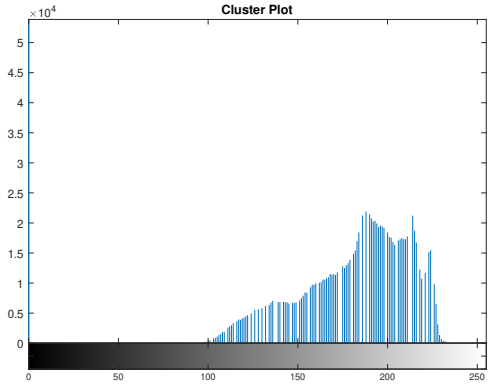

(b) Cluster Plot

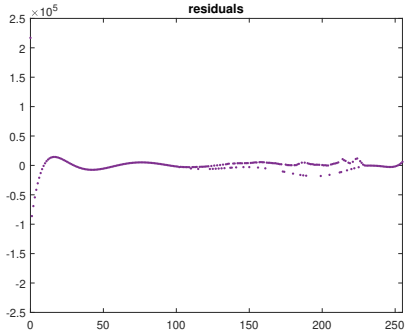

(c) Cluster Plot Residuals

Fig. 85: Clustering Plot and Segment,Day4

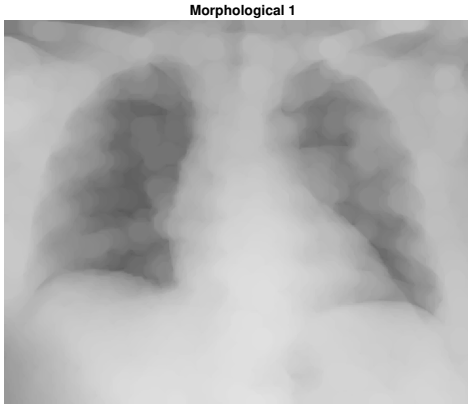

(a) Morphological Opening 1

(b) Background Approximation Removed from Fig. 19(a)

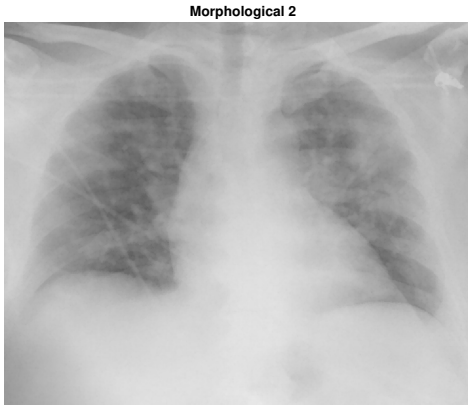

(c) [Morphological Opening 2

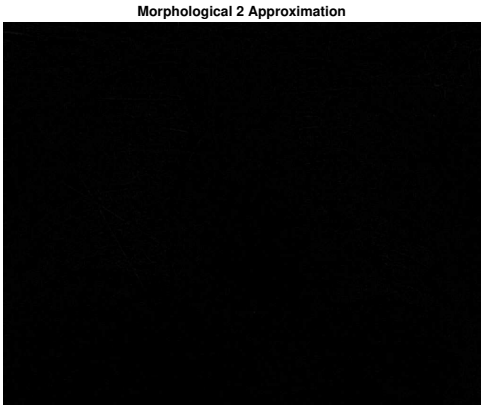

(d) Background Approximation Removed from Fig. 19(c)

Fig. 86: Morphological Segmentation,Day4

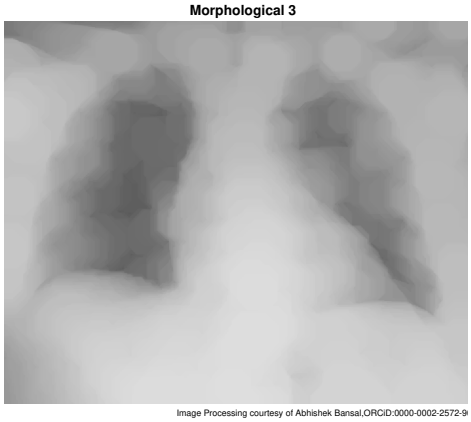

(a) Morphological Opening 3

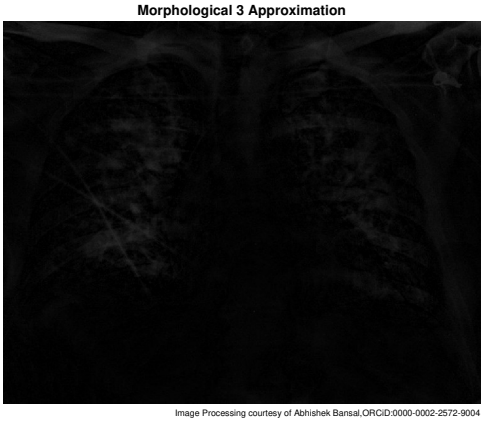

(b) Background Approximation Removed from Fig. 20(a)

Fig. 87: Morphological Segmentation,Day4

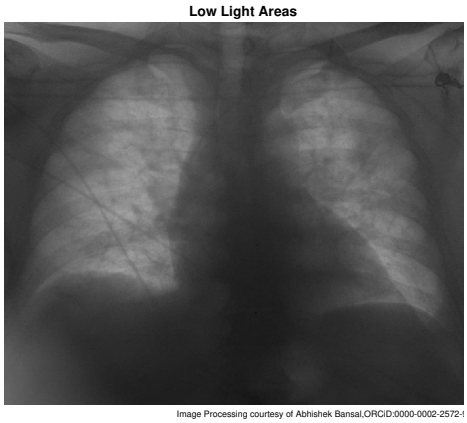

(a) X-Ray Inverted & Illuminated

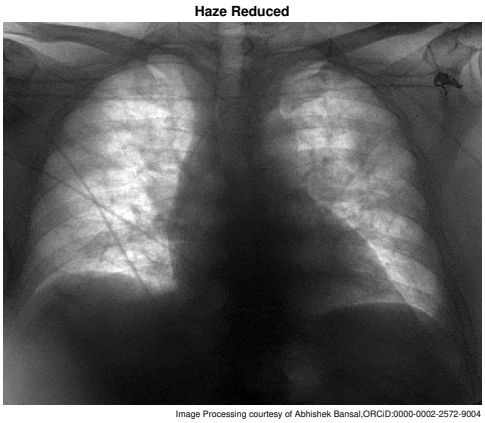

(b) Hazing Reduction Algorithm

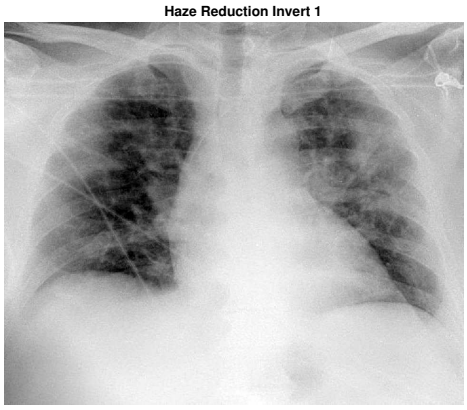

(c) Dehazing Algorithm

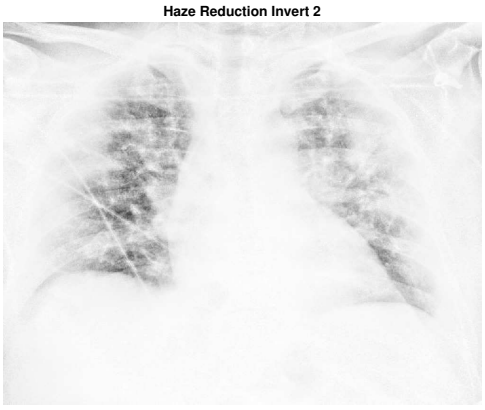

(d) Dehazing Algorithm

Fig. 88: Dehazing Algorithm,Day4

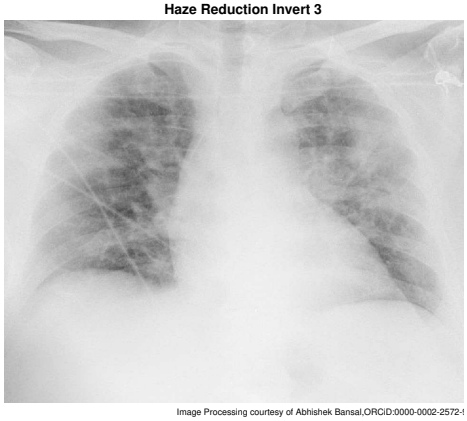

(a) Dehazing Algorithm

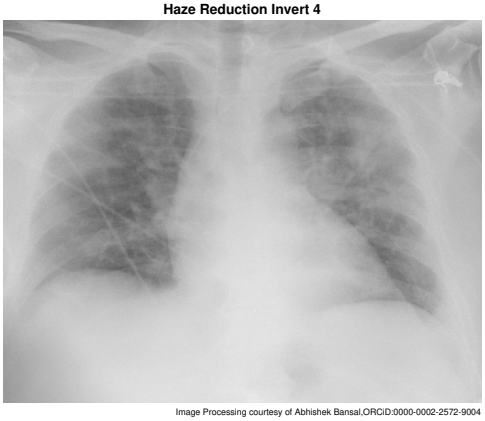

(b) Dehazing Algorithm

(c) Dehazing Algorithm

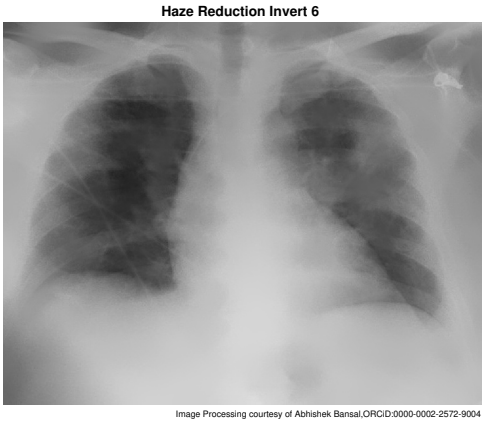

(d) Dehazing Algorithm

Fig. 89: Dehazing Algorithm,Day4

VII Results : Day 6, PA

1 X-Ray Converted

In this subsection, X-Ray(PA) of Day 6 is converted to single precision grayscale and double precision,on which all further image processings will be done. These are shown in Fig. 90.

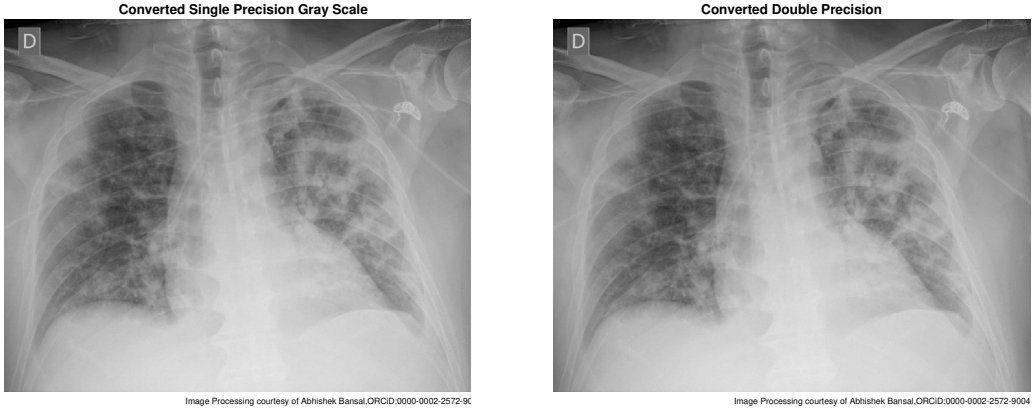

(a) Single Precision (b) Double Precision

Fig. 90: Converted to Single Precision & Double Precision,Day6

2 Double Precision Noise Addition

In this subsection, the double precision X-Ray of Day 6 (Fig 90(b)) of the previous subsection is subjected to noises namely Gaussian with variance 0.01, Poisson Noise and speckle noise with variance 0.05. These are shown in Fig. 91.

3 Gradient Magnitude and Direction

In this subsection, the gradient of the single precision X-Ray of Day 6 (Fig 90(a)) is obtained and its magnitude and direction is plotted using methods of Sobel, Prewitt, central difference and intermediate difference. These are shown in Fig. 92.

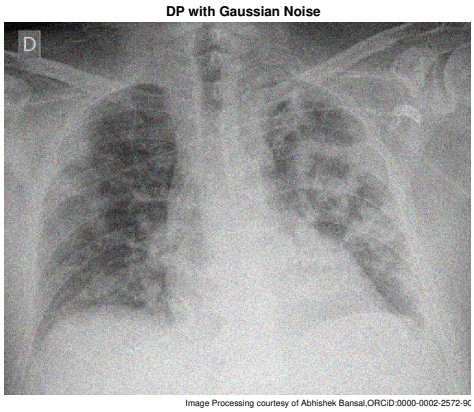

(a) Gaussian Noise

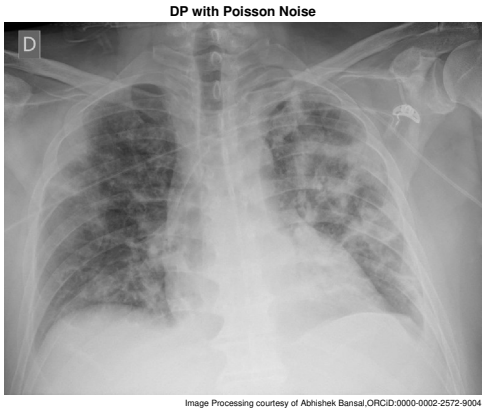

(b) Poisson Noise

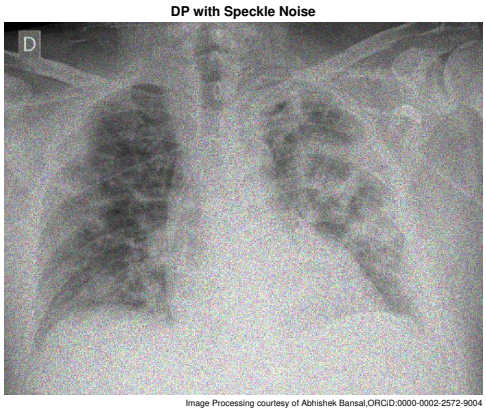

(c) Speckle Noise

Fig. 91: Noises Added to Double Precision,Day6

4 Directional Gradients

In this subsection, the directional gradient of the single precision X-Ray of Day 6 (Fig 90(a)) is plotted using methods of Sobel, Prewitt, central difference and intermediate difference. These are shown in Fig. 93.

5 Gaussian Noises & Sobel Gradient

In this subsection, the single precision X-Ray of Day 6 (Fig 90(a)) is subjected to Gaussian noise with three variances of 0.01, 0.001 and 0.0001. These are shown in Fig.

94. The gradient magnitude of these noisy X-Rays are plotted using Sobel method, which are shown in Fig. 95. The figures of gradient magnitude of Fig. 95 are further smoothed using 2-D Gaussian smoothing. The Gaussian smoothing and central difference gradient are shown in Fig. 96. The Gaussian smoothing and intermediate difference gradient are shown in Fig. 97.

6 Poisson Noise & Sobel Gradient

In this subsection, the single precision X-Ray of Day 6 (Fig 90(a)) is subjected to Poisson Noise,Fig. 98(a). The gradient magnitude of Poisson noise X-Ray is plotted using Sobel method, which are shown in Fig. 98(b). This is further smoothed using 2-D Gaussian smoothing and central difference gradient in Fig. 98(c); and 2-D Gaussian smoothing and intermediate difference gradient in Fig. 98(d).

7 Speckle Noise & Sobel Gradient

In this subsection, the single precision X-Ray of Day 6 (Fig 90(a)) is subjected to Speckle noise with four variances of 0.05, 0.01, 0.001 and 0.1. These are shown in Fig. 99[a-d]. The gradient magnitude of these noisy X-Rays are plotted using Sobel method, which are shown in Fig. 100. These are further smoothed using 2-D Gaussian smoothing. The Gaussian smoothing and central difference gradient are shown in Fig. 101. The Gaussian smoothing and intermediate difference gradient are shown in Fig. 102.

8 Pixel Intensities & Contrast

In this subsection, the original X-Ray (without converting to single precision or double precision) is contrasted for study and analysis.

Let the center fit $z = \frac{(x - 147.5)}{74.05}$, then from polynomial regression

$y = 2242 \times z^9 + 1964 \times z^8 - 1.405 \times 10^4 \times z^7 - 1.145 \times 10^4 \times z^6 + 2.975 \times 10^4 \times z^5 + 2.194 \times 10^4 \times z^4 - 2.698 \times 10^4 \times z^3 - 1.881 \times 10^4 \times z^2 + 1.266 \times 10^4 \times z + 1.133 \times 10^4$

Let $\bar{y}$ be the mean of y, $\hat{y}$ the calculated values of y, then the coefficient of determination, $R^2 = 1 - \frac{\sum_{\iota=1}^{n}(y_i - \hat{y})^2}{\sum_{\iota=1}^{n}(y_i - \bar{y})^2} = 0.9248$

The measure of the goodness of fit given by norm of residuals is 2.145×10^4. Here, the polynomial of degree 9 chosen here is the global which can be focused on the areas of interest (to be decided by infection part or researchers/doctors interest) and separate equations can be obtained for each particular area of interest. This gives insight in mathematical formulation and has been used in the Novel $\mathcal{B}$-Mathematical Modeling of Respiratory System.

TABLE IX: Data Statistics for Fig. 15(b)

	X	Y
min	0	0
max	255	1.516×10^4
mean	147.5	5516
median	147.5	4980
mode	0	0
std deviation	74.05	4898
range	255	1.516×10^4

The Fig.103(a) shows that X-Ray contrast is improved for analysis when compared

with Fig. 1(a). Fig. 103(b) shows the distribution of X-Ray pixel intensities. Fig. 103(c) shows the error estimation plot, which is the plot of the residuals. Fig. 103(d) shows the X-Ray histogram equalization which is the spreading of the intensity values over the full range.

In Fig. 104, X-Ray Contrast is improved with five local luminances. The original Fig. 90(a) X-Ray contrast is improved with four more local luminances by varying the intensity values at low and high intensities. These are shown in Fig 104(a), Fig. 104(b) and Fig. 104(c). In Fig. 104(d), the original Fig. 90(a) X-Ray is contrasted with fifth value of improvement but smoothing technique is applied after it.

9 Fuzzy Logic

In this subsection, the images obtained using fuzzy logic edge-detection algorithm and Fuzzy Inference System (FIS) are given. Two 2-D Convolution are performed. The x-axis of directional gradient is convolved with x-axis gradients of double-precision X-Ray obtained in Fig. 90(b) and the X-Ray gradient of fuzzy logic x-axis is given in Fig. 105(a). The y-axis of directional gradient is convolved with y-axis gradients of double-precision X-Ray obtained in Fig. 90(b) and the X-Ray gradient of fuzzy logic y-axis is given in Fig. 105(b). The edge detection is shown in Fig. 105(c).

10 K-means Clustering

In this subsection, the popular vector quantization technique of K-Means clustering is applied to X-Ray. In this technique, firstly CIE XYZ tristimulus technique is used to know the color information and thus, the information of luminosity layer

'L*', chromaticity-layer 'a*' and chromaticity-layer 'b*' is obtained. Then every pixel is clustered with its pixel label and partitioned into three clusters. The clustering obtained is shown in Fig. 106(a), Vector Quantization Cluster Label. And three clusters Cluster 1, Cluster 2 and Cluster 3 obtained are shown in Fig. 106(b), Fig. 106(c) and Fig. 106(d) respectively.

In Fig. 107(a), segmentation is applied and Fig. 107(b) and Fig. 107(c) shows respectively the cluster plot and the plot of error estimation, that is, the plot of residuals.

Moving in similar way as in the *Subsection-8* and choosing same $z = \frac{(x - 147.5)}{74.05}$, we have

$y = -7238 \times z^9 + 8947 \times z^8 + 3.917 \times 10^4 \times z^7 - 4.471 \times 10^4 \times z^6 - 7.035 \times 10^4 \times z^5 + 6.906 \times 10^4 \times z^4 + 4.169 \times 10^4 \times z^3 - 3.767 \times 10^4 \times z^2 - 1211 \times z + 1.086 \times 10^4$

$R^2 = 0.3247$ and Norm of Residuals $= 1.806 \times 10^5$

TABLE X: Data Statistics for Fig. 18(b)

	X	Y
min	0	0
max	255	2.108×10^5
mean	147.5	5516
median	147.5	3735
mode	0	0
std deviation	74.05	1.376×10^4
range	255	2.108×10^5

11 Morphological Segmentation

In this subsection, known morphological segmentation technique is applied on X-Rays. Three morphological openings are used. The morphological opening with struc-

turing element of disk shaped with three different radius are shown in Fig. 108(a), Fig. 108(c) and Fig. 109(a). The background approximation images of X-Ray obtained after subtracting from the original image are shown in Fig. 108(b), Fig. 108(d) and Fig. 109(b).

12 Dehazing Algorithm

In Fig. 110(a), the original Fig. 90(a) X-Ray is inverted and the low-light areas and focused and the new X-Ray is obtained. The hazing obtained in Fig. 110(a) is reduced by hazing reduction algorithm.

On the new X-Ray of Fig. 110(b), dehazing algorithm is applied and its result is in Fig.110(c,d). Fig. 111[a-d] hs four more such combinations on which dehazing algorithm is implemented.

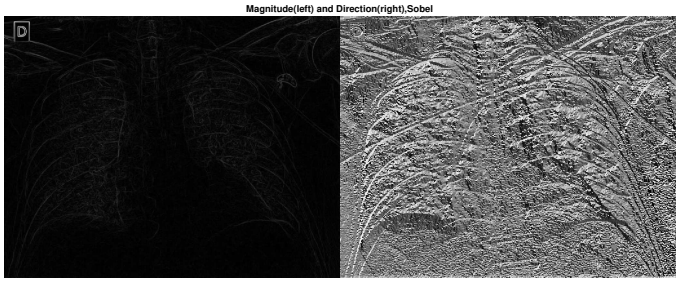

(a) Sobel Method

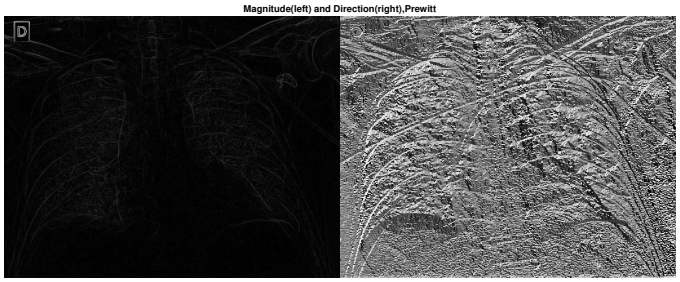

(b) Prewitt Method

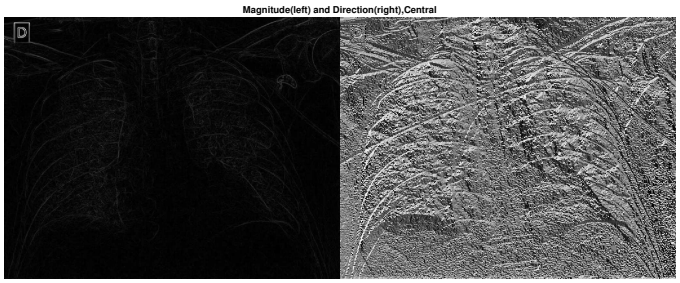

(c) Central Difference

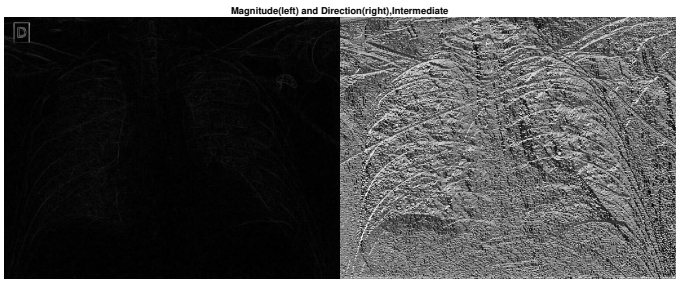

(d) Intermediate Difference

Fig. 92: X-Ray Gradient Magnitude and Direction,Day6

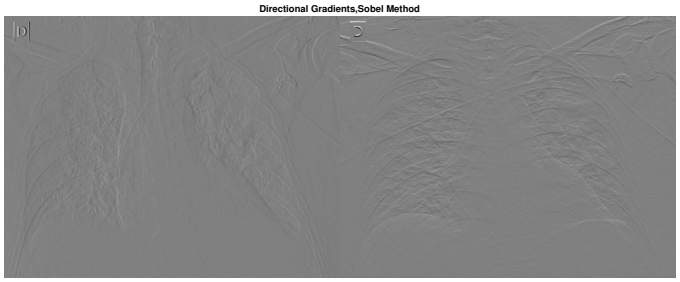

(a) Sobel Method

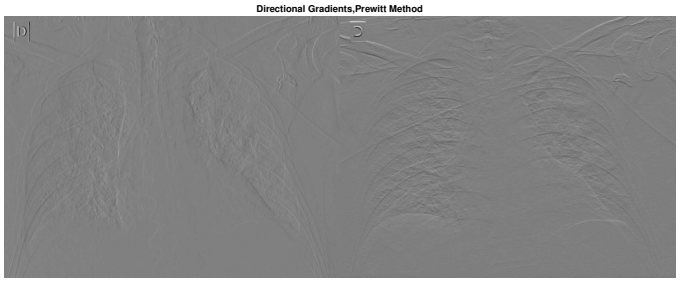

(b) Prewitt Method

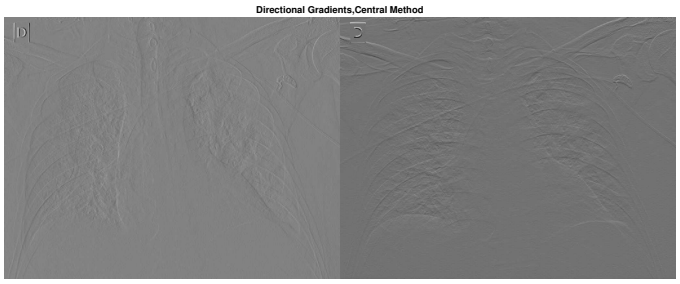

(c) Central Difference

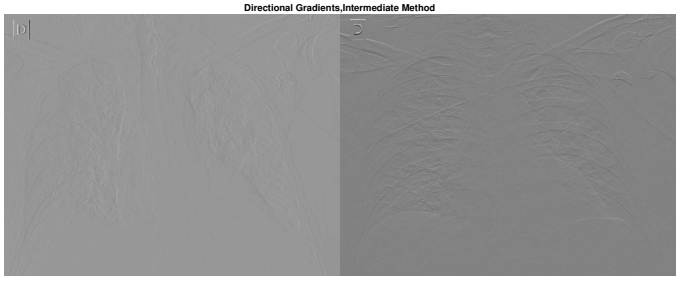

(d) Intermediate Difference

Fig. 93: Directional Gradients,Day6

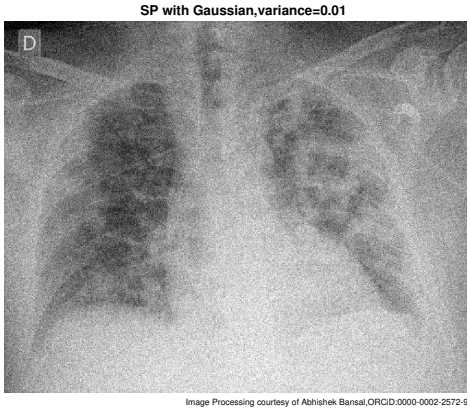

(a) Gaussian Variance = 0.01

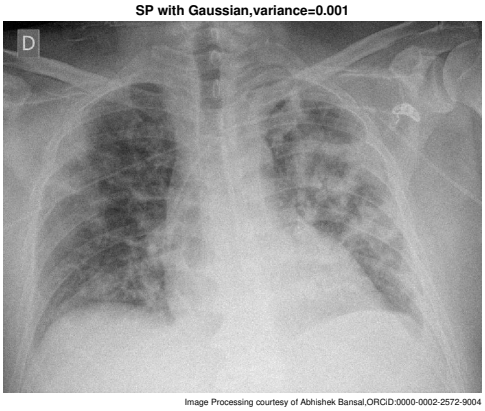

(b) Gaussian Variance = 0.001

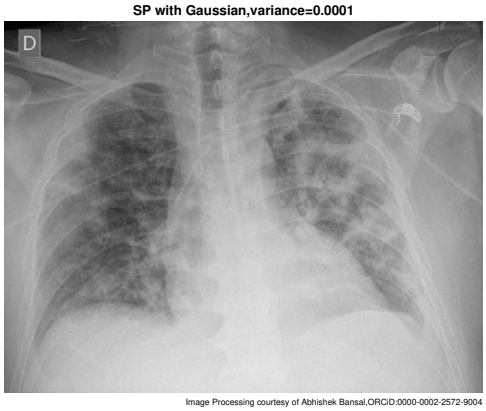

(c) Gaussian Variance = 0.0001

Fig. 94: Gaussian White Noise added to Image,Day6

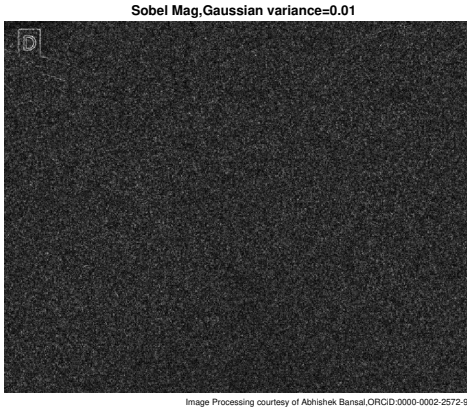

(a) Gaussian Variance = 0.01

(b) Gaussian Variance = 0.001

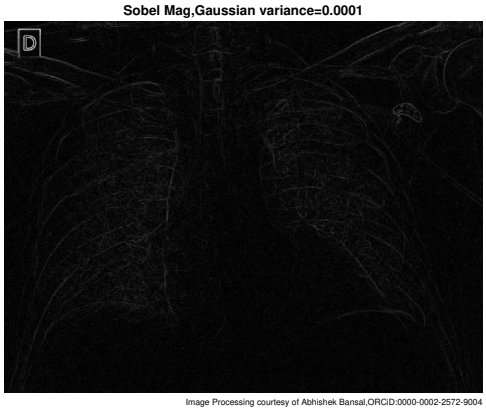

(c) Gaussian Variance = 0.0001

Fig. 95: Gradient of Noisy X-Ray using Sobel Method,Day6

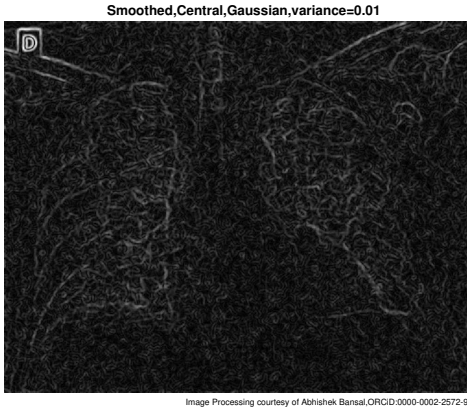

(a) Gaussian Variance = 0.01

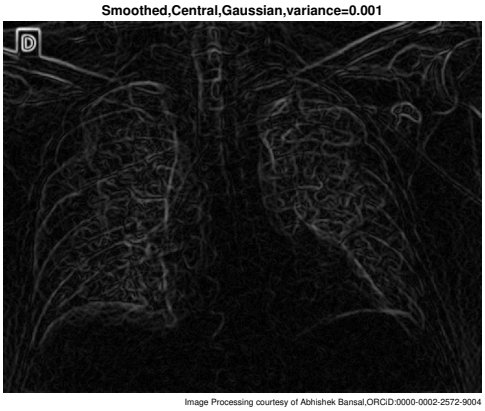

(b) Gaussian Variance = 0.001

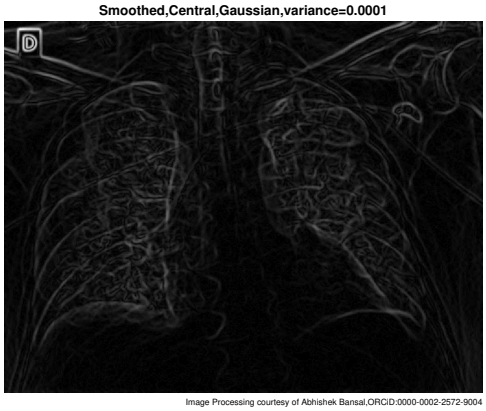

(c) Gaussian Variance = 0.0001

Fig. 96: Gaussian smoothing & central difference gradient,Day6

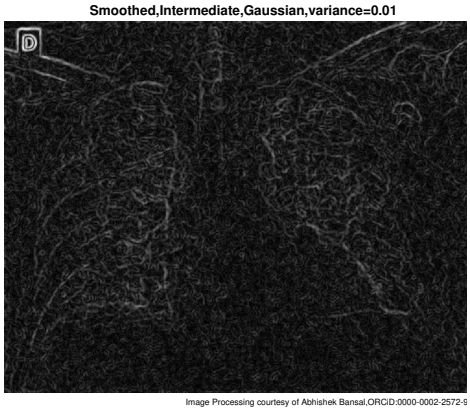

(a) Gaussian Variance = 0.01

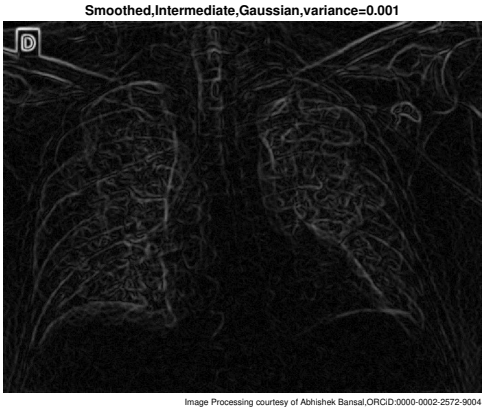

(b) Gaussian Variance = 0.001

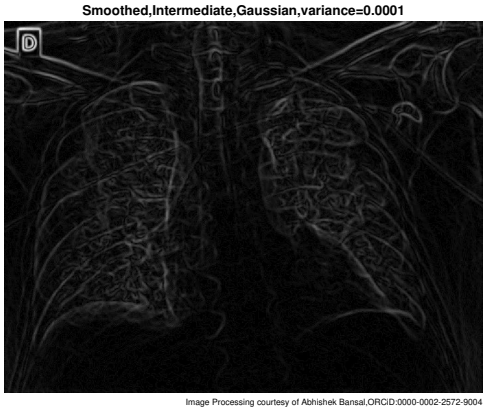

(c) Gaussian Variance = 0.0001

Fig. 97: Gaussian smoothing & intermediate difference gradient,Day6

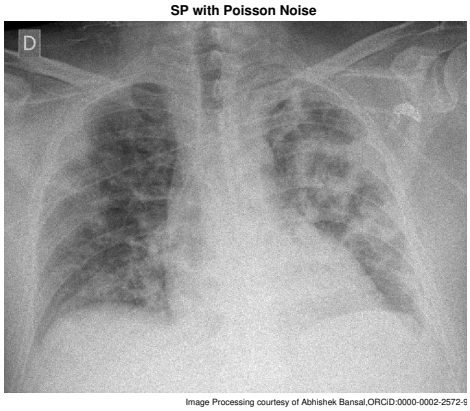

(a) Poisson Noise added

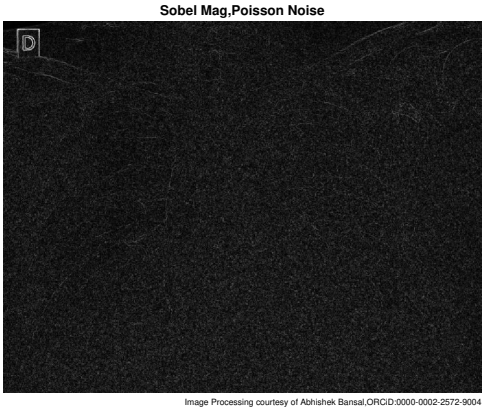

(b) Sobel Gradient Magnitude

(c) Smoothed by Central Difference

(d) Smoothed by Intermediate Difference

Fig. 98: Poisson Noise & Gradient Magnitude,Day6

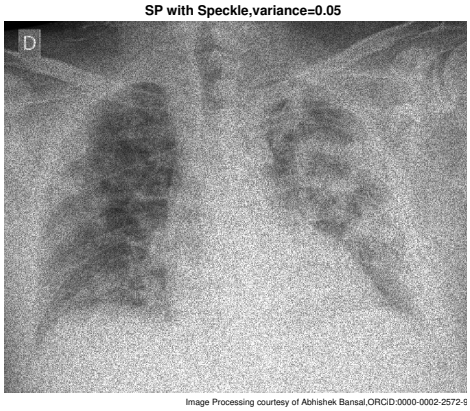

(a) Speckle Variance = 0.05

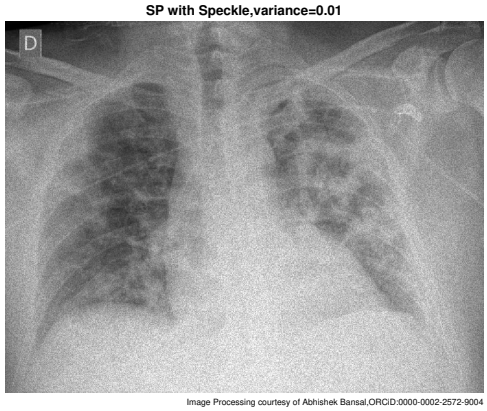

(b) Speckle Variance = 0.01

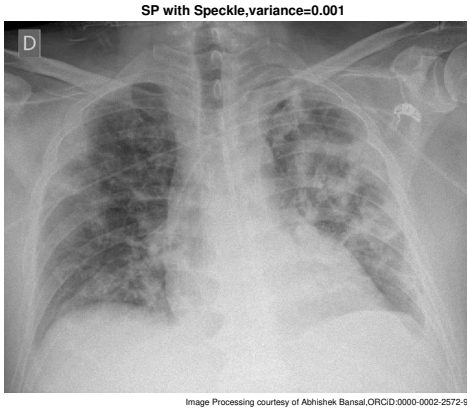

(c) Speckle Variance = 0.001

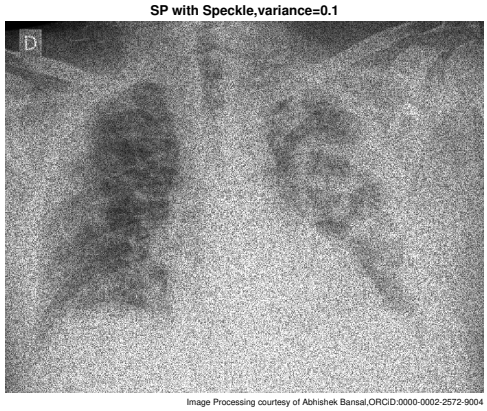

(d) Speckle Variance = 0.1

Fig. 99: Speckle Noise added to Image,Day6

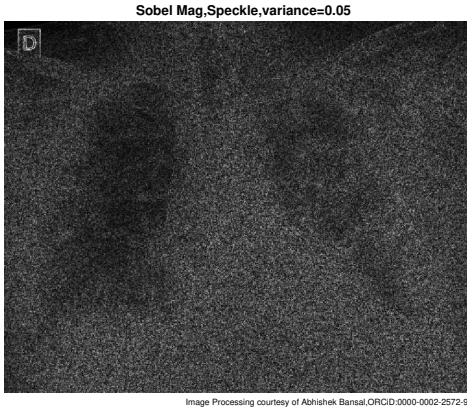

(a) Speckle Variance = 0.05

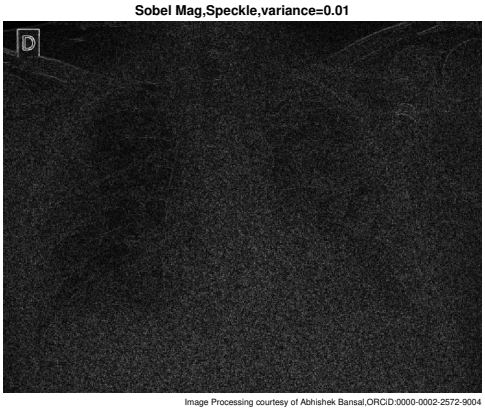

(b) Speckle Variance = 0.01

(c) Speckle Variance = 0.001

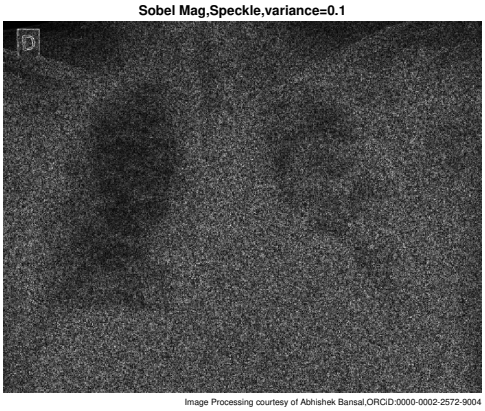

(d) Speckle Variance = 0.1

Fig. 100: Gradient of Noisy X-Ray using Sobel Method,Day6

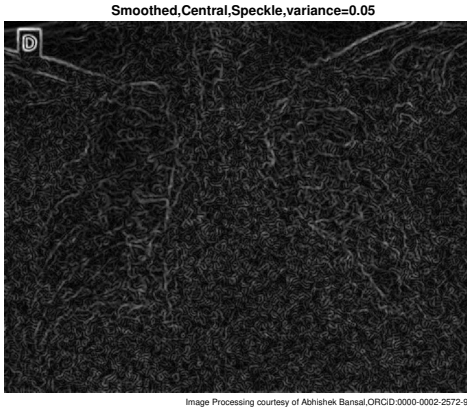

(a) Speckle Variance = 0.05

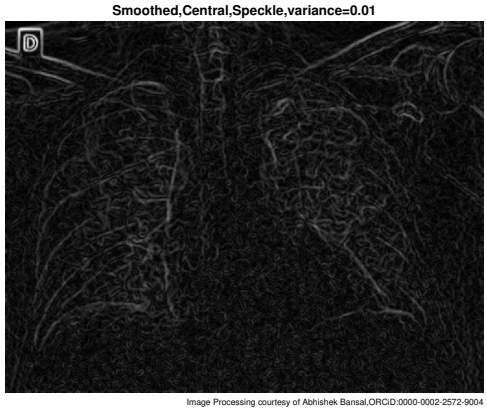

(b) Speckle Variance = 0.01

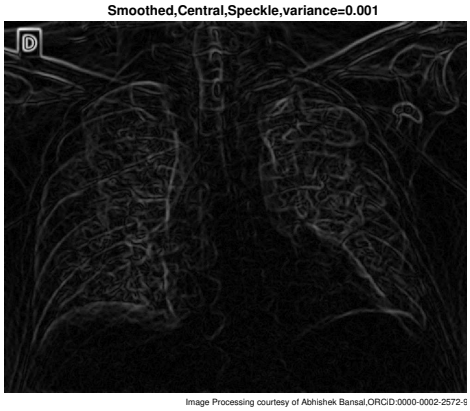

(c) Speckle Variance = 0.001

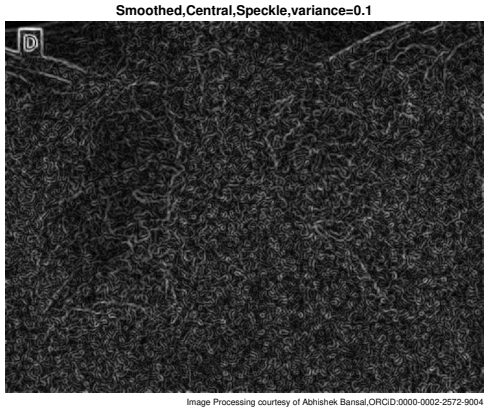

(d) Speckle Variance = 0.1

Fig. 101: Gaussian smoothing & central difference gradient,Day6

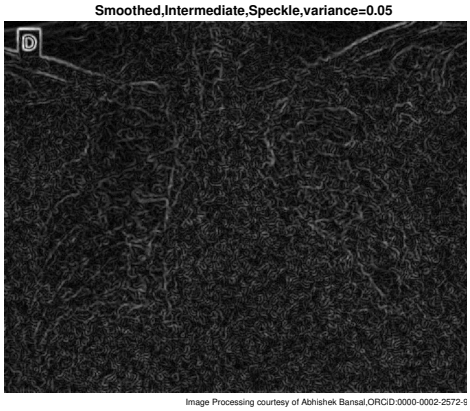

(a) Speckle Variance = 0.05

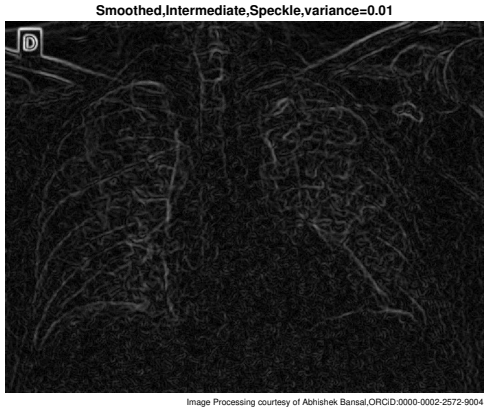

(b) Speckle Variance = 0.01

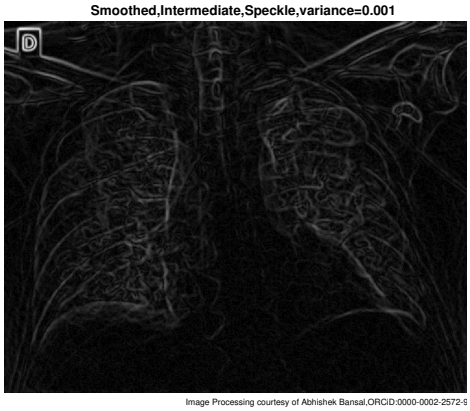

(c) Speckle Variance = 0.001

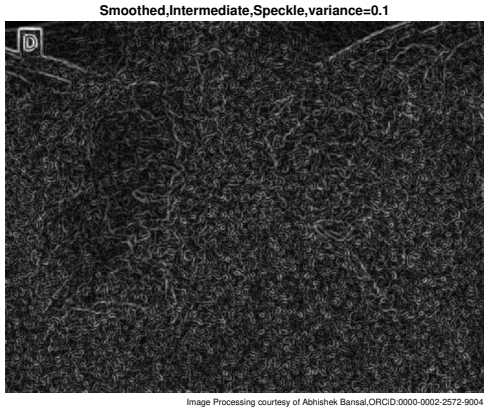

(d) Speckle Variance = 0.1

Fig. 102: Gaussian smoothing & intermediate difference gradient,Day6

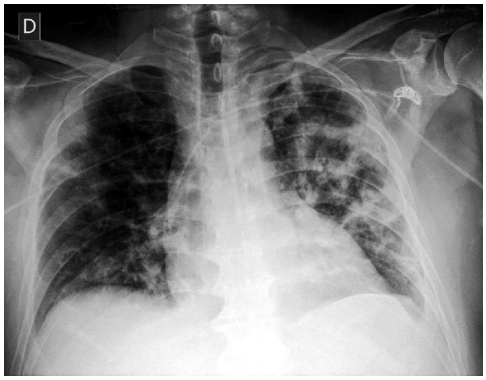

(a) X-Ray Contrast Improved

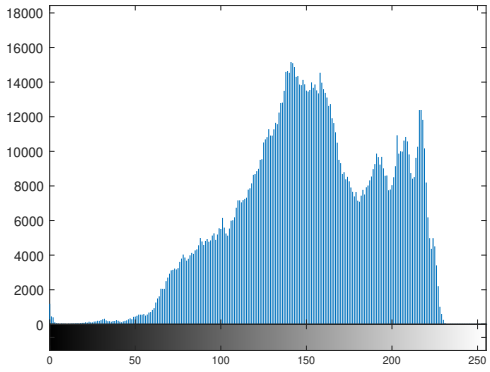

(b) Distribution of Pixel Intensities

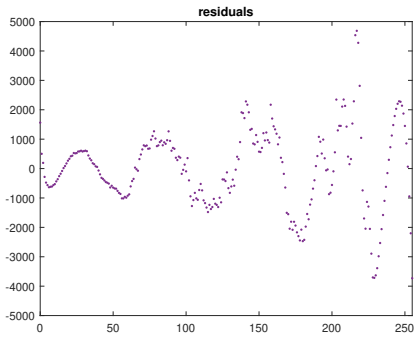

(c) Error Estimation Plot

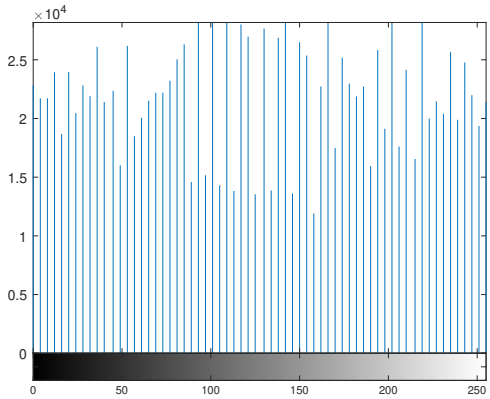

(d) X-Ray Histogram Equalization

Fig. 103: Distribution of Pixel Intensities in X-Ray,Day6

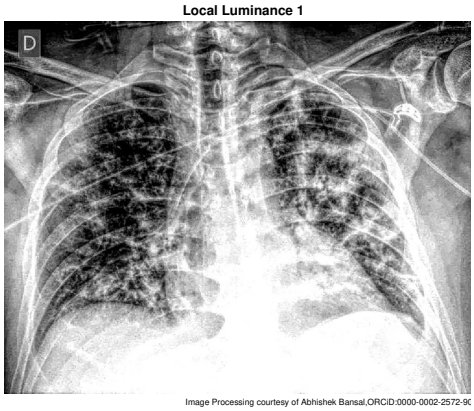

(a) X-Ray Contrast Improved 2

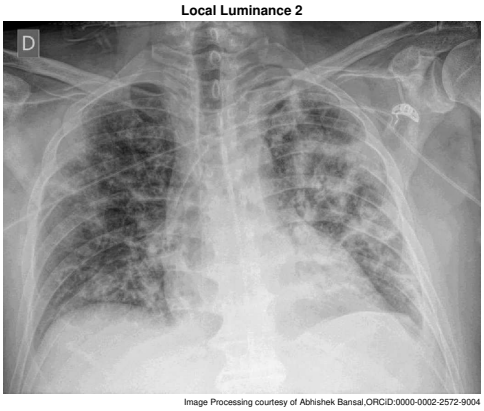

(b) X-Ray Contrast Improved 3

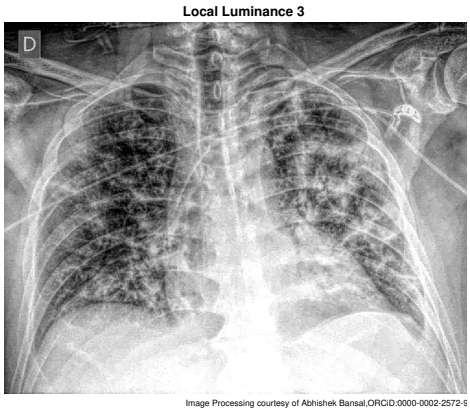

(c) X-Ray Contrast Improved 4

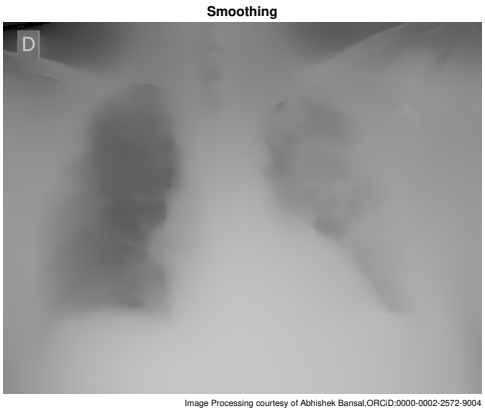

(d) X-Ray Contrast Improved & Smoothed

Fig. 104: X-Ray Contrast Improved with Five Local Luminances,Day6

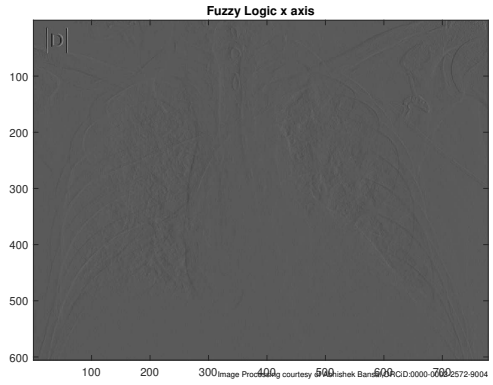

(a) x axis

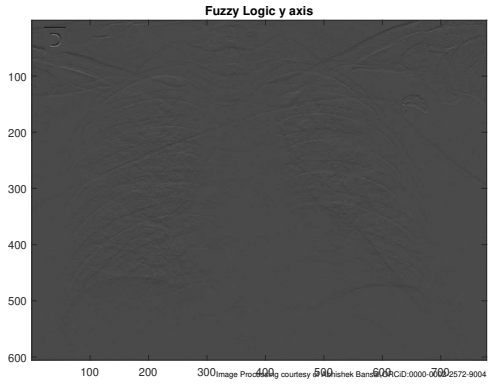

(b) y axis

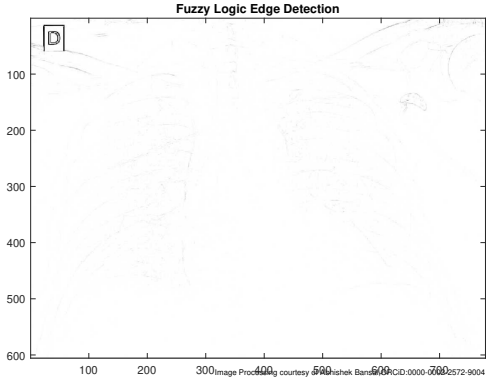

(c) Edge Detection

Fig. 105: Fuzzy Logic,Day6

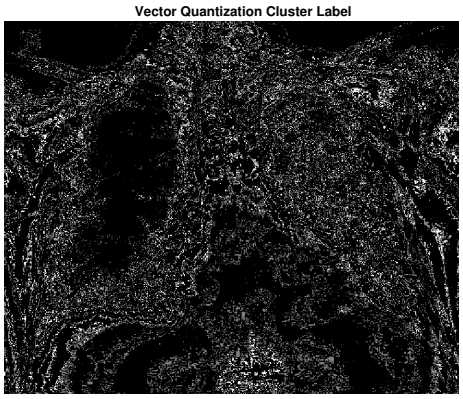

(a) Vector Quantization Cluster Label

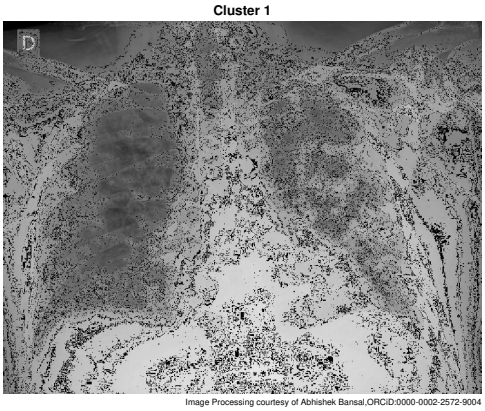

(b) Cluster 1

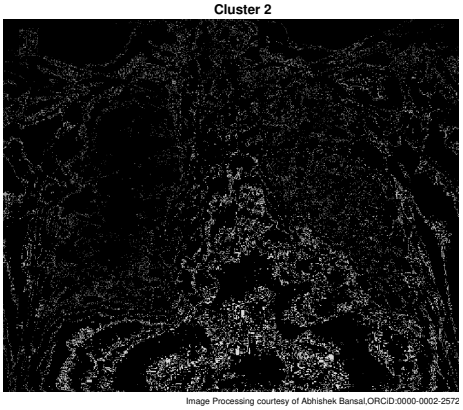

(c) Cluster 2

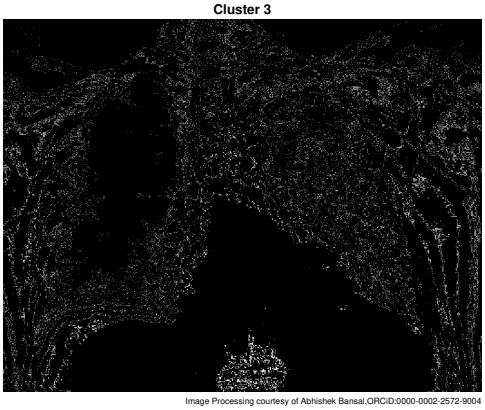

(d) Cluster 3

Fig. 106: Vector Quantization,K-means Clustering,Day6

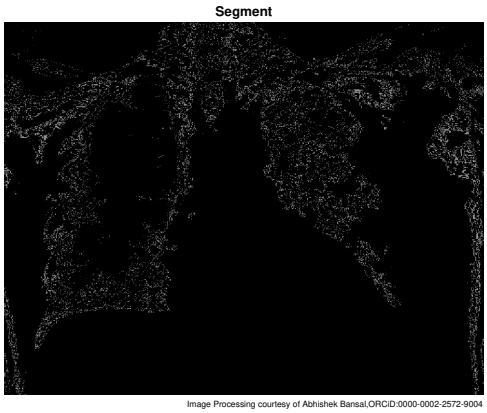

(a) Segmentation

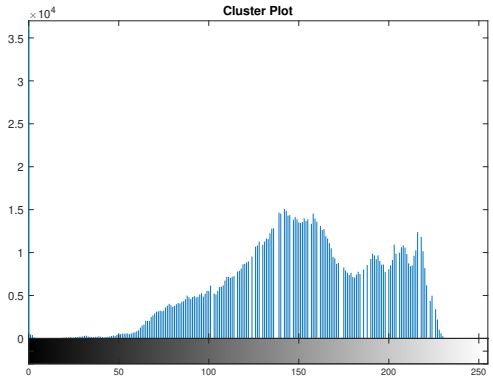

(b) Cluster Plot

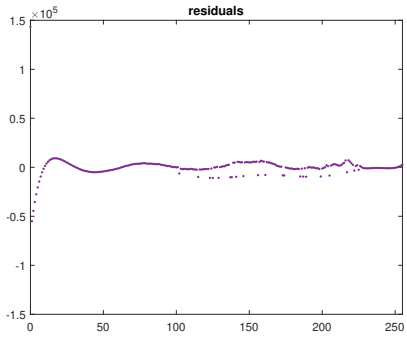

(c) Cluster Plot Residuals

Fig. 107: Clustering Plot and Segment,Day6

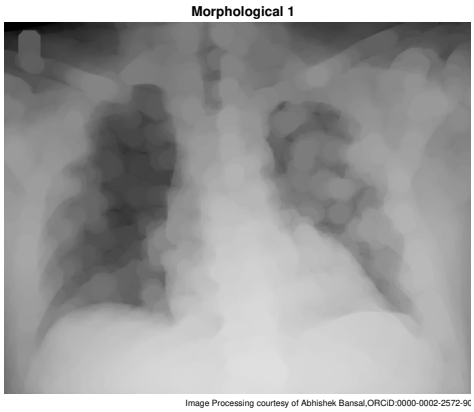

(a) Morphological Opening 1

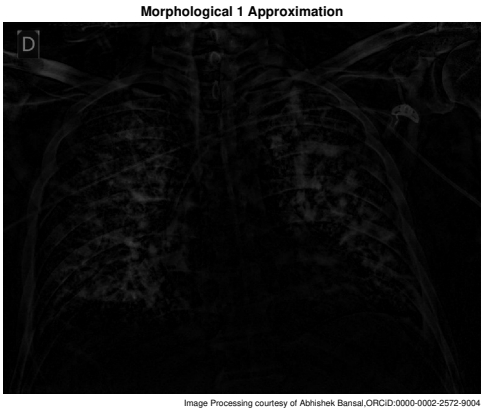

(b) Background Approximation Removed from Fig. 19(a)

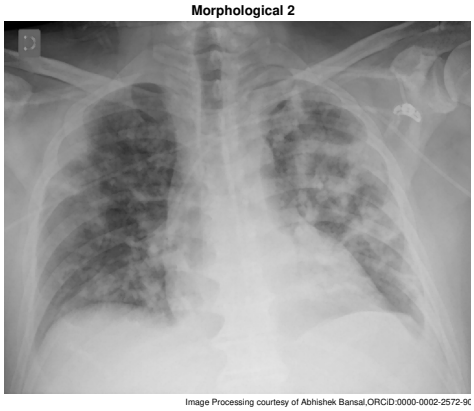

(c) [Morphological Opening 2

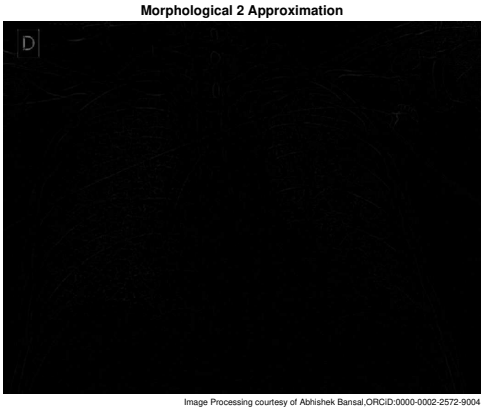

(d) Background Approximation Removed from Fig. 19(c)

Fig. 108: Morphological Segmentation,Day6

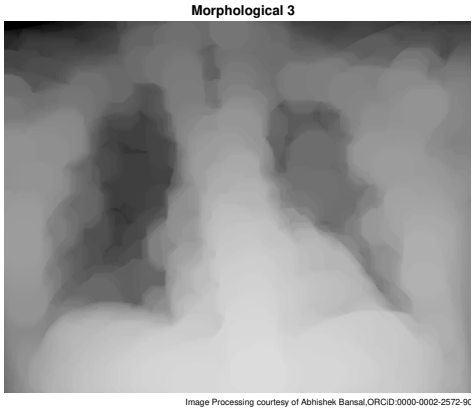

(a) Morphological Opening 3

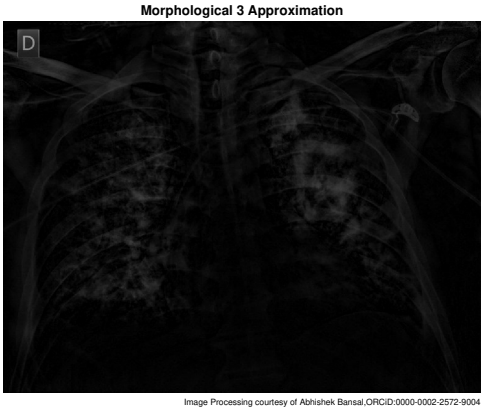

(b) Background Approximation Removed from Fig. 20(a)

Fig. 109: Morphological Segmentation,Day6

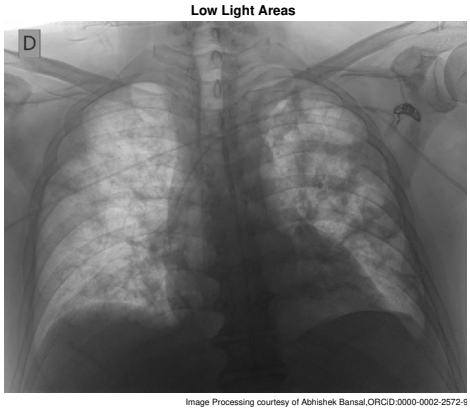

(a) X-Ray Inverted & Illuminated

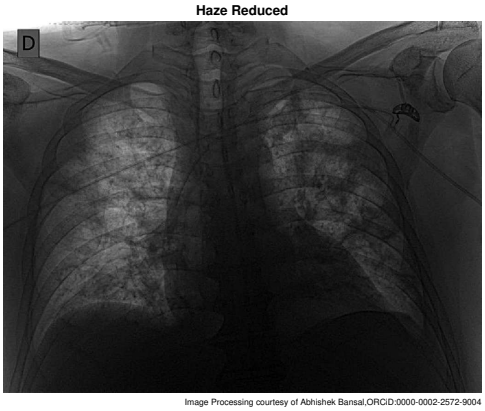

(b) Hazing Reduction Algorithm

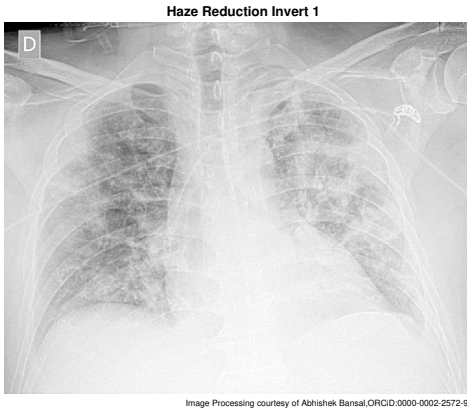

(c) Dehazing Algorithm

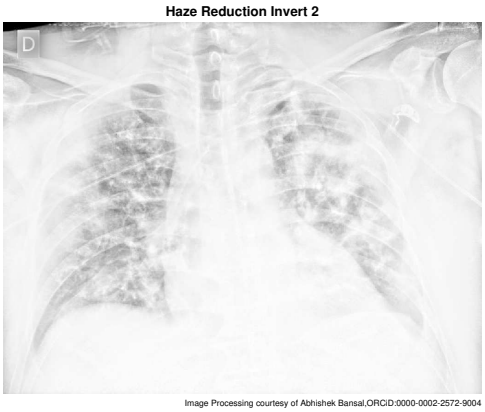

(d) Dehazing Algorithm

Fig. 110: Dehazing Algorithm,Day6

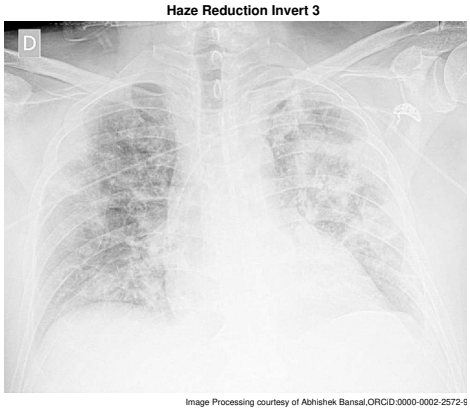

(a) Dehazing Algorithm

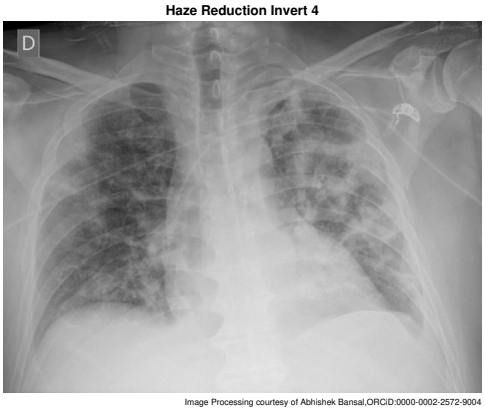

(b) Dehazing Algorithm

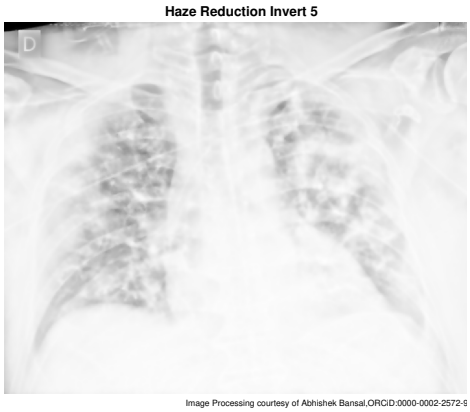

(c) Dehazing Algorithm

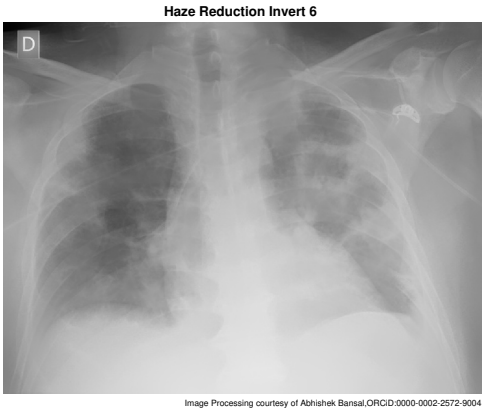

(d) Dehazing Algorithm

Fig. 111: Dehazing Algorithm,Day6

VIII Conclusion & Future Work

The author using various tools and techniques invested his time in order to help doctors or researchers and pharmacologists. The author has successfully presented his image processing results and shown different possible images that can be obtained for analysis and studying ailment.

Though there are already established straightforward rules to read X-rays, e.g. dark gray areas, light area, distances,penetration,adequacy of inspiration,silhouette sign etc., which are adequate; these submitted further processed images can help doctors in diagnosing and understanding deeper the phenomenon when the infection causes are different. Thus, these can help in the research of new medicine or treatment and can be used in designing of machine or therapy. It also gives researchers a perspective in deciding which image processing technique will not work at all, saving their time.

The submitted image processing results reveal certain patterns which are represented in mathematical form and can be used in the testing of machines. The polynomial fitting equations show the global formulation of complete lungs with various ailments is not possible mathematically whereas the local area (which would of interest) can be more accurately expressed in mathematical equations. The submitted mathematical equations can be more analysed with comparative study on other infections of lungs which the author may submit in future work. The author has used these in his novel model- Novel $\mathcal{B}$-Mathematical Modeling of Respiratory System and Novel $\mathcal{B}$-Bio Models Theory (to be submitted in few months or 20-30 years or never).

It must be also noted that the clinical usefulness is ***not claimed*** *in these results. As author has already mentioned, many researchers/post-doctorate fellows/clinical doctors, are performing*

same tasks which even the source[1] reveals, the author has submitted his work in this research paper.

Competing Interests

The author declares no competing interest. This manuscript has not been accepted or published by any journal.

Funding

There are no funders for this submission.The author has himself fully self-financed (with only objective to help) as it is only wastage of his time.

Acknowledgment

The work reported in this paper has been done independently and exclusively by the single author. The author has himself arranged himself various tools needed to submit this paper,with no support of any kind. The author as such thankful to none and does not have any special name to be acknowledged. He expects all these papers, would be nice Shroud for the passion and the price paid.

Disclosure statement

The author declares no potential conflict of interest.

Distribution/Reuse Options

References

[1] Joseph Paul Cohen and Paul Morrison and Lan Dao, Joseph Paul Cohen, Postdoctoral Fellow, University of Montreal, COVID-19 image data collection, covid-chestxray-dataset-master.zip, 525MB, https://github.com/ieee8023/covid-chestxray-dataset

[2] COVID-19 Image Data Collection: Prospective Predictions Are the Future Joseph Paul Cohen and Paul Morrison and Lan Dao and Karsten Roth and Tim Q Duong and Marzyeh Ghassemi arXiv:2006.11988, https://github.com/ieee8023/covid-chestxray-dataset, 2020

[3] OpenCV team, https://opencv.org/

[4] FuzzyLite, https://www.fuzzylite.com/

[5] Laplacian Operator, https://en.wikipedia.org/wiki/Laplace_operator

[6] Sobel–Feldman operator, https://en.wikipedia.org/wiki/Sobel_operator

[7] Mathematical morphology, https://en.wikipedia.org/wiki/Mathematical_morphology

[8] Fuzzy Logic, https://en.wikipedia.org/wiki/Fuzzy_logic

[9] Abhishek Bansal, December 9, 2020, "Data and Designs of $\mathcal{B}$-Medical Machines", IEEE Dataport, doi: https://dx.doi.org/10.21227/b58y-nb96.

[10] PyTorch, https://PyTorch.org

[11] TensorFlow,www.tensorflow.org